NIST GCR 17-917-46v2

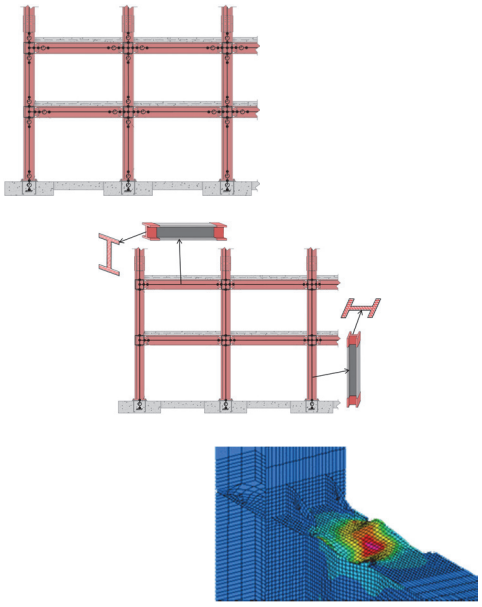

Guidelines for Nonlinear Structural Analysis for Design of Buildings

Part IIa – Steel Moment Frames

Applied Technology Council

This publication is available free of charge from:
https://doi.org/10.6028/NIST.GCR.17-917-46v2

National Institute of Standards and Technology
U.S. Department of Commerce

Disclaimer

This report was prepared for the Engineering Laboratory of the National Institute of Standards and Technology (NIST) under Contract SB1341-13-CQ-0009, Task Order 13-497. The contents of this publication do not necessarily reflect the views and policies of NIST or the U.S. Government.

This report was produced by the Applied Technology Council (ATC). While endeavoring to provide practical and accurate information, the Applied Technology Council, the authors, and the reviewers assume no liability for, nor express or imply any warranty with regard to, the information contained herein. Users of information contained in this report assume all liability arising from such use.

Unless otherwise noted, photos, figures, and data presented in this report have been developed or provided by ATC staff or consultants engaged under contract to provide information as works for hire. Any similarity with other published information is coincidental. Photos and figures cited from outside sources have been reproduced in this report with permission. Any other use requires additional permission from the copyright holders.

Certain commercial software, equipment, instruments, or materials may have been used in the preparation of information contributing to this report. Identification in this report is not intended to imply recommendation or endorsement by NIST, nor is it intended to imply that such software, equipment, instruments, or materials are necessarily the best available for the purpose.

NIST policy is to use the International System of Units (metric units) in all its publications. In this report, however, information is presented in U.S. Customary Units (inch-pound), as this is the preferred system of units in the U.S. engineering industry.

Cover image – Three model idealizations (concentrated hinge, fiber hinge, and continuum finite element) of a typical steel moment frame system/connection.

NIST GCR 17-917-46v2

Guidelines for Nonlinear Structural Analysis for Design of Buildings

Part IIa – Steel Moment Frames

Prepared for
U.S. Department of Commerce
Engineering Laboratory
National Institute of Standards and Technology
Gaithersburg, MD 20899-8600

By
Applied Technology Council
201 Redwood Shores Parkway, Suite 240
Redwood City, CA 94065

This publication is available free of charge from:
https://doi.org/10.6028/NIST.GCR.17-917-46v2

April 2017

U.S. Department of Commerce
Wilbur L. Ross, Jr., Secretary

National Institute of Standards and Technology
Kent Rochford, Acting NIST Director and Under Secretary of Commerce for Standards and Technology

Participants

National Institute of Standards and Technology

Steven L. McCabe, Acting NEHRP Director and Group Leader
Jay Harris, Research Structural Engineer
Siamak Sattar, Research Structural Engineer
Matthew S. Speicher, Research Structural Engineer
Kevin K. F. Wong, Research Structural Engineer
Earthquake Engineering Group, Materials and Structural Systems Division, Engineering Laboratory
www.NEHRP.gov

Applied Technology Council

201 Redwood Shores Parkway, Suite 240
Redwood City, California 94065
www.ATCouncil.org

Program Management

Jon A. Heintz (Program Manager)
Ayse Hortacsu (Associate Program Manager)
Veronica Cedillos (Associate Project Manager)

Program Committee on Seismic Engineering

Jon A. Heintz (Chair)
Michael Cochran
James R. Harris
James Jirsa
Roberto Leon
Stephen Mahin
James O. Malley
Donald Scott
Andrew Whittaker

Project Technical Committee

Gregory G. Deierlein (Project Director)
Stephen T. Bono
James O. Malley
Silvia Mazzoni
Chia-Ming Uang

Project Review Panel

Jerome F. Hajjar
Charles Roeder
Thomas Sabol
Mark Saunders
Kent Yu (ATC Board Contact)

Working Group

Gulen Ozkula
Zhi Zhou

Preface

In September 2014, the Applied Technology Council (ATC) commenced a task order project under National Institute of Standards and Technology (NIST) Contract SB1341-13-CQ-0009 to develop guidance for nonlinear dynamic analysis (ATC-114 Project). The need for such guidance is identified as high-priority research and development topic (Proposed Research Initiative 6) in NIST GCR 14-917-27 report, *Nonlinear Analysis Research and Development Program for Performance-Based Seismic Engineering* (NIST, 2013), which outlines a research and development program for addressing the gap between state-of-the-art academic research and state-of-practice engineering applications for nonlinear structural analysis, analytical structural modeling, and computer simulation in support of performance-based seismic engineering. In addition, the NIST GCR 09-917-2 report, *Research Required to Support Full Implementation of Performance-Based Seismic Design* (NIST, 2009), also identified the need to improve analytical models for buildings and their components in near-collapse seismic loading.

To help fill this gap, the ATC-114 Project developed a series of reports that provide general nonlinear modeling and nonlinear analysis guidance, as well as guidance specific to the following two structural systems: structural steel moment frames and reinforced concrete moment frames. This Part IIa report, referred to as *Guidelines* herein, provide practical guidance for nonlinear modeling and analysis specific to steel moment-resisting frames and their components. It is a companion to *Part I Guidelines* (NIST, 2017a) that provides general guidance on nonlinear analysis. Other Part II companion reports provide further details for selected system types.

These *Guidelines* were developed by the members of the ATC-114 *Steel Moment Frames* project team. ATC is indebted to the leadership of Greg Deierlein, who served as the Project Director. The Project Technical Committee, consisting of Stephen Bono, Jim Malley, Silvia Mazzoni, and Chia-Ming Uang, contributed to developing this report and guided the technical efforts of the Project Working Group, which included Gulen Ozkula and Zhi Zhou. The members of the Project Review Panel, who were charged with reviewing the report during the various stages of development and ensuring that technical results were accurate, are also gratefully acknowledged. These individuals consisted of Jerry Hajjar, Charles Roeder, Tom Sabol, Mark Saunders, and Kent Yu (ATC Board Contact). The names and affiliations of all who contributed to this report are provided in the list of Project Participants.

ATC also gratefully acknowledges Steven L. McCabe (Contracting Officer's Representative), Jay Harris, Siamak Sattar, Matthew Speicher, and Kevin Wong for their input and guidance throughout the project development process. Dimitrios Lignos and Amit Kanvinde contributed to the development of this report by providing source material, developing new equations, and helping with writing and reviewing the report. ATC staff members Veronica Cedillos and Carrie Perna provided project management support and report production services, respectively.

Ayse Hortacsu
Associate Program Manager

Jon Heintz
Program Manager

Table of Contents

Preface ..... **iii**

List of Figures ..... **ix**

List of Tables ..... **xiii**

1. Introduction and Scope **1-1**

2. Structural Behavior and Failure Modes **2-1**
2.1 Overview of Frame Behavior 2-1
2.2 Expected Behavior Modes for Steel Moment Frames 2-3
2.3 Composite Beam Behavior 2-6
2.4 Column Behavior 2-6
2.5 Panel Zone 2-8
2.6 Column Splices 2-9
2.7 Moment Frames with Non-Conforming Design Details 2-10
2.8 Gravity Framing 2-11
2.9 Loading History Effects 2-11

3. Nonlinear Modeling of Steel Moment Frames and Components **3-1**
3.1 Overview of Three Frame Model Idealizations 3-1
3.1.1 Concentrated Hinge Components Models 3-2
3.1.2 Fiber-Type Beam-Column Models 3-4
3.1.3 Continuum Finite Element Components Models 3-6
3.2 Column and Beam Modeling 3-7
3.3 Column Splices 3-8
3.4 Beam-Column Joint Panel Zones 3-8
3.4.1 Behavior and Shear Strength 3-8
3.4.2 Simplified Models 3-10
3.4.3 Concentrated Shear Model 3-11
3.4.4 Finite Size Kinematics and Flexibility 3-13
3.5 Floor Diaphragms and Collectors 3-15
3.6 Secondary Gravity Load-Carrying Systems 3-15
3.7 Modeling of Damping 3-16

4. Concentrated Hinge Component Models **4-1**
4.1 Overview of Concentrated Hinge Model 4-1
4.2 Beam Hinge Model 4-1
4.2.1 Monotonic Backbone 4-4
4.2.2 Cyclic Envelope 4-5
4.2.3 Beam Hinge – Illustrative Examples 4-7
4.2.4 Limiting Deformations 4-8
4.2.5 Composite Beam Effect 4-8

4.3 Column Hinge Model 4-11
4.3.1 Monotonic Backbone – Wide Flange Columns 4-11
4.3.2 Cyclic Backbone Curve – Wide Flange Columns 4-13
4.3.3 Monotonic Backbone – Square HSS Columns 4-14
4.3.4 Cyclic Skeleton – Square HSS Columns 4-15
4.4 Composite Gravity Beam-Column Connection 4-16
4.4.1 Positive Moment Capacity 4-17
4.4.2 Negative Moment Capacity 4-19
4.4.3 Moment at Connection Slip 4-20
4.4.4 Limitations on Procedure 4-21
4.4.5 Comparison of Liu and Astaneh-Asl versus ASCE/SEI 41 and FEMA 355D 4-21

5. Fiber-Type Beam-Column Models 5-1
5.1 Overview of Fiber-Type Models 5-1
5.2 Implementation of Section and Element Models 5-1
5.3 Fiber-Section Modeling 5-2
5.4 Uniaxial Moment and Axial Force Model 5-3
5.5 Biaxial Moment and Axial Force Model 5-4
5.6 Material Modeling Requirements 5-4
5.7 Implementation of Distributed-Inelasticity Elements 5-6
5.8 Hinge Length 5-7
5.9 Special Considerations for Fiber Sections in Steel Structures 5-7
5.9.1 Reduced Beam Section 5-7
5.9.2 Bolt Slip and Fracture 5-8

6. Continuum Finite Element Component Models 6-1
6.1 Overview 6-1
6.2 Quality Assurance 6-2
6.2.1 Virtual Testing 6-3
6.3 Element Type and Convergence Test 6-3
6.4 Nonlinear Material Models 6-4
6.5 Geometric Imperfections, Residual Stresses, and Post-Buckling Analysis 6-5
6.6 Strain Limits for Fracture and Low-Cycle Fatigue 6-7

Appendix A: Modeling Pre-Northridge (Fracture Critical) Connections A-1
A.1 Overview of Pre-Northridge Connections A-1
A.2 Pre-Northridge Beam-Column Connection A-2
A.2.1 Moment Frame Beam Hinge Model A-2
A.2.2 Critical Stress A-3
A.2.3 Critical Plastic Hinge Rotation A-6
A.2.4 Recommendations for Pre-Northridge Beam-Column Connections A-7
A.2.5 Concentrated Hinge Implementation A-8
A.2.6 Fiber Hinge Implementation A-8
A.3 Pre-Northridge Column Splice Connection A-10
A.3.1 Critical Stress A-11
A.3.2 Concentrated Hinge Implementation A-12
A.3.3 Fiber Hinge Implementation A-12

Appendix B: Steel Moment Frame Example Building B-1
B.1 Introduction B-1
B.2 Building Description B-1
B.3 Linear Structural Analysis and Design B-3
B.3.1 Modeling Criteria B-5
B.3.2 Fundamental Periods B-6
B.3.3 Modal Analysis B-6
B.3.4 Structural Design of Primary Moment-Resisting Members B-7
B.3.5 Structural Design of Secondary Members B-9
B.4 Nonlinear Modeling of Building B-10
B.4.1 Material Strengths B-14
B.4.2 Moment Frame Beam B-14
B.4.3 Moment Frame Column B-15
B.4.4 Panel Zone B-15
B.4.5 Diaphragm B-15
B.4.6 Gravity Beam B-16
B.4.7 Damping B-16
B.4.8 Ground Motions B-17
B.5 Nonlinear Response History Analysis B-18
B.5.1 Nonlinear Model Fundamental Periods B-19
B.5.2 Story Drift B-19
B.5.3 Story Shear and Overturning Moment B-21
B.5.4 RBS Hinges B-23
B.5.5 Columns B-25
B.5.6 Panel Zones B-27
B.5.7 Diaphragm Transfer at Fourth Floor B-28
B.5.8 Gravity System B-31
B.6 Conclusions B-31

References C-1

Project Participants D-1

List of Figures

Figure 2-1 Overview of typical steel moment frame system 2-2

Figure 2-2 Steel beam-to-column subassembly 2-2

Figure 2-3 Cyclic response of steel moment connection with composite slab 2-6

Figure 2-4 W14×176 (stocky) column with high axial load 2-7

Figure 2-5 W24×131 (deep) column with varying axial load levels 2-7

Figure 2-6 Failure modes of steel columns 2-8

Figure 2-7 Cyclic shear behavior of weak panel zone 2-9

Figure 2-8 Shear buckling of thin doubler plate in a retrofitted moment connection 2-9

Figure 2-9 Typical details and cyclic response of an interior beam-column subassembly with composite shear tab gravity connection 2-11

Figure 2-10 Beam moment versus story drift angle response of identical steel beam-column moment connection tests 2-12

Figure 2-11 Comparison of monotonic response curve versus a cyclic skeleton curve for a steel beam 2-13

Figure 3-1 Overview of a typical steel moment frame, showing concentrated hinge centerline model idealization 3-2

Figure 3-2 Fiber sections in distributed-inelasticity elements 3-5

Figure 3-3 Fiber sections in finite length hinge elements 3-6

Figure 3-4 An example of local buckling 3-7

Figure 3-5 Schematic of forces from beams and columns acting on panel zone and the resultant panel zone shear forces 3-9

Figure 3-6 Schematic of rigid end offsets for elastic PZ 3-11

Figure 3-7 Idealized panel zone shear force versus shear deformation 3-12

Figure 3-8 Values of PZ shear deformation at the fully plastic strength from Equation 3-3, recommended as a deformation limit to avoid flange fracture (for grade 50 steel) 3-13

Figure 3-9 Idealized panel zone models that capture finite size and panel deformations 3-14
Figure 4-1 Idealized monotonic and cyclic backbone curves for steel beams 4-2
Figure 4-2 Geometric offsets in concentrated hinge models 4-3
Figure 4-3 Comparison of monotonic and cyclic backbone curves and ASCE/SEI 41-13 curves for two steel sections 4-7
Figure 4-4 Rotation limit imposed where using models that do not simulate degradation for rotations beyond θ_p^* (corresponding to M^*_u) 4-8
Figure 4-5 Adjustments to monotonic backbone curve to account for composite beam action 4-9
Figure 4-6 Local transfer of longitudinal stresses resisted by floor slab into the steel column 4-10
Figure 4-7 Composite gravity framing connection 4-16
Figure 4-8 Cyclic skeleton curve for composite gravity framing connections 4-17
Figure 4-9 Equivalent bolt elements in shear tab connections 4-17
Figure 4-10 Force distribution in composite shear tab connection 4-18
Figure 4-11 Force distribution in non-composite (bare) steel shear tab connection 4-19
Figure 4-12 Calculation of M_{slip} in shear tab connections 4-20
Figure 4-13 Comparison of Liu and Astaneh-Asl (2000a, 2004) and ASCE/SEI 41-13 and FEMA 355D backbone curves 4-22
Figure 5-1 Fiber-section discretization of I-shape member 5-3
Figure 5-2 Engineering stress-strain curve for mild steel 5-5
Figure 5-3 Uniaxial cyclic stress-plastic strain curve 5-5
Figure 6-1 Simulation of cyclic response of a deep (W24) column with ABAQUS 6-2
Figure 6-2 Simulation of retrofitted beam-column connection response with ABAQUS 6-3
Figure 6-3 Beam-column subassembly modeling with mixed shell and brick elements 6-4
Figure 6-4 Beam-column subassembly global modeling and sub-modeling 6-4
Figure 6-5 Recommended steel stress-strain relationship (A992 steel) 6-5
Figure 6-6 Typical residual stress pattern 6-6

Figure A-1 Pre-Northridge beam-column connection A-3
Figure A-2 Moment-rotation response of pre-Northridge connection with fractured lower flange and intact top flange A-3
Figure A-3 Plastic hinge rotation at initial fracture in tests of pre-Northridge beam-column connections A-7
Figure A-4 Example calibration of fiber-hinge model A-10
Figure A-5 Typical column splice with partial penetration flange welds A-11
Figure B-1 Five story steel-framed building B-2
Figure B-2 Fourth floor framing plan of building B-3
Figure B-3 Structural model used for elastic analysis and design B-5
Figure B-4 Framing elevation on column lines A and D B-7
Figure B-5 Framing elevation on column line 4 ..... B-8
FigureB-6 Framing elevation on column line 5 ..... B-8
Figure B-7 Framing elevation on column line 1 ..... B-9
Figure B-8 Flow chart of analysis and assessment approach for force-controlled components B-11
Figure B-9 Flow chart of analysis and assessment approach for deformation-controlled components B-12
Figure B-10 Isometric view of nonlinear PERFORM-3D analysis model B-13
Figure B-11 Isometric view of nonlinear PERFORM-3D analysis model B-13
Figure B-12 Diaphragm model using shell finite elements B-16
Figure B-13 Response spectra of the eleven pairs of ground motions that are selected and scaled to the MCE Uniform Hazard Spectrum B-17
Figure B-14 Peak story drift ratios under MCE ground motions B-20
Figure B-15 Peak story drift ratios under MCE ground motion determined using an alternative model with pin-connected gravity beams B-21
Figure B-16 Peak story shear forces under MCE ground motions B-22
Figure B-17 Overturning moment under MCE ground motions B-22
Figure B-18 Peak RBS hinge rotations and acceptance criteria under MCE ground motions B-24
Figure B-19 First-story column hinge rotations under MCE ground motions B-25
Figure B-20 Panel Zone shear strains under MCE ground motions B-28

Figure B-21 Comparison of resultant shear and overturning moments in moment frames from analyses with variable floor diaphragm stiffness B-30

List of Tables

Table 2-1 Nonlinear Behavioral Effects to Consider in Nonlinear Analysis 2-4

Table 4-1 Ductile and Brittle Failure Modes in Composite Gravity Connection 4-17

Table A-1 Fracture Toughness Values at 70º F A-5

Table B-1 Building Seismic Design Information B-4

Table B-2 Summary of Equivalent Lateral Seismic Design Forces B-5

Table B-3 Dynamic Properties of Elastic Analysis Model B-6

Table B-4 Design Story Shears and Overturning Moment from MRSA B-6

Table B-5 Elastic Design Story Drifts and Drift Ratios from MRSA.....B-7

Table B-6 Beam Flange Cut Dimensions for RBS Connections B-9

Table B-7 Gravity Framing Connection Information B-9

Table B-8 Structural Steel Nominal and Expected Strengths B-14

Table B-9 Steel Bolts Nominal and Expected Strengths B-14

Table B-10 Concrete Nominal and Expected Strengths B-14

Table B-11 Concrete Reinforcement Nominal and Expected Strengths.....B-14

Table B-12 Demand Parameters and Acceptance Criteria for ASCE/SEI 7-16 MCE Analysis – Inelastic Behavior B-18

Table B-13 Demand Parameters and Acceptance Criteria for ASCE/SEI 7-16 MCE Analysis – Elastic Behavior.....B-18

Table B-14 Vibration Periods from Nonlinear PERFORM-3D Model B-19

Chapter 1
Introduction and Scope

This *Part IIa Guidelines* document is intended to provide practical guidance for nonlinear modeling and analysis specific to the design of steel moment-resisting frames and their components. It is a companion to NIST GCR 17-17-917-46v1, *Guidelines for Nonlinear Structural Analysis for Design of Buildings, Part I – General* (NIST, 2017a) that provides general guidance on nonlinear analysis that is applicable to several types of building structural systems. Readers are referred to *Part I Guidelines* for an overall introduction and for guidance on general topics. Although much of the guidance provided in this document is generally applicable to steel moment frames, the modeling criteria emphasize the seismic behavior of modern steel moment frames that adhere to current building code provisions for regions of high seismicity.

This *Part IIa Guidelines* document is meant to provide comprehensive guidelines for nonlinear analysis of steel moment frame structures, but it intentionally does not repeat material from other established standards and reference documents. Beyond the general reference standards cited in *Part I Guidelines*, this document is intended to build on the following documents:

- NIST GCR 16-917-41, N*EHRP Seismic Design Technical Brief No. 2: Seismic Design of Steel Special Moment Frames: A Guide for Practicing Engineers* (NIST, 2016)
- NIST GCR 10-917-5, NEHRP Seismic Design Technical Brief No. 4: Nonlinear Structural Analysis for Seismic Design: A Guide for Practicing Engineers (NIST, 2010)
- NIST GCR 16-917-42, N*EHRP Seismic Design Technical Brief No. 5: Seismic Design of Composite Steel Deck and Concrete-filled Diaphragms: A Guide for Practicing Engineers* (NIST, 2011)
- ANSI/AISC 341-16, Seismic Provisions for Structural Steel Buildings (AISC, 2016c)
- ANSI/AISC 360-16, *Specification for Structural Steel Buildings* (AISC, 2016d)

The intended audience for these *Part IIa Guidelines* is engineering practitioners, who are familiar with the concepts and limitations of nonlinear structural analysis, and who desire more detailed guidance on modeling of steel moment frame buildings. Similarly, the objective is not to cover basic principles of nonlinear

analysis, but rather to provide nonlinear modeling guidance to practitioners who are already experienced with these topics. These *Part IIa Guidelines* are written considering the analysis software capabilities that are currently available to practitioners, but also with a view towards emerging techniques that will become available in the future.

Chapter 2 of this document provides an overview of expected structural behavior and failure modes for steel moment frame buildings and Chapter 3 provides many of the general modeling guidelines. Chapters 4-6 provide specific guidelines for concentrated hinge component models (Chapter 4), fiber-type models (Chapter 5), and continuum finite element models (Chapter 6). In addition, Appendix A of this document provides guidance on modeling fracture in pre-Northridge steel moment frame buildings, which except for the fracture weakness, generally conform to current seismic design concepts for moment frames. An example application is provided in Appendix B to illustrate the use of these *Part IIa Guidelines* for a case-study building.

Chapter 2

Structural Behavior and Failure Modes

This chapter discusses the behavioral and failure modes of steel moment frame structures. Identifying and understanding these issues is an important step that allows an analyst to develop a model that captures all relevant behavior.

2.1 Overview of Frame Behavior

Figure 2-1 shows the major components of a steel moment frame, including the steel beams and columns, the beam-column joint panel region, the floor deck system, and the foundation system. In systems that employ seismic capacity design principles, the intent is for most of the inelastic behavior to occur through flexural hinging of the beams and limited shear yielding in the panel zone, although yielding is possible in the columns and column bases. For special moment frames, the connections of the beams to the columns and the column splices are designed to remain essentially elastic. Steel beams in moment frames are typically not designed as composite beams. However, these beams often act compositely with the floor deck (typically a concrete slab on a ribbed steel deck), which can affect the lateral stiffness, beam hinging, beam buckling mode, and connection response.

Figure 2-2a shows a finite element model of a beam-column subassembly that illustrates the distribution of deformations and yielding in the beams, columns, and panel zone. For overall frame analysis, the beam-column subassembly can be idealized as shown in Figure 2-2b, where common deformation parameters are shown. At the material level, the total strains are often considered to be comprised of elastic and plastic components, where the plastic component is the portion associated with energy dissipation that is not recovered upon unloading. Likewise, at the structural level, deformations and rotations are often distinguished between their elastic and plastic components, although the plastic (non-recoverable) deformations may be due to material yielding combined with other nonlinear actions such as local buckling and fracture. Using the discrete type models shown in Figure 2-2b, the plastic deformations are often assumed to be concentrated in plastic axial-flexural (*P*-*M*) hinges in the beams and columns along with plastic shear deformation of the panel zone. To the extent that plastic deformations are assumed to be concentrated in the plastic hinges, the plastic hinge rotations in flexural beam-column members can be obtained by subtracting the elastic chord rotations from the total chord rotations.

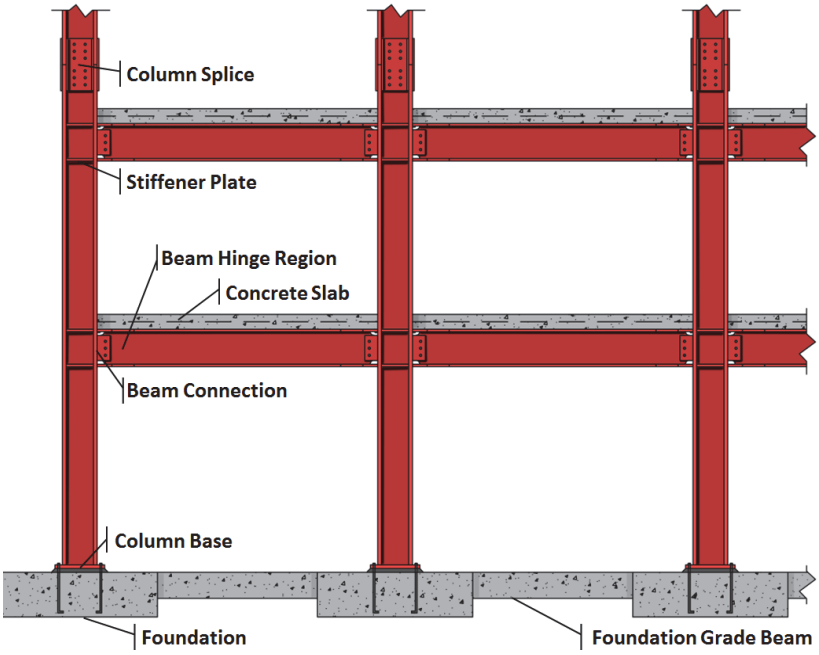

Figure 2-1 Overview of typical steel moment frame system.

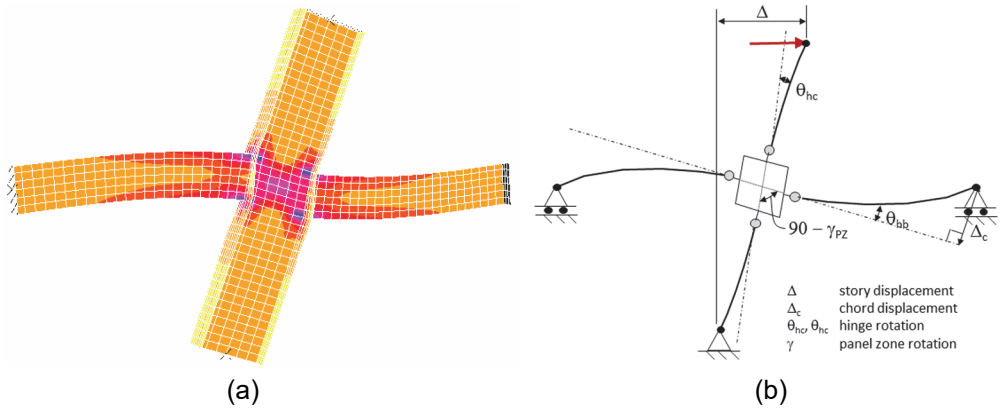

(a) (b)

Figure 2-2 Steel beam-to-column subassembly: (a) finite element model (Charney and Downs, 2004), and (b) idealized deformation components.

Ideally, the inelastic deformation is dominated by ductile yielding of steel, but other behavioral modes arise that can degrade the strength (force resistance) of members and connections. Deterioration generally occurs due to geometric instabilities (local or overall buckling) and/or material degradation (tearing or fracture). The following phenomena typically cause deterioration in beams and columns:

- **Local buckling of flanges or web.** This is dependent on the section slenderness.
- **Lateral-torsional buckling.** This is dependent on the member slenderness, associated with unbraced length, the radius of gyration about the weak axis, and boundary conditions.

- **Ductile tearing.** This refers to tearing due to large strains that concentrate in local buckles or other strain risers in plastic hinge regions.
- **Axial compression.** The presence of axial compression reduces flexural strength and exacerbates buckling.

The additional phenomena listed below can cause deterioration in the behavior of connections, including beam-column connections, column splices, and column base connections.

- **Crack propagation and fracture.** These arise when local stress or strain demands exceed the toughness of the materials. Depending on the situation, cracks can initiate and propagate through ductile or brittle fracture, although either mode can produce sudden failures.
- **Bolt slippage, yielding, and fracture.** This refers to a sequence of failure limit states in bolts that arises under bolt bearing, shear, tension, or combined shear and tension.
- **Local tearing in tension and shear.** This refers to ductile tearing arising at regions of concentrated tension, shear, and combined stress and strain states, including block shear of multiple failure planes.
- **Local plate bending.** This commonly occurs in base plate and end-plate connections, which increases connection flexibility and can lead to prying action that amplifies bolt tensions.
- **Plate compression buckling.** This is dependent on slenderness of connection plates in compression.

The degrading response due to these behavior modes must either be captured in the analysis or otherwise considered in the acceptance criteria, unless these deteriorating effects have been avoided through design (e.g., by proportioning stocky members or using capacity-design principles to limit imposed forces and deformations on the components or systems). In phenomenological type models (e.g., concentrated hinge models), these basic deterioration effects are often aggregated into cyclic strength and stiffness degradation of members and connections.

2.2 Expected Behavior Modes for Steel Moment Frames

Table 2-1 summarizes some possible nonlinear response phenomena in beams, columns, and beam-column connections. For each component, possible sequences of nonlinear response are described, including ones that respond in a ductile fashion and others that experience sudden and less predictable degradation.

Table 2-1 Nonlinear Behavioral Effects to Consider in Nonlinear Analysis

Component	Nonlinear Behavior	Moment Frame Types: *SMF*	*PN-SMF*	*IMF*	*OMF*	*NR-MF*
Beam	Yielding followed by gradual deterioration due to local buckling and/or lateral-torsional buckling and ductile tearing	■	▨	■	▨	▨
	SAME AS ABOVE – except with rapid deterioration			▨	■	■
	Yielding followed by rapid deterioration due to sudden connection fracture (ductile and/or brittle fracture)		■	▨	■	■
	No yielding or limited yielding followed by rapid deterioration due to local buckling and/or lateral-torsional buckling and ductile fracture				■	■
	No yielding or limited yielding followed by rapid deterioration due to sudden connection fracture (ductile and/or brittle		■		■	■
Column	Yielding followed by gradual deterioration due to local buckling and/or limited lateral-torsional buckling with possible ductile fracture (tearing)	▨	▨	▨	■	■
	SAME AS ABOVE – except with rapid deterioration			▨	■	■
	Yielding followed by rapid deterioration due to sudden column splice fracture (ductile and/or brittle fracture)		■		■	■
	No yielding or limited yielding followed by rapid deterioration due to local buckling and/or lateral-torsional buckling and ductile fracture				■	■
	No yielding or limited yielding followed by rapid deterioration due to sudden column splice fracture (ductile and/or brittle		■		■	■
Panel Zone	Limited yielding and strain hardening after beams have begun to yield	■	■	■	▨	▨
	Significant yielding prior to yielding in adjacent beams or columns			▨	■	■
Gravity Beam-Column Connection	Significant rotation capacity prior to gradual loss of flexural and/or shear capacity	■	■	▨	▨	▨
	Limited rotation capacity prior to sudden loss of flexural and/or shear capacity			■	■	■
Column Base	Full fixity with limited yielding and deformation	■	▨	▨	▨	▨
	Partial fixity with gradual yielding and deformation and significant rotation capacity			■	■	■
	Partial or full fixity with sudden deterioration due to fracture or rupture in the plate		■	■	■	■

Shading Legend

- ☐ *unlikely that phenomena will occur*
- ▨ *uncertain whether phenomena will occur*
- ■ *very likely that phenomena will occur*

The likelihood of occurrence of the nonlinear behavior is then related to frames whose design characteristics fall into one of the categories shown. It is important to recognize that these associations are approximate and only intended to provide some guidance about what type of response is likely to be encountered. Ultimately, the specific characteristics of each structure must be evaluated to determine which modes of behavior are likely to occur and should be modeled in design. The moment frame types in Table 2-1 are defined as follows:

- **Special Moment Frame (SMF).** This refers to a steel moment frame that is designed and constructed without any significant irregularities in accordance with the special moment frame requirements of ASCE/SEI 7-16, *Minimum Design Loads for Buildings and Other Structures* (ASCE, 2017a) and ANSI/AISC 341-16, *Seismic Provisions for Structural Steel Buildings* (AISC, 2016c).
- **Pre-Northridge Special Moment Frame (PN-SMF).** This refers to a steel moment frame that is characteristic of the welded frame construction that was prevalent in California and other high seismic regions of the West Coast prior to the Northridge earthquake (between about 1970 and 1994). Prior to the Northridge earthquake, such frames were expected to exhibit reliable ductile response, but the widespread weld fractures that were observed in beam-column connections revealed the high likelihood of sudden weld fractures. This changed beginning in about 1997 with FEMA 267, *Interim Guidelines for Steel Moment Resisting Frame Construction* (FEMA, 1997b), FEMA 350, *Recommended Seismic Design Criteria for New Steel Moment-Frame Buildings* (2000a), and the *Seismic Provisions for Structural Steel Buildings (1997)* (AISC, 1999).
- **Intermediate Moment Frame (IMF).** This refers to a steel moment frame that is designed and constructed without significant irregularities in accordance with intermediate moment frame requirements of ASCE/SEI 7 and ANSI/AISC 341.
- **Ordinary Moment Frame (OMF).** This refers to a steel moment frame that is designed and constructed without significant irregularities in accordance with ordinary moment frame requirements of the ASCE/SEI 7 and ANSI/AISC 341.
- **Non-Rated Moment Frame (NR-MF).** This refers to a steel moment frame that is not necessarily designed with any special capacity design or other requirements to ensure ductile response. This would include frames that are currently permitted by ASCE/SEI 7 in Seismic Design Categories C and lower, which only meet the minimum seismic strength requirements of ASCE/SEI 7 and the basic design and detailing provisions of ANSI/AISC 360, *Specification for Steel Buildings*. In such cases, there is no assurance that members or connections will respond in a ductile manner or that inelastic deformations will be not localized in the frame. This category also includes older existing steel frames in

higher seismic regions (Seismic Design Categories D or higher) that did not incorporate capacity design requirements and ductile connection details that were implemented following the Northridge earthquake.

2.3 Composite Beam Behavior

As noted earlier, beams in steel moment frames (of the seismic resisting system) are typically not designed as composite beams, although they often act compositely with the concrete floor slab. In cases where the composite action is significant (i.e., where calculations show that the composite action increases the flexural strength and stiffness in positive bending), it may be important to consider the flexural response of the beam in the model. Figure 2-3a shows the response of a two-sided beam-column connection test with composite action. The composite action results in non-symmetric response of each beam due to the increased flexural strength and reduced degradation because the slab restrains local buckling and lateral-torsional buckling when top beam flange is in compression (upper right quadrant in Figure 2-3a). This behavior can be modeled using a non-symmetric flexural hinge; or, for interior connections, the non-symmetric response of each hinge can be averaged between two opposing hinges. In such cases, the average strength will be higher and the cyclic degradation will be less than an equivalent bare steel beam. Figure 2-3b shows the much more symmetric response of a two-sided moment connection due to this averaging effect.

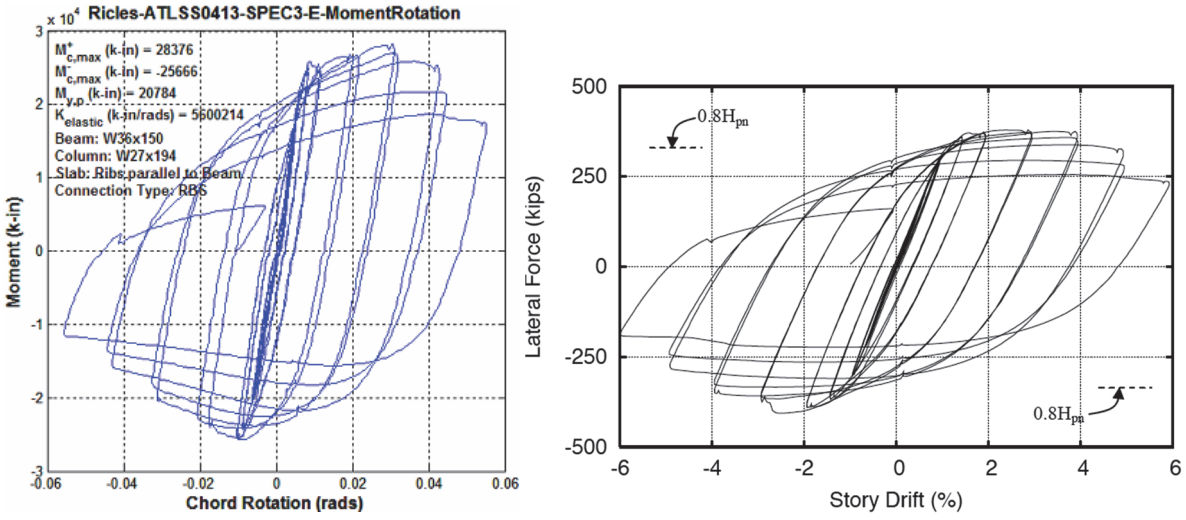

(a) (b)

Figure 2-3 Cyclic response of steel moment connection with composite slab: (a) moment-rotation relationship of one beam; and (b) lateral force-story drift relationship of a two-sided moment connection (Ricles et al., 2004).

2.4 Column Behavior

The flexural hinging response of columns can vary dramatically depending on its cross section, slenderness ratio, and the level of axial load. As shown in Figure 2-4,

very stocky columns, such as heavy W14 members, tend to have a remarkably stable hysteretic response. On the other hand, deep slender column sections, as shown in Figure 2-5, can experience rapid strength and stiffness degradation. The figure also shows that the level of axial load has a significant effect on the plastic rotation and energy dissipation capacities. While stocky shallow columns tend to form plastic hinges in the form of local buckling in the plane of bending, deep columns can exhibit global-type buckling in addition to local buckling as shown in Figure 2-6.

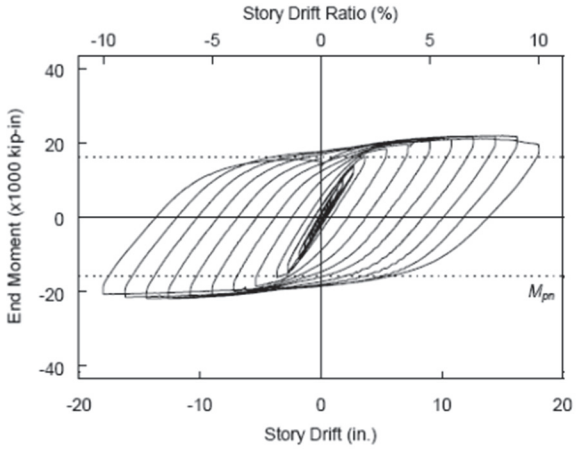

Figure 2-4 W14×176 (stocky) column with high axial load (Newell and Uang, 2008).

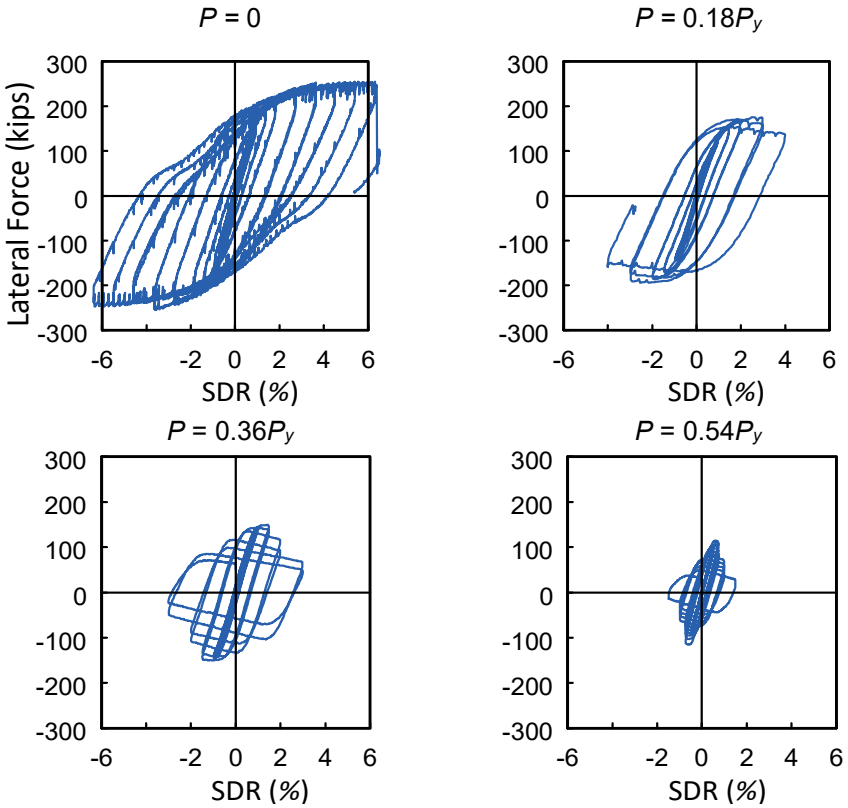

Figure 2-5 W24×131 (deep) column with varying axial load levels (Ozkula et al., 2015). (SDR = Story Drift Ratio)

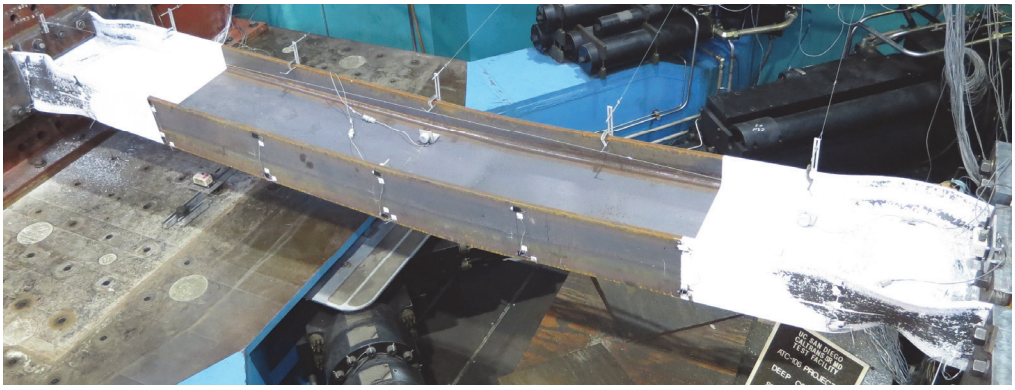

(a)

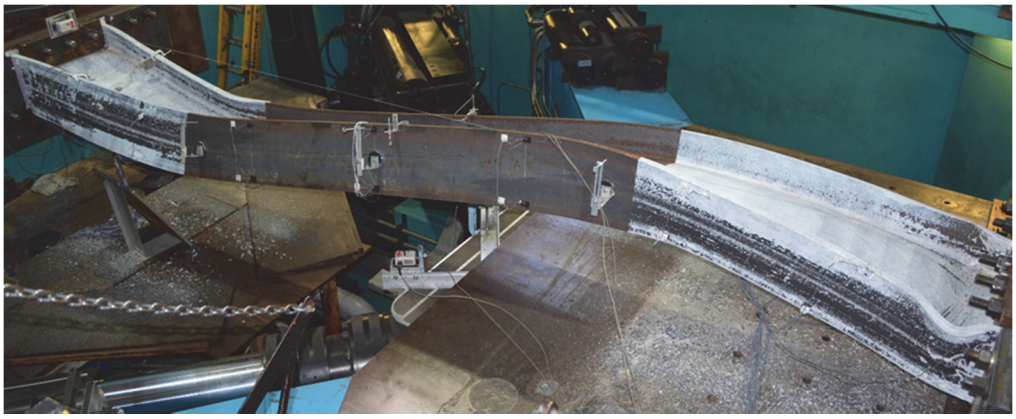

(b)

Figure 2-6 Failure modes of steel columns: (a) W24×131 with $P = 0.18P_y$; and (b) W24×176 with $P = 0.18P_y$ (Ozkula et al., 2015).

2.5 Panel Zone

Where beam-column joint panel zones yield in shear, as shown in Figure 2-7, the nonlinear response tends to be quite stable. This holds provided that: (1) the panel zone is thick enough with respect to its width and depth dimensions to avoid local buckling; and (2) the weld details of doubler plates, if used, are properly designed to develop the plate capacities. These conditions are typically met in seismically detailed frames that meet the recommendations of FEMA 350 or the requirements in standards that were subsequently developed. Typical beam-column geometries are such that most panel zones are sufficiently stocky to avoid local buckling, although buckling or fracture may occur if the panel zone is not seismically detailed (see Figure 2-8).

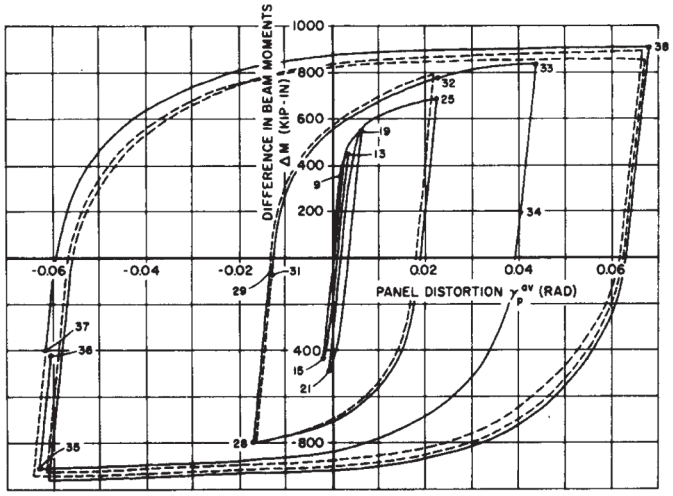

Figure 2-7 Cyclic shear behavior of weak panel zone (Krawinkler, 1978).

Figure 2-8 Shear buckling of thin doubler plate in a retrofitted moment connection (Newell et al., 2006).

2.6 Column Splices

Studies of the performance of existing high-rise steel building frames have highlighted that failure of under-capacity column splices may trigger collapse mechanisms (Shen et al., 2010; Almufti et al., 2012; Hall, 1995). Splices are susceptible to sudden failure when column splices are not properly designed and detailed. Splice failure is not expected to occur in modern (post-2000) special moment frames where either full strength splices are used or provisions are taken to ensure sufficient overstrength to avoid failure of partial strength splices. Splice failure is more likely in older frames, where partial strength splices are more common. Regardless of the design approach, it is generally recommended to confirm that the splice strength is sufficient to develop the forces that develop in the column

during the nonlinear analysis. Splices can fail suddenly with rapid strength deterioration; therefore, unless splices are modeled to capture this response, they should be treated as force-controlled components in the nonlinear analysis and acceptance criteria.

Welded splices of modern (post-2000) code-conforming special moment frames that are constructed of weld metal with high fracture toughness should have sufficient toughness to develop their calculated strengths. However, if the calculated strength of a partial strength splice (constructed with partial-joint-penetration (PJP) welds) is exceeded, the splice will fail suddenly, which can jeopardize the transfer of axial and shear forces and moments through the splice. Recent tests and fracture mechanics analyses of column splices (Sillmaker et al., 2015; Shaw et al., 2015) have demonstrated that under certain design and detailing conditions, PJP welds can be used to develop ductility commensurate with complete-joint-penetration (CJP) welds, but that is not generally the case.

Welded column splices with insufficient toughness (such as in frames constructed prior to the introduction of toughness requirements after the Northridge earthquake) may experience brittle fracture before reaching their nominal strength. Therefore, splices in pre-Northridge frames should be evaluated based on strength limits that take into account the tendency for brittle fracture. Guidelines for establishing effective strengths of PJP column splices and for modeling partial strength splices using a fiber-type approach are provided in Appendix A.

2.7 Moment Frames with Non-Conforming Design Details

The response plots described previously for beams, columns, and joint panel zones are all for cases where modern capacity design and ductile design and detailing provisions are applied to prevent premature fractures or other instabilities. When such requirements are not applied, frames may experience sudden loss of strength and stiffness that is difficult to predict reliably, as was demonstrated by the fractures to welded flange-bolted web moment connections in the 1994 Northridge earthquake. This presents particular challenges when analyzing older existing buildings that may not have been designed and constructed with capacity design and ductility. Similar concerns arise in new steel moment frames that are designed with less stringent requirements in moderate to low seismic regions, such as systems designed without any seismic detailing (with $R = 3$) as in Seismic Design Category C and lower. Guidance for evaluating the fracture-critical response of connections in "pre-Northridge" moment frames are provided in Appendix A. To the extent that these frames have failure modes that are otherwise fairly well controlled (i.e., where members are highly ductile and not prone to lateral buckling), the nonlinear response of the frames can be modeled using the guidelines of Appendix A combined with modeling recommendations from other sections of this *Guidelines* document.

2.8 Gravity Framing

The gravity load-resisting system in steel-framed buildings typically consists of steel beams that are attached to columns with connections that are designed only to resist beam shear, assuming that the rotational stiffness is low enough that connections do not resist much moment. While gravity connections are not designed to resist moment, typical shear tab or angle gravity connections can, in fact, resist significant moment, particularly when they act compositely with the concrete floor slab. An example of a typical gravity connection and moment-drift response from a cyclic interior beam-column connection test is shown in Figure 2-9. Such studies have shown that shear tab connections can resist moments on the order of 30% to 50% of the plastic moment of the connected beam with considerable ductility. The connection behavior will, of course, depend on the specific connection detail (e.g., strengths of shear tab and its connections of the beam and proportion of the beam). Nevertheless, depending on the connection detail, the framing plan configuration, and the proportion of seismic resisting frames to gravity framing, the gravity framing can contribute significantly to the lateral stiffness and strength of the building. While standard design methods do not formally recognize this contribution, it can be included in nonlinear dynamic analyses, provided that the analysis model reliably represents the construction detail (e.g., shear tab connection and composite action between the steel beam and column, and strength of gravity columns and their splices). Further details on modeling gravity framing is provided in Section 4.4.

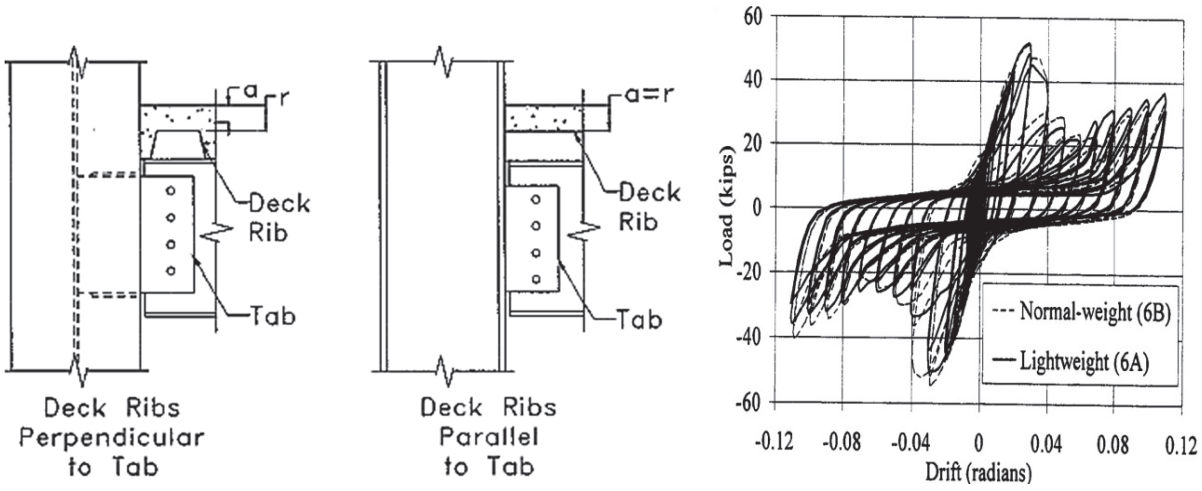

Figure 2-9 Typical details and cyclic response of an interior beam-column subassembly with composite shear tab gravity connection (Liu and Astaneh-Asl, 2004).

2.9 Loading History Effects

Loading history plays a significant role in a structure's response. Figure 2-10 shows beam moments versus chord rotation response curves from two identical reduced beam section (RBS) moment connection tests under different loading histories. The response shown in Figure 2-10a is for a specimen subjected to symmetric cyclic

loading, which is a standard protocol used in many tests. The loading protocol used in that test is similar to the one in Appendix K of ANSI/AISC 341-16, *Seismic Provisions for Structural Steel Buildings* (AISC, 2016c). Of particular note in the test is the peak point in the response curve, at a story drift angle of about 0.02 radians, beyond which the moment drops off due to local buckling and lateral-torsional buckling of the beam. Under continued cyclic loading, the moment resistance degrades to about one-half of the maximum moment at a maximum story drift angle of 0.05 radians. Under a near-fault type loading, as shown in Figure 2-10b, the specimen exhibits a slightly reduced peak response, but post peak degradation varies significantly depending on the number and amplitude of loading cycles. In particular, under the large positive push out to nearly 0.06 radians, this connection maintains considerably more (about two-thirds) of the peak resistance than that maintained by the specimen that was loaded symmetrically (Figure 2-10a). The strength retention under large monotonic-like pulses (Figure 2-10b) can significantly improve collapse resistance, compared to what may be inferred from the degradation in Figure 2-10a.

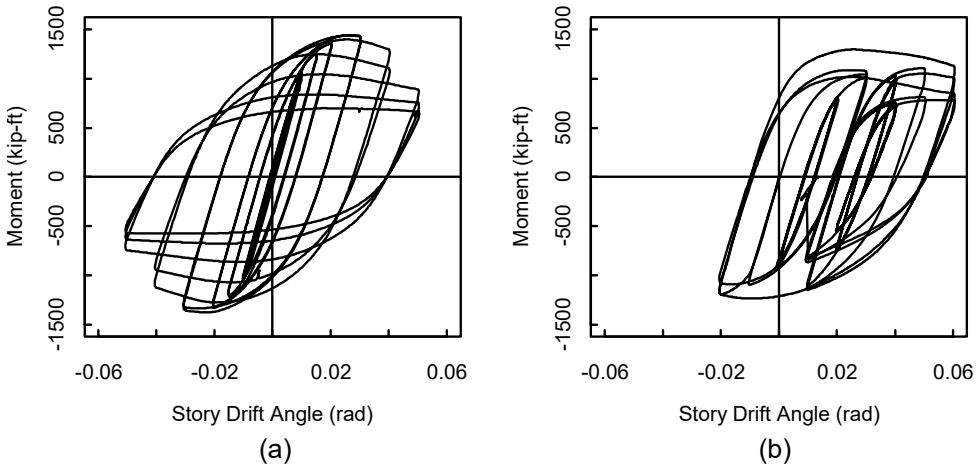

Figure 2-10 Beam moment versus story drift angle response of identical steel beam-column moment connection tests: (a) under symmetric cyclic loading; and (b) under random cyclic loading (Yu and Uang, 2001).

The influence of loading history on response is further illustrated in Figure 2-11, where data from a cyclically loaded test is superimposed with data from a monotonic test. The comparison in this figure demonstrates the distinction between a monotonic backbone curve (solid red line) and a cyclic skeleton curve (dashed black line). Whereas the monotonic response curve is considered as a characteristic property of the specimen, the cyclic skeleton curve will vary depending on the loading history applied.

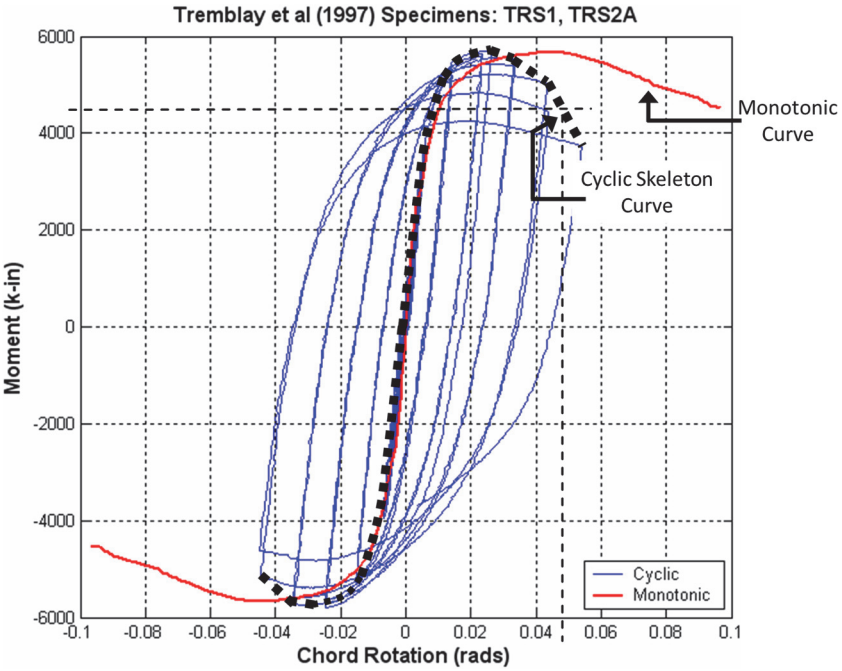

Figure 2-11 Comparison of monotonic response curve versus a cyclic skeleton curve for a steel beam (Tremblay et al., 1997).

Chapter 3
Nonlinear Modeling of Steel Moment Frames and Components

Idealized analysis models for steel moment frames can generally be distinguished between: (1) concentrated hinge models; (2) fiber-type models; or (3) continuum finite element models. The choice of model depends on the goals of the analysis and scope of the investigation. In general, continuum finite element models are best for simulating localized effects in members and connections, whereas concentrated hinge or fiber-type discrete models are better suited in practical applications for modeling overall response of entire frame systems. General background on these different model is provided in the *Part I Guidelines*. This chapter presents more detailed information and guidelines for applying these model types for the nonlinear analysis of steel moment frames.

3.1 Overview of Three Frame Model Idealizations

For analysis of steel moment frames, discrete concentrate hinge or fiber-type models are commonly used to represent beams, columns, and connections. Such models are usually semi-empirically calibrated to data from component and material tests and/or, to a lesser extent, to data from detailed finite element analyses. These discrete models have the advantage of being computationally efficient and amenable to definition using mechanics-based equations for member and connection strengths and stiffness properties. Discrete models for beams and columns are further distinguished based on how the member cross section is idealized and how inelastic effects are modeled along the member length. The cross section behavior is usually modeled using either pre-defined functions (uniaxial functions or multi-axial yield surface functions) that describe the component strength and stiffness, or by fiber-type numerical discretization through the member cross section. Numerical discretization through the member cross section generally requires some type of kinematic assumption (e.g., plane sections remain plane) to relate generalized cross section deformations to material strains. Inelastic behavior along the member length may be concentrated at one (hinge) location or distributed along the member based on assumed interpolation functions where the section response is calculated at discrete integration points. To the extent that inelastic effects concentrate over a small portion of the member length, the concentrated hinge models generally suffice. However, distributed models may be warranted in members with small moment gradients and/or high axial forces.

In contrast to discrete models, which rely on one or more behavioral assumptions to simplify the section or member response into line elements, continuum finite element models represent the entire structural continuum more explicitly. However, the advantage of modeling members and components at a more fundamental level comes with a larger computational cost. Nevertheless, continuum finite element analyses are sometimes warranted to analyze members or connections with complex geometries or laterally unbraced (slender) members, whose behavior cannot be reliably represented by discrete models or where calibration test data are not available.

3.1.1 Concentrated Hinge Components Models

Concentrated hinge models are the ones most commonly used in practice to simulate the overall response of steel moment frames because they are straightforward and efficient to calibrate and use. To the extent that the strength and stiffness degradation is present in calibration test data that represents conditions in real buildings, the phenomenological hinge models can simulate nonlinear behavior from the onset of yielding up through strength and stiffness degradation due to local buckling and other effects. Figure 3-1 shows an idealized model of a frame where concentrated hinges are inserted at locations that are expected to yield in an analysis.

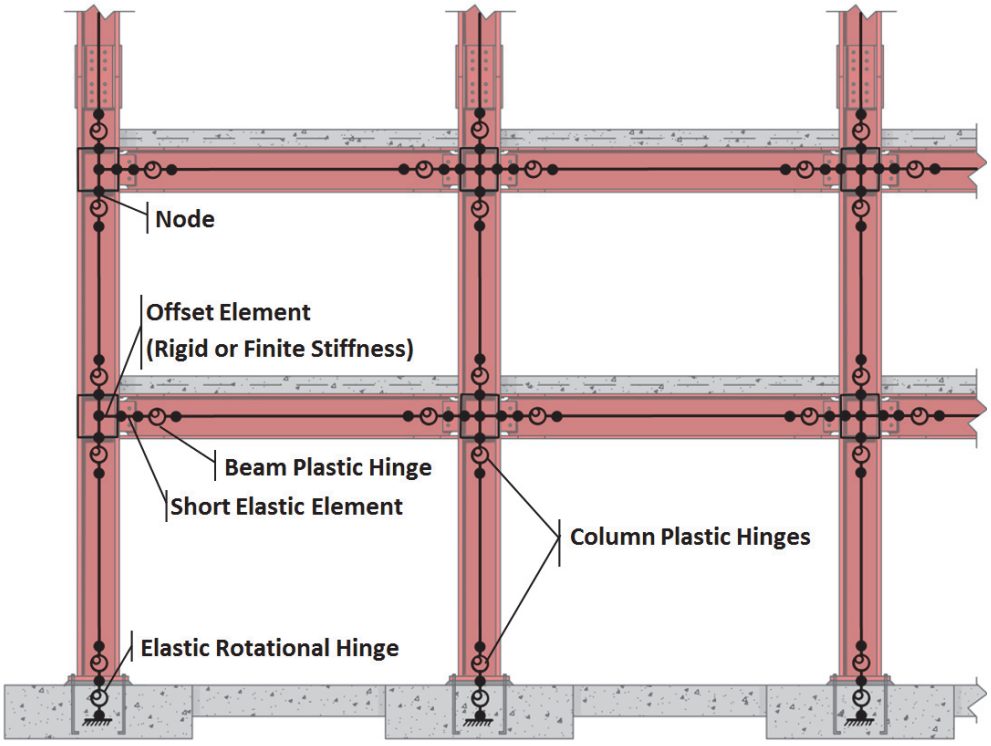

Figure 3-1 Overview of a typical steel moment frame, showing concentrated hinge centerline model idealization.

Components of the frame where inelastic behavior may occur should be modeled accordingly and include the following:

- **Beams.** Steel beams are often composite with the floor slab with stud anchors, which provides lateral support to the top flange and, depending on the relative size of the beam and slab, may affect the moment-rotation response. If composite action significantly increases the beam strength and stiffness (e.g., enough of an increase in strength to shift yielding from the beam to the column), it should be considered in defining inelastic hinge properties. Bracing (or lack of bracing) should, likewise, be considered in establishing the hinge properties, recognizing that concentrated hinge models may not be sufficient for slender laterally unbraced beams. Concentrated hinges should be located to reflect the anticipated plastic hinge region, either directly adjacent to the beam-column joint or offset in the case of reduced beam section (RBS) connections. AISC 358, *Prequalified Connections for Special and Intermediate Steel Moment Frames for Seismic Applications*, provides information on the plastic hinge location for the commonly used prequalified connections.
- **Columns.** While steel columns are often designed following the strong-column weak-beam provisions, this minimum criterion does not necessarily prevent column yielding. Therefore, unless it is demonstrated that the columns will remain elastic, inelastic hinges should be included at both ends of columns. While inelastic moment-rotation response is the dominant effect, the flexural response should be adjusted for axial loads, such as by reducing the moment resistance based on a *P-M* yield strength relationship. The unbraced length, slenderness, and restraint conditions at the column ends should be considered in defining hinge properties (NIST, 2017b; Elkady, 2016; Elkady and Lignos, 2016).
- **Beam-Column Connections.** Finite connection sizes and panel zone flexibility can have a significant effect on frame stiffness and response. Where deep beams are used, finite connection size can be particularly significant in reducing the effective column length. Inelastic panel zone deformations will depend on the panel zone strength, relative to the induced panel zone shear forces. Further guidance on modeling panel zones is presented in Section 3.4. In welded beam-column connections, the deformations of the connection between the beam and column are generally negligible, but these may need to be considered in bolted end plate or other connections with flexible connection plates.
- **Column Splices.** In frames designed in accordance with modern seismic requirements, splices are typically designed using capacity-design principles, such that inelastic deformations are not anticipated in the splices. Accordingly, the splices do not need to be explicitly modeled in such cases, but checks should be made to ensure that the induced forces do not exceed the strength of the

splices. In cases where the force demands in the splice exceed the splice strength, then the splice should be modeled with an inelastic spring (for shear and/or flexural effects).

- **Column Bases.** Flexibility of column base plates and foundations should be reflected in the model. For most frames the dominant effect is rotational stiffness, although axial stiffness of the column base may be important for slender frames with significant seismic uplift effects.

Further details to define concentrated hinge properties are provided in Chapter 4.

3.1.2 Fiber-Type Beam-Column Models

Fiber-type beam-column models, combined with either a fiber-hinge or distributed-inelasticity fiber beam-column element, are similar to concentrated hinge models to the extent that both are suitable to simulating overall frame response. Since stresses and strains are integrated through the cross section during the analysis, fiber-type elements are well suited for modeling arbitrary cross section shapes, hybrid cross sections (with mixed materials), and sections with variable axial load and moment (P-M) or with biaxial moment (P-M_y-M_z) interaction. Fiber sections typically employ uniaxial cyclic stress-strain properties of the steel material. However, strict adherence to uniaxial engineering stress-strain behavior and classical beam theory assumptions (i.e., plane sections remaining plane) limits the ability of fiber-type elements to simulate degradation due to flange and web buckling, fracture, and other localized effects. While the stress-strain response can be modified to simulate degradation, this requires phenomenological calibration that tends to negate some of the advantages of the fiber-type idealizations over phenomenological concentrated hinge models. Fiber-hinge and distributed-inelastic elements are primarily geared toward modeling beam-columns, and when used for modeling complete moment frames they are usually combined with concentrated hinge models to simulate member connections and deformations in joint panel zones.

As illustrated in Figures 3-2 and 3-3, inelastic yielding along the member length with fiber sections is generally represented by one of the following two formulation types:

- **Distributed-Inelasticity Elements** (Figure 3-2). In distributed-inelasticity elements, inelastic effects along the member length are evaluated at numerical integration points, whereby the model parameters are integrated along the length by assuming displacement or force interpolation functions. In theory, distributed models offer more accuracy than a hinge model by avoiding the need for pre-set hinge lengths. However, distributed models can be sensitive to strain localization. Therefore, some type of material model and mesh regularization method may need to be employed to control strain localization, particularly when

simulating degradation effects in materials and members. The fiber hinge approach (Figure 3-3) offers one way to avoid these issues.

- **Fiber Hinge Elements** (Figure 3-3). In this combination of fiber section and element models, yielding is assumed to occur over a pre-defined finite hinge length, where the controlling axial load and moment are usually evaluated at the mid-point or ends of the hinge. Inelastic strains are then integrated over the hinge length, assuming either a constant or linear distribution, to recover member forces and calculate the inelastic member stiffness. While this requires the user to pre-define the hinge length, it avoids potential numerical problems with strain localization that may be encountered with the distributed-inelastic elements.

Further information on these types of sections and elements is presented in Chapter 5.

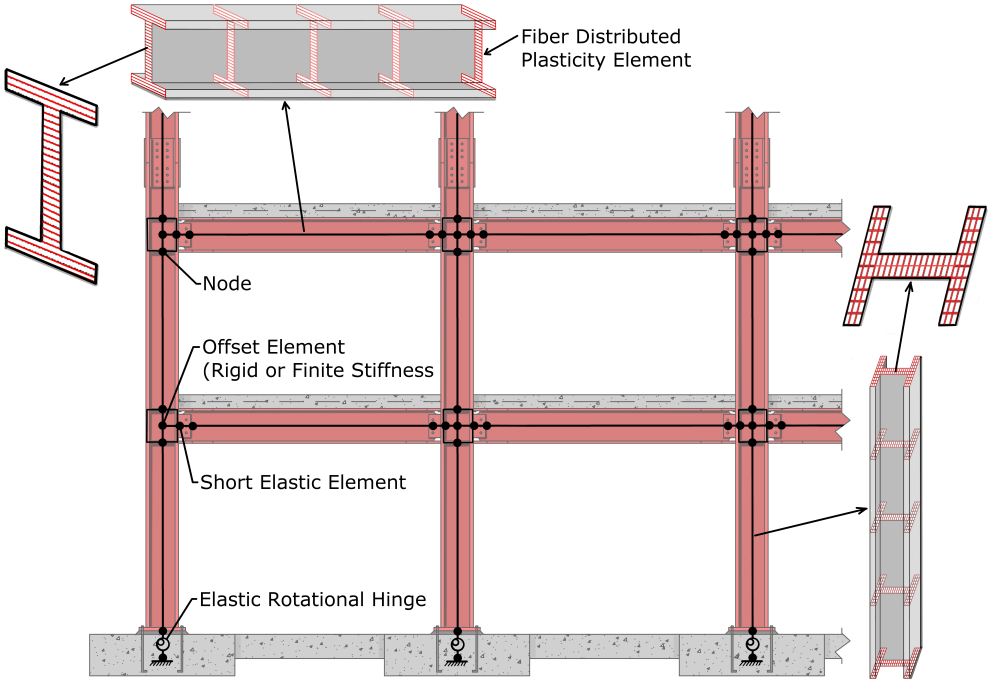

Figure 3-2 Fiber sections in distributed-inelasticity elements.

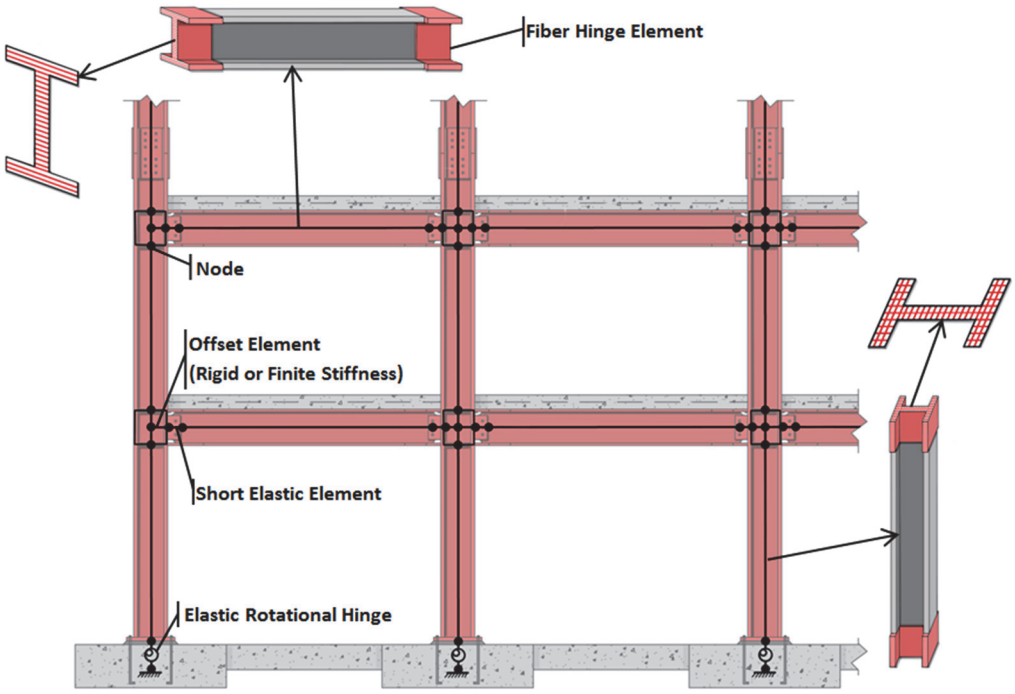

Figure 3-3 Fiber sections in finite length hinge elements.

3.1.3 Continuum Finite Element Components Models

Shell or solid (brick) finite element models can simulate yielding, buckling, and fracture behavior using a more fundamental representation of nonlinear material response than other approaches. Figure 3-4 shows an example of a finite element continuum model of a beam-column connection. In contrast to concentrated hinge or fiber-type models that can be used to simulate overall building response, current computing technologies tend to limit the practicality of continuum finite element methods to detailed modeling of only selected components of buildings. Such models can be reliably employed to characterize the nonlinear response and limit states of components for which test data does not exist and this information can then be used to calibrate and inform the use of discrete models of the complete building system. Further details on continuum finite element models are provided in Chapter 6.

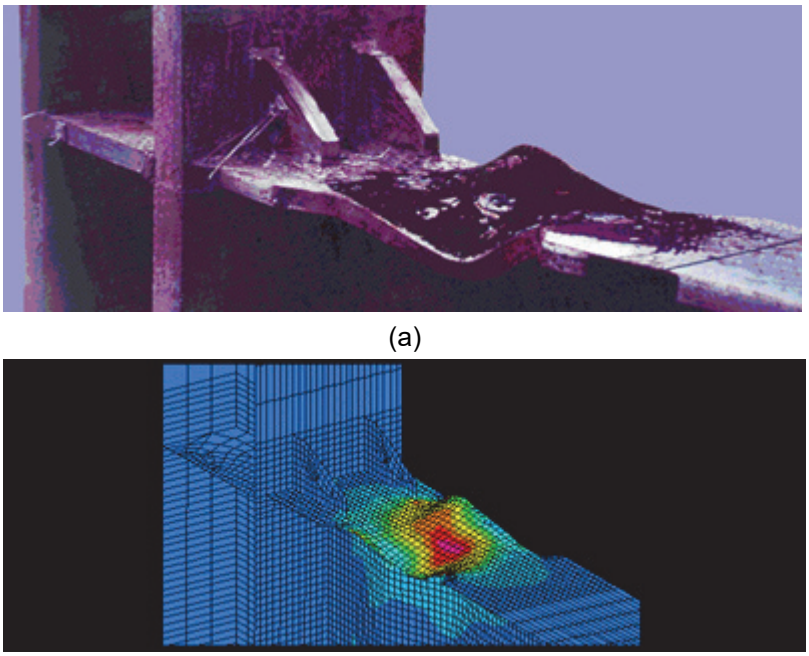

Figure 3-4 An example of local buckling: (a) of a test specimen; and (b) of a continuum finite element model simulation of a reinforced beam connection (provided by M. Willford, ARUP)

3.2 Column and Beam Modeling

As described in Chapter 2, the primary behavioral modes of steel moment frame components typically involve yielding, buckling, and fracture, which can occur independently or in combination with one another. To the extent that these phenomena may occur under the design earthquake ground shaking, they should be considered in the nonlinear analysis, either through direct simulation of the effects or through post-analysis limit state checks.

In the absence of project-specific data, expected properties of steel and concrete materials provided in Table 3-1 of *Part I Guidelines* can be used for modeling. These properties should be used in conjunction with the guidelines for modeling columns and beams as described in Chapters 4 through 6 in this *Guidelines* document. To the extent possible, models should represent all major modes of behavior, including strain hardening and post-peak degradation due to buckling and fracture. Otherwise, the acceptance criteria applied to the analysis results must be established, based on available data and judgment, to account for deterioration effects that are not captured by the analysis.

3.3 Column Splices

Column splices in seismically designed moment frame systems may be designed with sufficient strength to sustain forces imposed by the surrounding frame. Where this is the case, then the column splices are usually not modeled. For example, ANSI/AISC 341-16, *Seismic Provisions for Structural Steel Buildings* (AISC, 2016c) requirements for steel IMF and SMF frames will generally ensure that column splices are sufficiently strong to resist the forces induced during large earthquakes. However, it is recommended to always check the force demands on column splices, and to either model the splices or make other modifications to the analysis if the induced forces exceed the expected splice strength. Splices that are not sufficient to develop the required strength are likely to have limited ductility. Appendix A includes guidance for evaluating the strength and inelastic response of column splices constructed with partial penetration welds.

3.4 Beam-Column Joint Panel Zones

3.4.1 Behavior and Shear Strength

As shown in Figure 3-5, the panel zone (PZ) region that is common to adjacent beams and columns is subjected to a combination of axial forces, shear forces, and moments from the connected members. The two major considerations in modeling PZ behavior are: (1) influence of the finite size of the panel zone on the kinematics around the connection and effective free-span lengths of the connected beams and columns; and (2) elastic and inelastic deformations in the PZ region. While it is generally accepted that the dominate factors affecting the PZ response are the shears resisted by the PZ ($V_{pz,h}$ and $V_{pz,v}$, shown in Figure 3-5), the PZ region may also experience significant strains due to axial column forces and axial strains in the column flanges and continuity plates from moments in the columns and beams (so-called "strain penetration" into the joint). Explicit modeling of all these effects will generally require continuum finite element modeling. However, the two dominant effects of finite joint size and PZ shear can be modeled using discrete joint models.

Referring to Figure 3-5, and assuming that the beam and column moments are resisted primarily by a force couple in their flanges, the nominal horizontal shear force resisted by the PZ is calculated as:

$$V_{pz,h} = \frac{M_{b1} + M_{b2}}{d_b - t_{fb}} - \frac{V_{c1} + V_{c2}}{2} \tag{3-1}$$

where M_{b1} and M_{b2} are the moments in the beams, acting at the face of the column, V_{c1} and V_{c2} are the shear forces in the columns, d_b is the depth of the beams, and t_{fb} is the thickness of the beam flanges. Note that the panel zone shear is usually defined in terms of its horizontal component, $V_{pz,h,}$ since this is consistent with how the joint

panel shear strength as specified in the ANSI/AISC 360-16, *Specification for Steel Buildings* (AISC, 2016d). Given the horizontal joint shear force resultant, the corresponding vertical joint shear force resultant can be determined by moment equilibrium, i.e., $V_{pz,h}\,(d_b\text{-}t_{fb}) = V_{pz,v}\,(d_c\text{-}t_{fc})$.

Under earthquakes and other lateral load effects, shear forces increase and the PZ may yield, initially at its center and propagating outwards. Provided that the PZ deformations are not excessive and the connection is not prone to fracture, the PZ yielding is fairly ductile and can be modeled as such. Two exceptions, where this is not the case and fracture would be of concern, are: (1) pre-Northridge type connections; and (2) connections with shallow beam depths and thick column flanges where large inelastic shear deformations of the PZ can contribute to the initiation and propagation of fracture at beam flange welds in the vicinity of the column web (Kim et al., 2015). In such cases, it is recommended to either avoid significant PZ yielding by strengthening the PZ (with larger column sections or by adding PZ doubler plates) or to confirm that PZ deformation is less than the deformation at which column kinking is likely to cause weld or flange fracture (Kim et al., 2015).

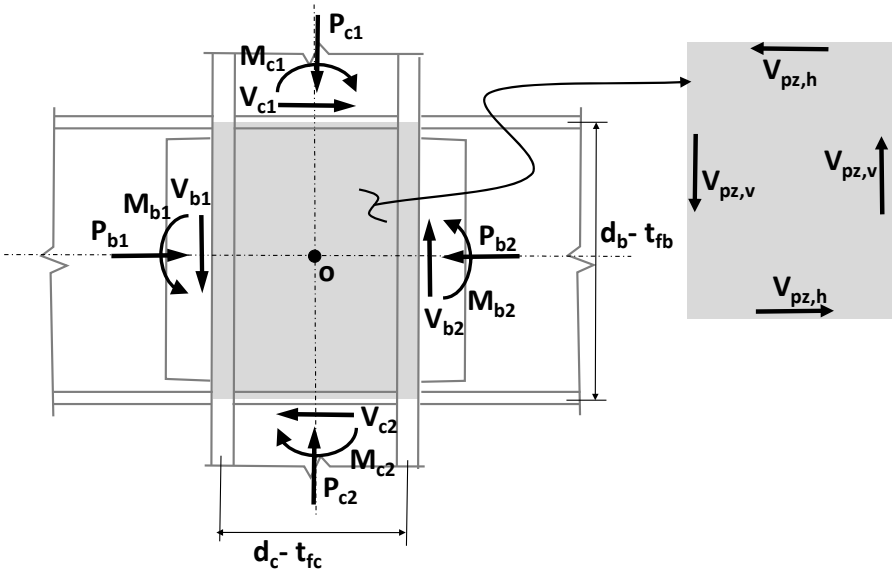

Figure 3-5 Schematic of forces from beams and columns acting on panel zone and the resultant panel zone shear forces.

To assess the likelihood of PZ yielding, the nominal PZ shear demand given by Equation 3-1 can be compared to the PZ strengths determined using equations in Section J10.6 of ANSI/AISC 360-16. To assess the expected behavior, the PZ strength can be evaluated using member forces from nonlinear analyses and the expected steel yield strength ($F_{y,exp} = R_y F_y$) in the PZ strength equations from ANSI/AISC 360-16. Where the PZ shear force does not exceed the expected strengths evaluated per Section J10.6a of ANSI/AISC 360-16 (Equations J10-9 and

J10-10), it is probably not necessary to model panel zone yielding. On the other hand, when the PZ shear forces exceed these expected strengths, panel zone yielding should be modeled. In such cases, one should be careful that PZ deformations do not become excessive by comparing the induced PZ shear force (Eq. 3-1) to the expected upper bound strengths given in Section J10.6b of ANSI/AISC 360-16 (Equations J10-11 and J10-12).

3.4.2 Simplified Models

A first-pass to account for PZ deformations and expected design drifts is to model centerline dimensions of beams and columns and not include a rigid end zone as described in the previous section. Provided that the PZ stays elastic, neglecting the finite size of the PZ will usually more than compensate for the neglect of PZ deformations, such that in most cases the calculated drifts will be larger than that from an analysis including an elastic PZ. While centerline models are certainly appropriate for preliminary member sizing and prescriptive design methods, they are generally not recommended for nonlinear analyses where significant efforts have been invested in modeling other effects. If centerline models without PZs are used in nonlinear analyses, the inelastic flexural strength of the beam hinge should be modified by increasing its capacity such that the yield force at the expected hinge location matches the flexural strength of the beam. In addition, the calculated inelastic flexural deformations (hinge rotations) should be increased by the difference in span ratios; or alternatively, the effective rotation parameters in the models should be reduced. Guidance for making these adjustments are provided in Section 4.2.

Where PZ are expected to remain elastic, an alternative to the centerline model is to approximate the finite size and stiffness of the PZ by including rigid offsets at the ends of beams and columns (see Figure 3-6). The rigid end offset may be implemented using stiff elements at the member ends (usually with an element stiffness on the order of 10 times that of the connected beam or column) or using kinematic constraint techniques (when available in the analysis software). The offset may be specified as the full PZ size, however, it is generally recommended to perform a sensitivity study to calibrate the stiffness modifier to match test data or detailed finite element analyses of similar PZs. In tall and slender buildings where axial deformations of columns is a significant percentage of overall building drift, consideration should be given to how the column rigid stiffness modifier will affect the column axial stiffness.

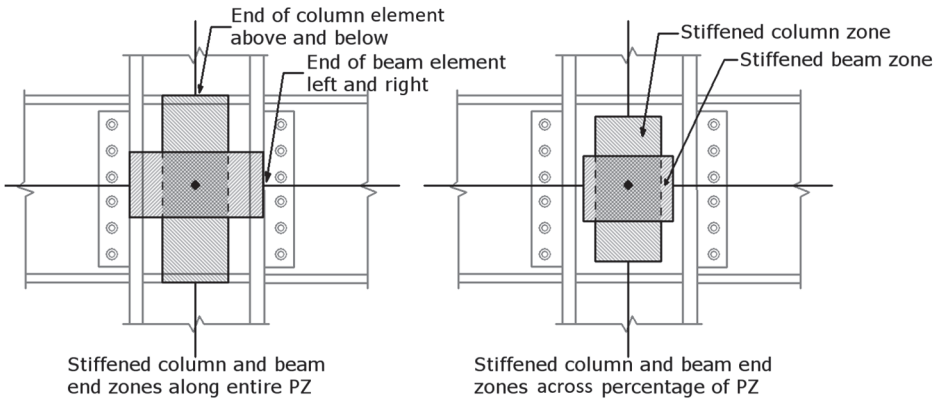

Figure 3-6 Schematic of rigid end offsets for elastic PZ.

3.4.3 Concentrated Shear Model

Where the shear force demands indicate that the induced PZ shear (Eq. 3-1) exceeds the PZ yield strength (Section J10.6a in ANSI/AISC 360-16), the inelastic panel zone response can be idealized by the tri-linear response curve for PZ shear force versus shear deformation, as shown in Figure 3-7. For panel zones that are fairly compact and not prone to buckling, the hysteresis response is very stable and the backbone curve is essentially the same for monotonic and cyclic loading. While this is usually the case for modern seismically detailed connections, it may not be the case for older or non-conforming designs, where buckling may need to be considered.

For compact panel zones, the expected PZ strengths given by equations in Sections J10.6a and J10.6b of ANSI/AISC 360-16 can be used to establish the PZ shear yield strength, $V_{y.pz}$ and fully plastic strength $V_{p,pz}$, respectively. When doing so, the expected steel yield strength ($R_y F_y$) should be used in lieu of the nominal yield strength. These equations take into account gross shear yielding of the web shear panel, the so-called "frame action" provided by the column flanges, and the influence of axial column load. Assuming that seismic column axial forces are not too significant, the applied axial load, P_r, in the ANSI/AISC 360-16 equations can be taken as the gravity load from the nonlinear analysis.

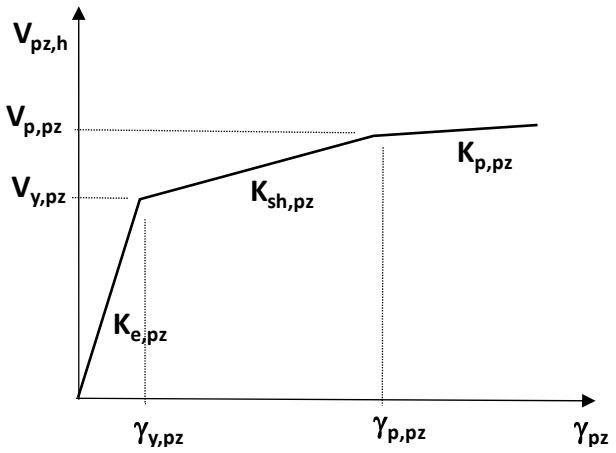

Figure 3-7 Idealized panel zone shear force versus shear deformation.

The elastic shear stiffness of the panel zone is given by the following:

$$K_{e,pz} = GA_{s,pz} \tag{3-2}$$

where G is the elastic shear modulus of steel, and $A_{s,pz}$ is the cross sectional area of the web in plan, equal to the column depth times the web thickness, including any web doubler plates. The shear yield strain, $\gamma_{y,pz}$, is the shear yield force, $V_{y,pz}$, divided by the elastic stiffness, $K_{e,pz}$. For steel with a an expected yield strength of $F_{y,exp}$ equal to 55 ksi, the shear yield strain $\gamma_{y,pz}$ is about 0.003. The fully plastic strength, $V_{p,pz}$, corresponds to a shear deformation of $\gamma_{p,pz} = 4\gamma_{y,pz}$ (about 0.012 for 55 ksi steel) which defines the hardening slope, $K_{sh,pz}$. The slope beyond $\gamma_{p,pz}$, $K_{p,pz}$ is usually very small, on the order of 0.01 to 0.02 times the elastic slope. An alternative PZ model has recently been developed by Kim et al. (2015), which can result in PZ shear strengths and stiffness that can be in the range of 80% to over 150% of that calculated per ANSI/AISC 360-16 equations. Kim et al. (2015) provide further details of the strength and stiffness expressions.

In addition to alternative expressions for strength and stiffness, Kim et al. (2015) propose a parameter to estimate the deformation at the fully plastic strength of the PZ, which they also recommend as a limit on deformations to avoid fracture due to high localized strains (due to kinking) in the column flange. This deformation is calculated as follows:

$$\gamma_{p,pz} = \frac{0.475F_{yc}}{E}\left(\frac{d_b}{t_{fc}} + 3.45\frac{t_{fc}}{d_b}\right) \tag{3-3}$$

where F_{yc} steel yield strength of the column flanges, E is the elastic modulus of steel, d_b is the beam depth, and t_{fc} is the column flange thickness.

As indicated by Equation 3-3, the deformation capacity reduces with increasing column flange thickness and decreasing beam depth. Values of $\gamma_{y,pz}$ from Equation

3-3 are shown as a function of column flange thickness for several beam depths in Figure 3-8, assuming grade 50 steel ($F_{y,exp}$ = 55 ksi). Traditionally, it has been assumed that the plannel zone will reach its fully plastic strength at a shear strain of of 0.012 radian (roughly $4\gamma_{y,pz}$). The plots in Figure 3-8 indicates that the fully plastic condition will be reached at lower shear deformations for columns with flange thicknesses thicker than 1.5 to 3 inches and at higher shear deformations for columns with thicknesses less than 1.5 to 3 inches (depending on beam depth).

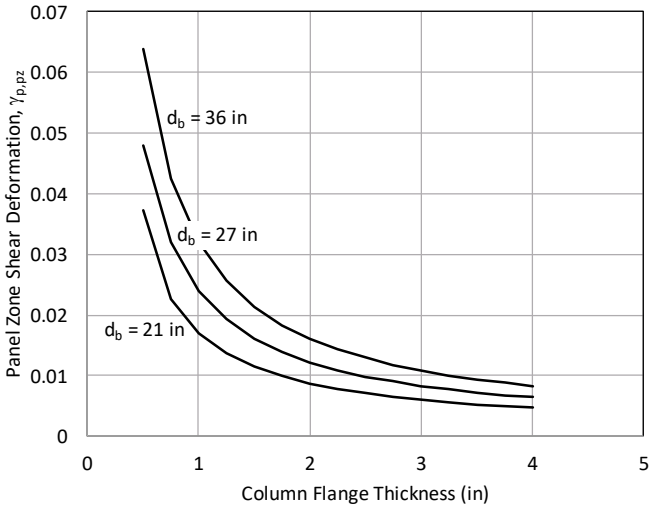

Figure 3-8 Values of PZ shear deformation at the fully plastic strength from Equation 3-3, recommended as a deformation limit to avoid flange fracture (for grade 50 steel).

3.4.4 Finite Size Kinematics and Flexibility

A practical but fairly complete PZ model is one that considers both finite connection geometry and panel zone flexibility. Figure 3-9 illustrates three possible ways that these effects can be implemented in analysis programs. The illustration in Figure 3-8a demonstrates a literal interpretation of the so-called "Krawinkler model" (PEER/ATC, 2010) where the PZ is modeled with stiff members with pinned connections to simulate the panel zone kinematics, and rotational spring (at the upper right corner of the PZ) is used to represent the PZ shear stiffness. The beams and columns are connected through nodes to the stiff PZ members. Yielding in the beams and columns may be modeled using concentrated hinges (as shown in Figure 3-9a) or by fiber-type models.

The model shown in Figure 3-9b is conceptually similar to that of Figure 3-9a, except that it uses kinematic constraint equations to connect the four surrounding beam and column nodes to the central PZ node. Compared to Figure 3-9a, the approach in Figure 3-9b is more efficient since it has fewer nodes and degrees of freedom. This model has been implemented in the OpenSees software and documented by Altoontash (2004).

A third and simpler alternative to model the PZ is the so-called "scissors model," shown in Figure 3-9c, where the beam and column are each modeled as rigid within the PZ, but are allowed to rotate relative to each other to account for PZ shear deformation (Charney and Marshall, 2006). The shear flexibility of the PZ is represented by a nonlinear rotational spring at the single hinge point at the beam-column centerline intersection. This model can be conveniently implemented by defining two nodes at the PZ, whose translational degrees of freedom are constrained to one another and whose rotational degrees of freedom are independent and connected by the PZ rotational spring. A disadvantage, compared to the previous two models (Figures 3-9a and 3-9b), is that the joint panel kinematics and equilibrium are not properly captured in the scissors model, which can lead to inaccuracies when the panel zone size is large compared to the column and beam lengths and as the panel zone deformations become large. For this reason, the joint models of Figures 3-9a or 3-9b are preferred.

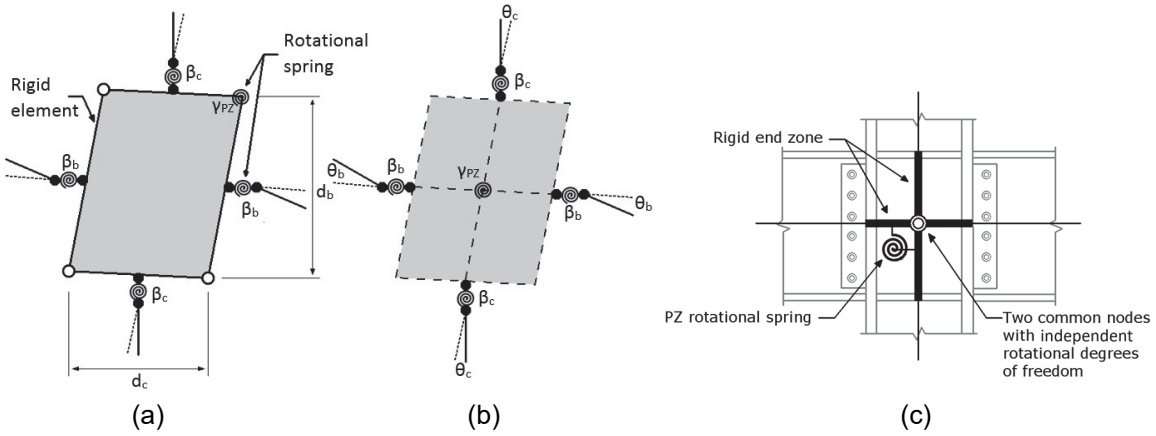

Figure 3-9 Idealized panel zone models that capture finite size and panel deformations: (a) "Krawinkler model" constructed with rigid elements, (b) kinematic constraint model, (c) "scissor model" constructed with rigid end offsets and double node.

Common to all three of approaches in Figure 3-9 are: (1) the assumption that the PZ can only deform in shear; (2) the PZ response is controlled by a single shear spring, which can be elastic or inelastic; and (3) inelastic deformations in the connected beams and columns is modeled independently in the member models. The specific implementation details often differ, including how rigorously the PZ assemblies (or constraint relationships) capture large deformation/rotation response. In addition, all of these model idealizations ignore axial deformations in the panel zones, which tends to overestimate the stiffness in instances where column axial strains or beam or column flexural strains penetrate into the PZ. These limitations will cause the elastic stiffness to be overestimated, particularly if the PZ are relatively large and the axial deformation of columns is significant (e.g., tall building frames). Column axial flexibility could be maintained by modeling the vertical links as rigid only in flexure, with vertical flexibility equivalent to that of the column section. Alternatively, the

stiffnesses of connected columns and beams could be modified to account for axial and flexural deformations that are suppressed in the PZ.

In all three models, the shear panel zone strength and stiffness must be translated from a shear force-shear deformation relationship (Figure 3-7) to equivalent PZ spring moments and rotations. For the Krawinkler and kinematic constraint models (Figures 3-9a and 3-9b), the PZ hinge is typically described in terms of an equivalent shear panel moment, M_{pz}, where the yield and fully plastic strengths and associated stiffness parameters (K_{Mpz}) are calculated by multiplying the shear forces and stiffnesses from Figure 3-7 by the panel zone height (Figure 3-5), as follows:

$$M_{pz} = V(d_b - t_{fb}) \tag{3-4a}$$

$$K_{M,pz} = K(d_b - t_{fb}) \tag{3-4b}$$

where d_b is the beam depth and t_{fb} is the beam flange thickness. For the scissors model (Figure 3-9c), the moment strength and stiffness parameters are determined by multiplying the shear forces from Figure 3-7 by the panel zone height, plus additional terms to adjust for discrepancies in the joint kinematics (Charney and Marshall, 2006):

$$M_{pz} = V\left(d_b - t_{fb}\right) / \left(1 - d_b / H - d_c / L\right) \tag{3-5a}$$

$$K_{M,pz} = K\left(d_b - t_{fb}\right) / \left(1 - d_b / H - d_c / L\right)^2 \tag{3-5b}$$

Where d_c is the column depth, H is the story height, and L is the column spacing. Since details of the joint implementation may vary in different computer software, users should familiarize themselves with specific software capabilities by creating test-case models for one or more cruciform beam-column assemblies with well-defined loading and boundary conditions.

3.5 Floor Diaphragms and Collectors

The typical diaphragm in steel moment frame building are composite steel deck with reinforced concrete fill (with steel reinforcing bars or welded-wire fabric reinforcement) and shear stud connectors to the steel beams. At the roof level, the diaphragm might be either composite or bare steel deck. Guidelines for modeling of floor diaphragms and collectors are covered in Section 3.6 of the *Part I Guidelines*.

3.6 Secondary Gravity Load-Carrying Systems

It is generally considered acceptable and conservative to ignore the strength and stiffness of gravity framing and to simply include the destabilizing geometric stiffness (P-Δ) effects of the gravity system in the nonlinear analysis. This can be accomplished by adding one or more pin-ended "gravity" or "leaning" columns, or alternatively, some software has built-in features for adding the geometric stiffness

effects of the entire gravity load. For buildings prone to torsion, it is important to capture the destabilizing twisting effect, either by locating gravity columns to represent the spatial distribution of gravity loading or through a torsional geometric stiffness term (analogous to a torsional mass moment of inertia).

Since typical composite gravity connections can develop considerable moment restraint, the gravity framing system may contribute significantly to the overall strength and stiffness of moment frame buildings. As such, it may be appropriate to include the gravity framing in the analysis model, especially where analyses are being performed to gage the full performance (as opposed to minimum safety) of the building. To do so, the gravity framing elements should be modeled as follows:

- **Beams.** Since the gravity framing connections are usually weaker than the connected beams, the beams can usually be modeled as elastic as either bare steel beams or composite beams. Guidance for considering composite stiffness is provided in Chapter 4.
- **Columns.** Under moderate levels of story drift (~0.02 radians), the gravity columns will probably remain elastic and can be modeled as such. However, for analysis to larger drifts, especially where there is a tendency for story mechanisms to form in the building, the columns should be modeled as inelastic. This is necessary even with partial strength connections, owing to the vertical continuity of the columns across multiple stories (where resistance can develop through back-stay type response). Provided that the gravity columns meet the moderately to highly ductile requirements of ANSI/AISC 341-16 their inelastic response can be modeled using the hinge models presented in Section 4.3 or the fiber-section models in Chapter 5. Otherwise, if columns may not have sufficient inelastic rotation capacity to be modeled with concentrated hinges (e.g., columns with slender sections), then their contribution to the lateral resistance should be ignored and their ability to sustain gravity loads under the induced drifts should be checked using continuum finite element analyses or other methods (e.g., test data or stability design equations).
- **Connections.** The connections should be modeled to represent their realistic moment-rotation response, which can be significant (i.e., on the order of 20% or more of the beam moment capacity), especially where composite action with the slab is considered. Guidelines for modeling the connections are provided in Section 4.4.

3.7 Modeling of Damping

Modeling recommendations for equivalent viscous damping are included in Section 3.7 of the *Part I Guidelines*.

Chapter 4

Concentrated Hinge Component Models

4.1 Overview of Concentrated Hinge Model

This chapter provides detailed guidance to determine properties of concentrated hinges for modeling steel beams, columns, and gravity system beam-to-column connections. As described in *Part I Guidelines*, Chapter 2, component hinge guidelines may be distinguished by the extent to which strength and stiffness degradation are represented in the computational model. Accordingly, backbone model criteria are provided for the monotonic and cyclic backbone curves. Where appropriate, criteria are also specified for critical limit states that are not captured in the model, but should be considered as either force or deformation limits in the analysis and design.

The guidelines in this chapter are geared toward the analysis of ductile moment frames that generally meet the ANSI/AISC 341-16, *Seismic Provisions for Structural Steel Buildings* (AISC, 2016c) seismic design criteria for members and connections in special moment frames. Thus, the modeling criteria are for members whose inelastic response occurs primarily in plastic hinge regions of beams, along with some hinging in columns and yielding of panel zones. This also implies that the steel beams are adequately laterally-braced and highly (or moderately) ductile, with seismic conforming beam-to-column connections that are not prone to premature fracture. Appendix A provides guidance for modeling "pre-Northridge" type moment frames that meet many of the criteria for modern steel special moment frames, but are prone to premature fracture in welded beam-to-column and column splice connections. While the general concepts in this chapter and Appendix A can apply to other types of moment frames, such frames might have other degradation modes due to phenomena such as excessive local buckling or lateral-torsional instabilities that are not addressed in the models provided in this chapter or Appendix A.

4.2 Beam Hinge Model

This section provides guidelines for characterizing the nonlinear concentrated hinge properties for steel beams based on the generalized moment versus hinge rotation response shown in Figure 4-1. The recommended modeling parameter equations throughout this section originated from ATC-72-1, *Modeling and Acceptance*

Criteria for Seismic Design and Analysis of Tall Buildings (PEER/ATC, 2010; Lignos and Krawinkler, 2011) with updates based on more recent research (NIST, 2017b; Hartloper and Lignos, 2016). Equations are provided for both reduced beam section (RBS) and non-RBS beam hinges, based on physical test data for beams with depths up to 36 inches. These equations reflect test data for laterally-braced beam components where local-buckling causes initial deterioration and the final failure mode is cyclic fracture at θ^*_{ult}. The model parameters beyond this point (e.g., the monotonic backbone curve out to θ_{pc} in Figure 4-1) are shown dashed since they are primarily intended to define the slope of equations up to the ultimate point. The parameters are statistically calibrated to median values and the variability in these parameters is described in terms of a dispersion equal to the standard deviation of parameters in natural log space, σ_{ln}, which is similar to a coefficient of variation.

As discussed in *Part I Guidelines*, use of the monotonic backbone curve parameters should be limited to nonlinear dynamic analyses where the component models degrade under cyclic loading. The model by Ibarra et al. (2005) is an example of one such model that has been applied to steel moment frames. Otherwise, in cases where the model parameters do not cyclically degrade, or for nonlinear static (pushover) analyses, the first-cycle envelope parameters should be used. The first-cycle envelope parameters presented in this chapter incorporate the latest test data for seismically conforming steel moment frame members, and as such, are generally recommended instead of the component response parameters in ASCE/SEI 41-17, *Seismic Evaluation and Retrofit of Existing Buildings* (ASCE, 2017b). For seismically non-conforming frames, the values from ASCE 41-17 are more appropriate.

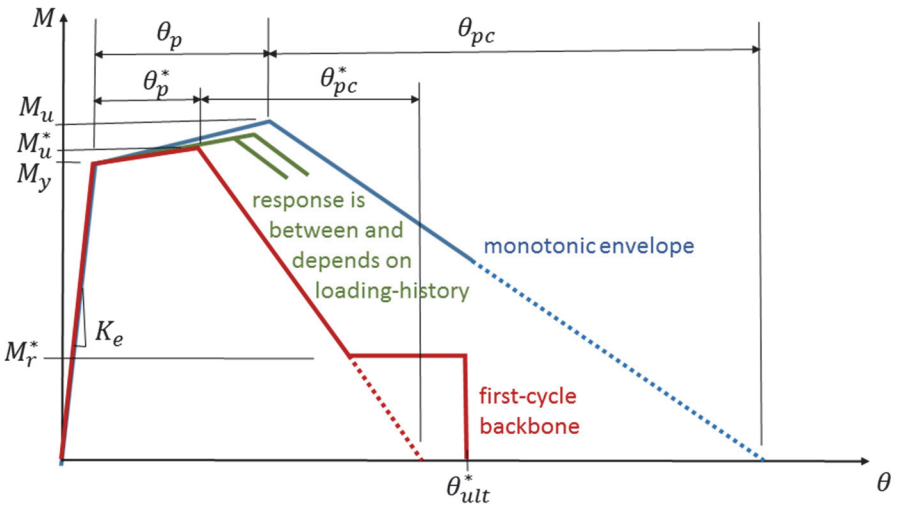

Figure 4-1 Idealized monotonic and cyclic backbone curves for steel beams. Adapted from from Figure 2-5 in *Part I Guidelines* (NIST, 2017a).

Note that the hinge properties are defined based on moments and rotations occurring in the hinge itself. Option 3 shown in Figure 4-2 is the most explicit model as it includes a panel zone (including both finite connection geometry and panel zone flexibility) and the offset between the column face and center of the beam hinge. Other common modeling approaches, shown in Figure 4-2, are Option 1, where centerline dimensions are used, and Option 2, where the finite connection geometry is considered, but other offsets are ignored. The significance of these differences will depend on the difference in effective span lengths of the beam models. For example, in a frame with 30 foot bays, W14 columns and W30 beams, the ratio in effective spans between Option 1 and 3 would be about 0.9 and could probably be ignored. On the other hand, in a frame with 20 foot bays, W27 columns and W30 beams with an RBS connection, the ratio in effective spans would be about 0.8, which is more significant. Ignoring the offsets in assigning hinge properties (e.g., in Option 1 versus Option 3) will tend to underestimate the beam strengths and, for a given drift demand, underestimate the beam hinge rotations. In addition, ignoring the offsets will tend to underestimate the frame stiffness.

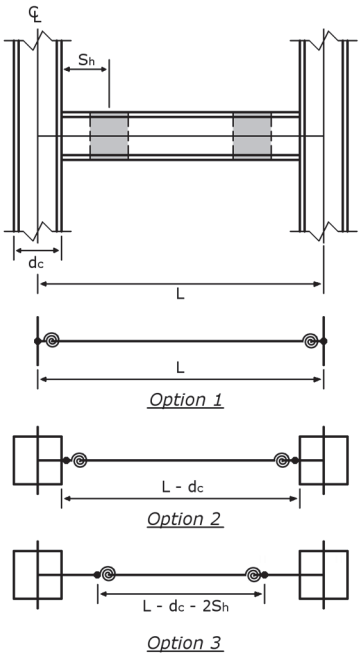

Figure 4-2 Geometric offsets in concentrated hinge models.

For the purpose of defining hinge properties, discrepancies in the dimensional offsets can be accounted for approximately by a linear adjustment based on the ratio of the beam length in the model (L_{model}) to the actual length between hinges in the building (Option 3 in Figure 4-2):

$$L_{ratio} = L_{model} / (L - d_c - 2s_h) \quad (4\text{-}1)$$

The properties assigned to the model can be adjusted from the properties provided later in this section as follows:

$(M_y, M_{max}, M_r)_{model} = (L_{ratio})(M_y, M_{max}, M_r)$

= beam moment strengths

$(\theta_p, \theta_{pc}, \theta_{ult}^*)_{model} = (1/L_{ratio})(\theta_p, \theta_{pc}, \theta_u^*)$

= beam rotation parameters

4.2.1 Monotonic Backbone

The key modeling parameters of the idealized monotonic backbone curve (Figure 4-1) are defined below (based on NIST, 2017b; Hartloper and Lignos, 2016).

Yield Moment (M_y). For practical modeling purposes, the yield moment is not distinguished between monotonic and cyclic loading, and the yield moment is increased (by the factor β) above the expected plastic beam moment, $M_{p,exp}$, to account for a moderate amount of cyclic strain hardening. The effective yield moment is given as:

$$M_y = \beta M_{p,exp} = \beta Z R_y F_y \qquad \text{(COV = 0.1)} \qquad (4\text{-}2)$$

where R_y provides the adjustment from nominal to expected steel yield strength. For standard beam connections, β=1.2, and for reduced beam section (RBS) connections, β=1.1. Further, for RBS beams, $M_{p,exp}$ should be evaluated based on the plastic section modulus of the reduced section, Z_{RBS}. Equation 4-2 also indicates the coefficient of variation (COV) on the effective yield moment. The COV is generally reported throughout this chapter for other parameters.

Peak Moment (M_u). The peak moment strength is increased 10% above the yield moment to account for additional strain hardening beyond yield, given as:

$$M_u = 1.1 M_y \qquad \text{(COV = 0.1)} \qquad (4\text{-}3)$$

Elastic Stiffness (K_e). The beam hinge may be modeled as rigid-plastic where the hinge is modeled with a finite, but large elastic stiffness. Where the zero-length hinge is modeled with a finite elastic stiffness, it is recommended to make the initial hinge stiffness, K_e, large relative to the entire beam. This can be expressed as:

$$K_e = \alpha_e EI/L \qquad (4\text{-}4)$$

where EI and L are the cross section stiffness and length of the beam, and α_e is the stiffness coefficient. It is suggested to make the hinge stiffness about 10 times the stiffness of the beam in reverse curvature (i.e., $6EI/L$), in which case α_e should be set to 60. The stiffness of the elastic beam connected to the hinges should then be increased to account for the flexibility of the hinge. Assuming the characteristic beam stiffness is the moment-rotation response in reverse curvature, the effective beam stiffness, EI^*, is as follows:

$$EI^* = EI/(1–6/\alpha_e) = 1.1EI \text{ for } \alpha_e = 60 \qquad (4\text{-}5)$$

Pre-Peak Rotation (θ_p). The pre-peak plastic rotation, θ_p (radians), may be determined as follows:

for standard (non-RBS) beams:

$$\theta_p = 0.07\left(\frac{h}{t_w}\right)^{-0.3}\left(\frac{b_f}{2t_f}\right)^{-0.1}\left(\frac{L}{d}\right)^{0.3}\left(\frac{d}{21"}\right)^{-0.7} \qquad \text{(COV = 0.3)} \qquad \text{(4-6a)}$$

for RBS beams:

$$\theta_p = 0.09\left(\frac{h}{t_w}\right)^{-0.3}\left(\frac{b_f}{2t_f}\right)^{-0.1}\left(\frac{L}{d}\right)^{0.1}\left(\frac{d}{21"}\right)^{-0.8} \qquad \text{(COV = 0.3)} \qquad \text{(4-6b)}$$

where h/t_w is the web depth-to-thickness ratio, $b_f/2t_f$ is the flange width-to-thickness ratio, L/d is the clear span-to-depth ratio, and d is the section depth in inches. These section parameters should be based on the full cross section for both standard and RBS beams.

Post-Peak Rotation (θ_{pc}). The post-peak plastic rotation, θ_{pc} (radians), may be determined as follows:

for standard (non-RBS) beams:

$$\theta_{pc} = 4.6\left(\frac{h}{t_w}\right)^{-0.5}\left(\frac{b_f}{2t_f}\right)^{-0.8}\left(\frac{d}{21"}\right)^{-0.3} \qquad \text{(COV = 0.3)} \qquad \text{(4-7a)}$$

for RBS beams:

$$\theta_{pc} = 6.5\left(\frac{h}{t_w}\right)^{-0.5}\left(\frac{b_f}{2t_f}\right)^{-0.9} \qquad \text{(COV = 0.3)} \qquad \text{(4-7b)}$$

Residual Strength (M_r). The residual strength for both standard and RBS beams may be assumed as $M_r = 0.4\ M_y$ (Equation 4-2), although, as a practical matter the rotations are usually limited by other criteria before this limit is reached.

4.2.2 Cyclic Envelope

When cyclic deterioration is not explicitly captured in the beam component hinge model, the model should be based on the cyclic envelope (see Figure 4-1), whose parameters are defined using statistics of the first-cycle envelope curves from cyclic tests (NIST, 2017b; Hartloper and Lignos, 2016). The parameters for the cyclic backbone curve are defined as described below.

Effective Yield Strength and Elastic Stiffness (M_y and K_e). These parameters are the same as defined previously in Section 4.2.1 for the monotonic backbone curve.

Peak Moment (M_u^*). The peak strength increases above the effective yield moment due to cyclic hardening to the following:

$$M_u^* = 1.15 M_y \qquad \text{(COV = 0.1)} \qquad (4\text{-}8)$$

where M_y is calculated from Eq. 4-2. Note that compared to the ratio for monotonic loading (Equation 4-3), the multiplier on M_y is larger under cyclic loading to account for cyclic strain hardening effects.

Pre-Peak Rotation (θ_p^*). The cyclic pre-peak plastic rotation, θ_p^* (radians), may be determined as follows:

for standard (non-RBS) beams:

$$\theta_p^* = 0.3\left(\frac{h}{t_w}\right)^{-0.3}\left(\frac{b_f}{2t_f}\right)^{-1.7}\left(\frac{L_b}{r_y}\right)^{-0.2}\left(\frac{L}{d}\right)^{1.1} \qquad \text{(COV = 0.34)} \qquad (4\text{-}9a)$$

for RBS beams:

$$\theta_p^* = 0.55\left(\frac{h}{t_w}\right)^{-0.5}\left(\frac{b_f}{2t_f}\right)^{-0.7}\left(\frac{L_b}{r_y}\right)^{-0.5}\left(\frac{L}{d}\right)^{0.8} \qquad \text{(COV = 0.42)} \qquad (4\text{-}9b)$$

where L_b/r_y is the laterally unbraced length divided by the weak-axis radius of gyration.

Post-Peak Rotation (θ_{pc}^*). The cyclic pre-peak plastic rotation, θ_{pc}^* (radians), may be determined as follows:

for standard (non-RBS) beam:

$$\theta_{pc}^* = 24.0\left(\frac{h}{t_w}\right)^{-0.9}\left(\frac{b_f}{2t_f}\right)^{-0.2}\left(\frac{L_b}{r_y}\right)^{-0.5} \qquad \text{(COV = 0.45)} \qquad (4\text{-}10a)$$

for RBS beams:

$$\theta_{pc}^* = 20.0\left(\frac{h}{t_w}\right)^{-0.8}\left(\frac{b_f}{2t_f}\right)^{-0.1}\left(\frac{L_b}{r_y}\right)^{-0.6} \qquad \text{(COV = 0.31)} \qquad (4\text{-}10b)$$

Residual Strength (M_r^*). The cyclic residual strength for both RBS and non-RBS beams may be assumed as $M_r^* = 0.3\ M_y$ (Equation 4-2).

Ultimate Rotation (θ_{ult}^*). The ultimate plastic rotation capacity is likely to be controlled by ductile fracture. Based on available cyclic test data, the ultimate rotation under cyclic loading is equal to $\theta_{ult}^* = 0.08$ (radians) with a COV = 0.3.

Limitations on Use of Equations. Based on the available data used in the calibration, the suggested range of applicability of the above equations is as follows:

$$20 \le h/t_w \le 55$$

$$4 \le b_f/2t_f \le 8$$

$$20 \le L_b/r_y \le 65$$

$$2.5 \le L/d \le 7$$

$$4 \le d \le 36 \text{ for standard beams; } 21 \le d \le 36 \text{ for RBS beams}$$

4.2.3 Beam Hinge – Illustrative Examples

Shown in Figure 4-3 are examples of the hinge parameters for two steel sections. The W27×147 is a stocky section with relatively low $b/2t_f$ and h/t_w and the W30×108 has a less stocky section. Parameters from the proposed models are contrasted with the corresponding criteria from ASCE/SEI 41-13, *Seismic Evaluation and Retrofit of Existing Buildings* (ASCE, 2014). Collapse analysis studies by Lignos and Krawinkler (2012) have generally shown that frames will begin to become unstable before the plastic hinges reach the ductile fracture rotations, and thus the most influential aspects of the hinge response are the plastic rotation up to unloading, θ_p, and the descending slope of the post-peak response. They also note how the slope of the post-peak descending branch will significantly influence the onset of ratcheting drift response. In both of these respects, the models recommended in this *Guidelines* document, which have been calibrated to a large database of steel beam-column subassembly tests, should be more realistic than the ASCE/SEI 41-13 models for moderately and highly ductile members (NIST, 2017b; Hartloper and Lignos, 2016). Note that in both examples shown in Figure 4-3, the rotation limit for ductile fracture under cyclic loading generally limits the post-peak response to values below the point where the residual strength parameter is important.

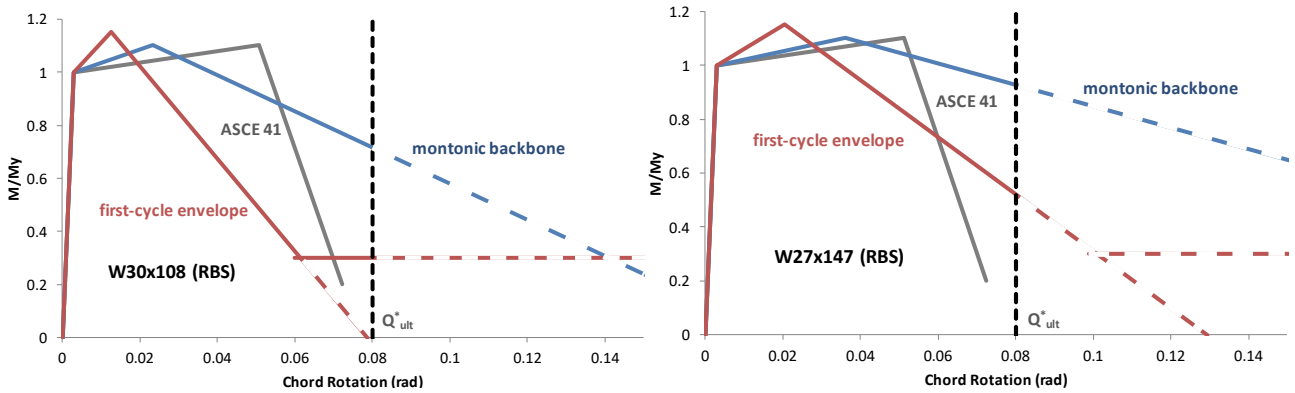

Figure 4-3 Comparison of monotonic and cyclic backbone curves and ASCE/SEI 41-13 curves for two steel sections.

4.2.4 Limiting Deformations

In models that do not capture in-cycle strength degradation (i.e., as represented by the descending post-peak portion of the backbone curves), the calculated nonlinear response should be limited to the deformation at which inelastic loss in stiffness and strength will initiate large drifts and ratcheting response. In such cases, it is recommended to limit response to a maximum deformation limit determined by the rotation along the first-cyclic envelope curve at a resistance equal to 80% of the maximum strength, M_u^*. Using the strength and rotation values mentioned previously, the plastic rotation limit is as follows:

$$\theta_{limit} = \theta_p^* + 0.2\theta_{pc}^* \tag{4-11}$$

If this approach is used, the rotation limit can be incorporated in the nonlinear hinge model, or can be checked in the post-processing of the analysis. Where any component exceeds the failure deformation, then the response would need to be classified as an unacceptable response, since it is beyond the range of the modeling capability. As shown in Figure 4-4, the inability of the model to simulate post-peak degradation would generally limit the rotation demand to a significantly smaller value than might otherwise be considered acceptable (i.e., comparing the limit in Figure 4-4 to the previous plot for the W27×147 beam in Figure 4-3).

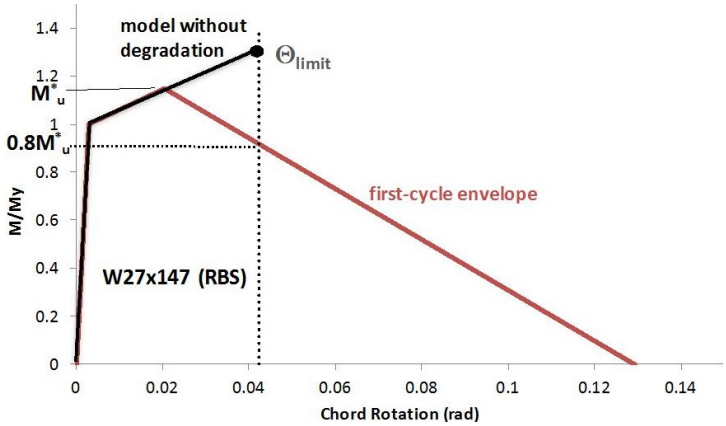

Figure 4-4 Rotation limit imposed where using models that do not simulate degradation for rotations beyond θ_p^* (corresponding to M_u^*).

4.2.5 Composite Beam Effect

Where beams are connected to composite floor slabs with sufficient shear studs to provide significant composite action, the component modeling approach should be modified to account for the presence of the slab. As shown in Figure 4-5, the modifications involve increasing the beam: (1) stiffness; (2) strengths in positive and negative bending; and (3) rotation parameters for positive bending (slab in compression). These changes would transfer to the cyclic backbone curve in the

same proportions as given in Section 4.2.2. The modifications outlined below will have a greater effect on smaller beam sizes, relative to the ratio of slab depth to steel beam depth.

Effective Slab Width (b_{eff}). For the purposes of adjusting the beam strength and stiffness for lateral load resistance, the effective slab width for positive bending (slab in compression), b_{eff}, can be taken as the sum of contributions from each side of the beam, each of which is limited to the minimum widths given by ANSI/AISC 360-16, *Specification for Structural Steel Buildings* (AISC, 2016d) (i.e., $^1/_8$ of the beam span, one-half the distance to the centerline of the adjacent girder, or distance to the edge of the slab). If there is significant reinforcement in the slab, which is anchored at or past the connected column, the negative bending strength can likewise be adjusted to account for tension resisted by the slab reinforcing steel within b_{eff}. The additional strength provided by the slab or slab reinforcement should not exceed the: (1) the maximum compression or tension forces in the slab that that can be transferred by shear studs over the beam shear span (between the point of inflection and the maximum moment); and (2) the maximum slab force that can be transferred through bearing into the steel column. Shown in Figure 4-6 is a schematic diagram of how the forces in the composite slab are transferred into the steel column through localized bearing. Based on this mechanism, it is recommended to limit the maximum axial force resultant in the slab due to moment transfer into the column to $3f_c'b_f t_s$, where f_c' is the nominal compression strength of the slab concrete, b_{fc} is the steel column flange width, and t_s is the thickness of the concrete slab in the portion bearing against the column. The factor of 3 accounts for: (1) transfer of bearing into both column flanges; and (2) confinement to the localized concrete bearing region against the column.

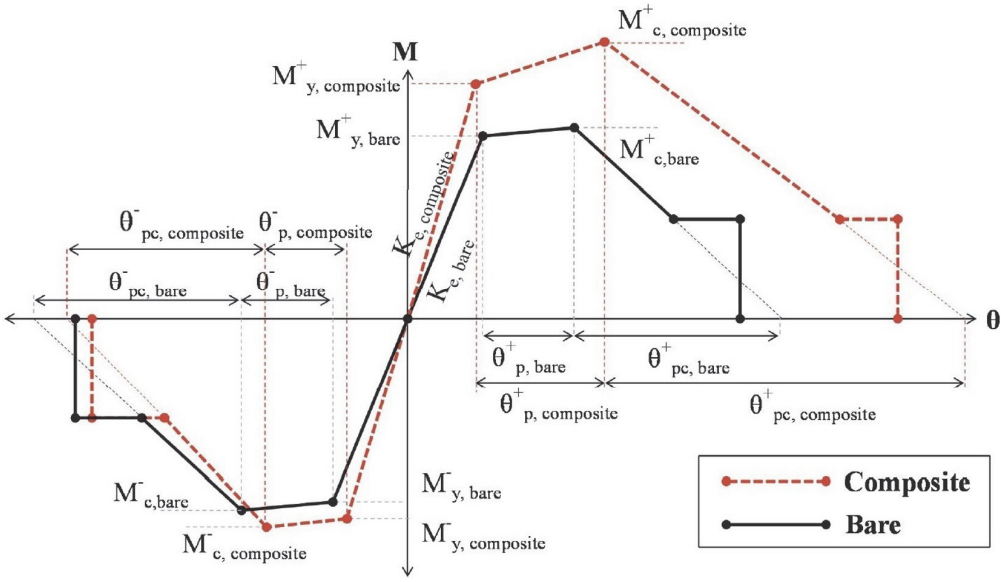

Figure 4-5 Adjustments to monotonic backbone curve to account for composite beam action (Elkady and Lignos, 2014).

Effective Stiffness (EI_{eff}). To account for composite action, it is recommended to use an effective beam stiffness that is the average of the bare steel beam and the composite beam stiffness, (i.e., $EI_{eff} = ½(EI_{steel} + EI_{comp})$, where EI_{comp} can be calculated for the transformed section, using the effective slab width). Based on tests of W36 beams with composite slabs (~3-inch slabs on 3-inch deck) all obtained from interior beam-to-column connection subassemblies (Elkady and Lignos, 2014; NIST, 2017b) have reported the effective stiffness to be about 1.4 times the stiffness of the bare steel beam. This 1.4 times increase, as measured by isolated connection subassemblies, is likely to be a lower bound on the stiffness in building frames with continuity between framing bays.

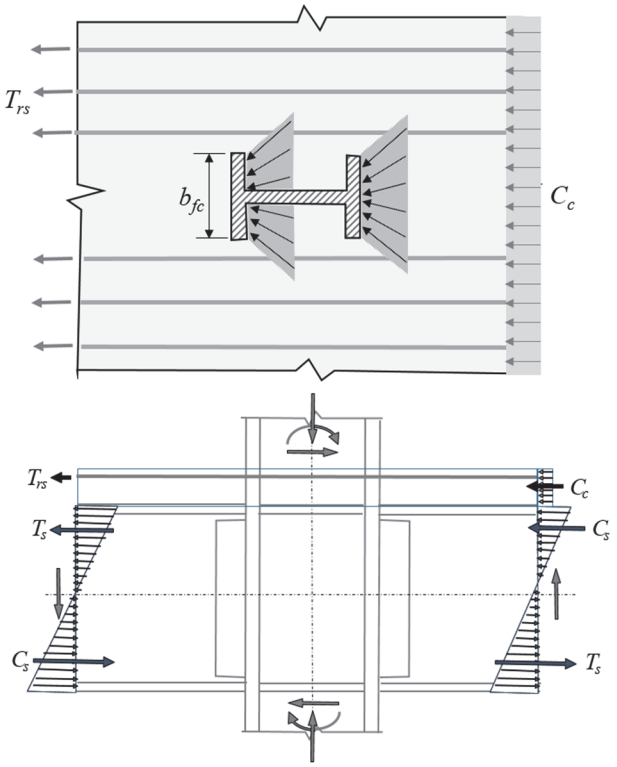

Figure 4-6 Local transfer of longitudinal stresses resisted by floor slab into the steel column.

Composite Yield Moment (M_c). Provided that sufficient shear studs are provided to generate significant composite action, the beam hinge yield strengths in positive and negative bending can be calculated using Equation 4-2, except where the $M_{p,exp}$ is calculated with composite beam action, using the effective slab width defined above, taking account of concrete in compression and slab reinforcement in tension.

Peak Moment (M_c). The peak moment, M_c, can then be calculated using the composite M_y values in Equations 4-3 or 4-8. For the loading direction with the slab in compression, based on tests of W6 beams with composite slabs (~3-inch slabs on 3-inch deck), Elkady and Lignos (2014) and NIST (2017b) have reported the peak moment M_c^+ to be about 1.3 times the moment strength of the bare steel beam.

Pre-Peak Plastic Rotation (θ_p or θ_p^*). For positive bending (slab in compression), the pre-peak rotation parameters, θ_p or θ_p^*, calculated by Equations 4-6 or 4-9 for either standard or RBS beams can be increased by a factor of 1.8 to account for the stabilizing effect of the floor slab (NIST, 2017b).

Post-Peak Plastic Rotation (θ_{pc} or θ_{pc}^*). For positive bending (slab in compression), the post-peak rotation parameters, θ_{pc} or θ_{pc}^*, calculated by Equations 4-7 or 4-10 for either standard or RBS beams can be increased by a factor of 1.35 to account for the stabilizing effect of the floor slab (NIST, 2017b).

Other parameters for composite beams (rotation parameters in negative bending and residual strengths) are essentially the same as those for non-composite beams.

4.3 Column Hinge Model

This section provides guidelines characterizing the nonlinear concentrated hinge properties for steel columns (i.e., beam-columns) that generally conform to the ANSI/AISC 341-16 seismic design criteria for columns that are classified as moderately and highly ductile. The recommended modeling parameter equations are based on test data for wide flange steel columns ranging in size from W8 to W36 and for HSS columns (Suzuki and Lignos, 2015; Elkady and Lignos, 2015, 2016; Ozkula et al., 2017). These equations reflect test data for columns with axial load and lateral drift where local flange and web buckling and sometimes lateral-torsional buckling cause deterioration.

The following guidelines for columns are described in terms of uniaxial bending. Based on data from tests of several W24 wide flange columns under biaxial bending, the proposed modeling recommendations for nonlinear modeling of beam-columns subjected to unidirectional loading may be used to assess the nonlinear behavior of wide-flange beam-columns subjected to bidirectional lateral loading (NIST, 2017b).

4.3.1 Monotonic Backbone – Wide Flange Columns

The key modeling parameters of the idealized monotonic backbone curve shown in Figure 4-1 are defined as described below.

Elastic Flexural Stiffness. The column hinge may be modeled with a finite elastic flexural stiffness or as rigid-plastic using similar provisions as recommended in Section 4.2.1 for beams.

Yield Moment (M_y^*). For a steel column this quantity refers to its effective flexural yield strength $M_{y,p}$ reduced by the applied compressive axial load. The effective flexural yield moment strength, accounting for some cyclic hardening, is computed as follows:

$$\text{If } P_g/P_{ye} \le 0.20, \quad M_y^* = 1.15 Z R_y F_y \left(1 - P_g/P_{ye}\right)$$
$$\text{If } P_g/P_{ye} > 0.20, \quad M_y^* = 1.15 Z R_y F_y \left[\frac{9}{8}\left(1 - P_g/P_{ye}\right)\right] \qquad \text{(COV = 0.10)} \qquad \text{(4-12)}$$

where P_g is the axial compression force due to gravity loads, P_{ye} is the expected yield strength of the column (= $R_y F_y A$), and the other terms are as defined previously. The 1.15 factor accounts for the effects of cyclic hardening.

Peak Moment (M_p). The peak flexural strength of the column can be determined as a multiple of the effective yield moment (Equation 4-12) to account for additional strain hardening at larger deformations, based on the following:

$$M_p = a\, M_y^* \qquad \text{(4-13)}$$

This coefficient a depends on the web local slenderness, h/t_w, and global slenderness of the member, L_b/r_y (L_b is the unbraced length of the column; r_y is the radius of gyration of the column cross-section with respect to the weak-axis), and the applied axial load ratio, P_g/P_{ye}, as follows:

$$a = 12.5\left(\frac{h}{t_w}\right)^{-0.2}\left(\frac{L_b}{r_y}\right)^{-0.4}\left(1 - \frac{P_g}{P_{ye}}\right)^{0.4} \ge 1.0 \text{ and } < 1.3 \qquad \text{(COV = 0.10)} \qquad \text{(4-14)}$$

Pre-Peak Plastic Rotation. The pre-peak plastic rotation, θ_p (radians), may be determined as follows:

$$\theta_p = 294\left(\frac{h}{t_w}\right)^{-1.7}\left(\frac{L_b}{r_y}\right)^{-0.7}\left(1 - \frac{P_g}{P_{ye}}\right)^{1.6} \le 0.20 \qquad \text{(COV = 0.39)} \qquad \text{(4-15)}$$

Post-Peak Plastic Rotation. The pre-peak plastic rotation, θ_{pc} (radians), may be determined as follows:

$$\theta_{pc} = 90\left(\frac{h}{t_w}\right)^{-0.8}\left(\frac{L_b}{r_y}\right)^{-0.8}\left(1 - \frac{P_g}{P_{ye}}\right)^{2.5} \le 0.30 \qquad \text{(COV = 0.14)} \qquad \text{(4-16)}$$

Residual Strength. The residual flexural strength, M_r, may be determined as:

$$M_r = \left(0.5 - 0.4\frac{P_g}{P_{ye}}\right) M_y^* \qquad \text{(COV = 0.27)} \qquad \text{(4-17)}$$

Limitations on Use of Equations. Equations 4-13 to 4-17 were derived for members of Grade 50 steel based on the following range of parameters (Elkady and Lignos 2014; NIST, 2017b):

$$3.71 \le h/t_w \le 57.5$$

$$1.82 \le b_f/2t_f \le 8.52$$

$$38.4 \le L_b/r_y \le 120$$

$$0 \le P_g/P_{ye} \le 0.75$$

Steel wide flange beam-columns under compressive axial load ratios $P_g/P_{ye} > 0.6$ that have $h/t_w > 43$ and $KL/r_y > 120$ should be treated as force-controlled elements per ASCE/SEI 41-17. Steel beam-columns that utilize stocky cross-sections with gravity load ratios $P_g/P_{ye} > 0.6$ have a finite plastic deformation capacity. However, beam-columns with gravity loads over $0.6P_{ye}$ may become unstable after hinging, and it is suggested to limit column yielding in such cases (Bech et al., 2016).

4.3.2 Cyclic Backbone Curve – Wide Flange Columns

When cyclic deterioration is not explicitly included in the analytical model, the modeling parameters for columns need to be modified to account for cyclic deterioration effects in a similar way as is done for beams. The parameters for the cyclic backbone curve are defined as described below.

Effective Yield Moment and Elastic Stiffness (M_y and K_e). These parameters are the same as defined previously in Section 4.2.1 for the monotonic backbone curve.

Peak Moment (M_u^*). The peak moment strength for beam-columns under cyclic loading increases above the effective yield moment due to cyclic hardening, which may be taken as:

$$M_u^* = a^* M_y \tag{4-18}$$

where a^* is determined as:

$$a^* = 9.5\left(\frac{h}{t_w}\right)^{-0.4}\left(\frac{L_b}{r_y}\right)^{-0.16}\left(1-\frac{P_g}{P_{ye}}\right)^{0.2} \ge 1.0 \text{ and } < 1.3 \qquad \text{(COV = 0.07)} \tag{4-19}$$

Pre-Peak Rotation (θ_p^*). The pre-peak plastic rotation, θ_p^*, for beam-columns under cyclic loading may be taken as:

$$\theta_p^* = 15\left(\frac{h}{t_w}\right)^{-1.6}\left(\frac{L_b}{r_y}\right)^{-0.3}\left(1-\frac{P_g}{P_{ye}}\right)^{2.3} \le 0.10 \qquad \text{(COV = 0.31)} \tag{4-20}$$

Post-Peak Plastic Rotation (θ^*_{pc}). The post-peak plastic rotation, θ^*_{pc} for beam-columns under cyclic loading may be taken as:

$$\theta^*_{pc} = 14\left(\frac{h}{t_w}\right)^{-0.8}\left(\frac{L_b}{r_y}\right)^{-0.5}\left(1-\frac{P_g}{P_{ye}}\right)^{3.2} \le 0.10 \qquad \text{(COV = 0.40)} \qquad (4\text{-}21)$$

Residual Moment (M^*_r). The residual flexural strength, M^*_r, under cyclic loading may be taken as:

$$M^*_r = \left(0.4 - 0.4\frac{P_g}{P_{ye}}\right)M^*_y \qquad \text{(COV = 0.35)} \qquad (4\text{-}22)$$

Ultimate Rotation, (θ^*_{ult}). For steel beam-columns with flexural hinging, the ultimate rotation capacity is likely to be controlled by loss of the column axial carrying capacity. It is recommended to assume that:

$$\theta^*_{ult} = 0.08\left(1 - 0.6\frac{P_g}{P_{ye}}\right) \qquad \text{(COV = 0.51)} \qquad (4\text{-}23)$$

4.3.3 Monotonic Backbone – Square HSS Columns

For square HSS columns, the elastic stiffness and yield moments can be determined using the same equations as for W-shape columns. Other parameters of the monotonic backbone curve are defined as outline below, based on evaluation of HSS beam-column tests (Lignos and Krawinkler, 2010, 2012).

Peak Moment. The peak flexural strength of the HSS beam-column can be determined using Equation 4-13, but with the following hardening ratio:

$$a = 0.04\left(\frac{D}{t}\right)^{-0.3}\left(1-\frac{P_g}{P_{ye}}\right)^{1.3}\left(\frac{E}{F_{ye}}\right)^{0.75} \ge 1.0 \text{ and} < 1.3 \qquad \text{(COV = 0.23)} \qquad (4\text{-}24)$$

where D is the width and t is the thickness of the HSS cross section.

Pre-Peak Plastic Rotation. The pre-peak plastic rotation, θ_p, for HSS columns may be taken as:

$$\theta_p = 0.3\left(\frac{D}{t}\right)^{-0.95}\left(1-\frac{P_g}{P_{ye}}\right)^{1.1}\left(\frac{E}{F_{ye}}\right)^{0.1} \qquad \text{(COV = 0.26)} \qquad (4\text{-}25)$$

Post-Peak Plastic Rotation. The post-peak plastic rotation, θ_{pc}, for HSS columns may be taken as:

$$\theta_{pc} = 5.4\left(\frac{D}{t}\right)^{-1.2}\left(1-\frac{P_g}{P_{ye}}\right)^{3.0}\left(\frac{E}{F_{ye}}\right)^{0.14} \qquad \text{(COV = 0.35)} \qquad (4\text{-}26)$$

Residual Moment. The residual flexural strength, M_r, for HSS columns may be taken as:

$$M_r = \left(0.5 - 0.6\frac{P_g}{P_{ye}}\right) M_y^* \geq 0 \qquad \text{(COV = 0.34)} \qquad (4\text{-}27)$$

4.3.4 Cyclic Skeleton – Square HSS Columns

When cyclic deterioration is not explicitly included in the analytical model, the parameters for the cyclic backbone curve of square HSS columns are defined as described below.

Effective Yield Moment, Fully Plastic Moment and Elastic Stiffness (M_y^*, M_p^* and K_e). Same as defined previously for the monotonic backbone curve.

Pre-Peak Plastic Rotation. The pre-peak plastic rotation, θ_p^*, of HSS columns may be taken as:

$$\theta_p^* = 0.1\left(\frac{D}{t}\right)^{-1.1}\left(1 - \frac{P_g}{P_{ye}}\right)^{1.4}\left(\frac{E}{F_{ye}}\right)^{0.3} \qquad \text{(COV = 0.53)} \qquad (4\text{-}28)$$

Post-Peak Plastic Rotation (θ_{pc}^*). The post-peak plastic rotation, θ_{pc}^*, of HSS columns may be taken as:

$$\theta_{pc}^* = 2.8\left(\frac{D}{t}\right)^{-1.3}\left(1 - \frac{P_g}{P_{ye}}\right)^{2.6}\left(\frac{E}{F_{ye}}\right)^{0.17} \qquad \text{(COV = 0.27)} \qquad (4\text{-}29)$$

Residual Strength. The residual flexural strength, M_r^* may be taken as:

$$M_r^* = \left(0.4 - 0.6\frac{P_g}{P_{ye}}\right) M_y^* \geq 0 \qquad \text{(COV = 0.40)} \qquad (4\text{-}30)$$

Ultimate Rotation, θ_{ult}^* . The ultimate rotation capacity that the column losses its axial carrying capacity is recommended to be:

$$\theta_{ult}^* = 0.08\left(1 - \frac{P_g}{P_{ye}}\right) \qquad \text{(COV = 0.50)} \qquad (4\text{-}31)$$

Limitations on Use of Equations. The range of applicability of the above equations for HSS steel beam-columns is indicated as follows:

$$20 \leq D/t \leq 40$$

$$0 \leq P_g/P_{ye} \leq 0.60$$

$$40 \text{ ksi} \leq F_y \leq 72.5 \text{ ksi}$$

Hollow structural steel beam-columns under compressive axial load ratios, $P_g/P_{ye} >$ 0.60 must be treated as force-controlled elements per ASCE/SEI 41-17.

4.4 Composite Gravity Beam-Column Connection

Shown in Figure 4-7 is a standard shear plate connection, which can provide significant rotational restraint, particularly when it acts compositely with the concrete floor slab. Figure 4-8 shows a cyclic envelope response curve for a composite connection, where the lower left quadrant represents negative bending (top beam flange is in tension) and the upper right quadrant represents positive bending in a composite section. Where a slab is not present, both positive and negative bending would have the properties shown in the lower left quadrant.

The response shown in Figure 4-8 is for a ductile connection, whose governing failure modes must be evaluated as part of the connection model development. Table 4-1 lists possible shear and tension ductile and non-ductile failure modes for the composite gravity connection. To evaluate the governing failure mode, the shear tab is discretized at each bolt location based on bolt spacing and edge distances as shown in Figure 4-9. The discretized segments are called equivalent bolt elements. The shear and tension capacity of an equivalent bolt element is compared to the bolt and weld fracture capacity to establish which failure mode will govern in the loading directions parallel and perpendicular to the beam. The lowest capacity governs connection capacity and expected connection behavior and is referred to as $F_{\parallel\, equiv\, bolt\, cap}$ for shear and $F_{\perp\, equiv\, bolt\, cap}$ for tension. These capacities should be evaluated using the strength equations of ANSI/AISC 360-16, where the expected material strengths are used instead of nominal material strengths and the resistance factors are set to unity. Provided that the non-ductile modes do not govern, then the connection is assumed to be ductile and can be represented by the cyclic backbone curve of Figure 4-8. The rotation values shown in Figure 4-8 and the associated moments, determined by modeling equations presented later in this section, are based on research by Liu and Astaneh-Asl (2000a, 2004).

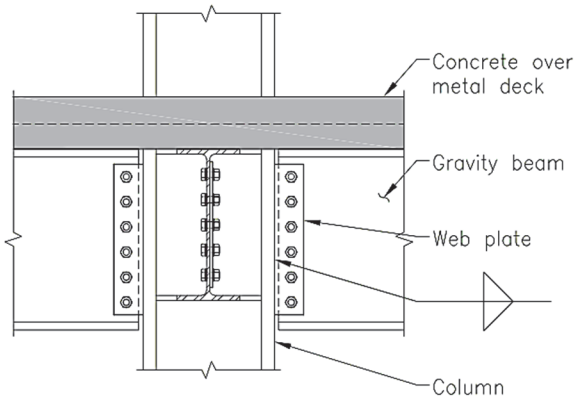

Figure 4-7 Composite gravity framing connection (Liu and Astaneh-Asl, 2000b).

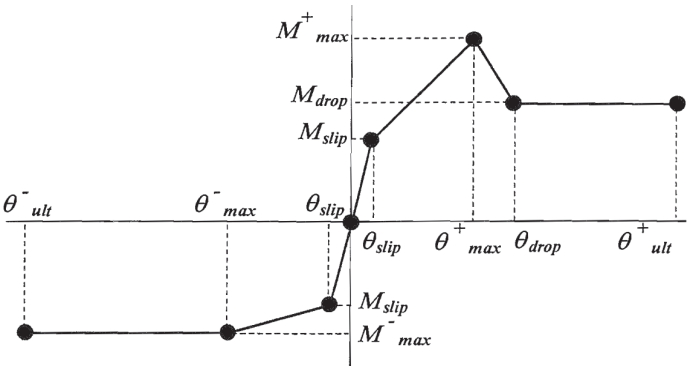

θ_{slip} = 0.0042 rad

θ^+_{max} = 0.03 rad, composite slab
= 0.05 bare steel

θ^-_{max} = 0.02 rad, composite slab
= 0.05 bare steel

θ^+_{drop} = 0.04 rad, composite slab
$\theta_{ult} = g/d_f$; where g = gap between beam and column and d_f = distance from CG of shear tab or bolt group to furthest beam flange

Figure 4-8 Cyclic skeleton curve for composite gravity framing connections (Liu and Astaneh-Asl, 2004).

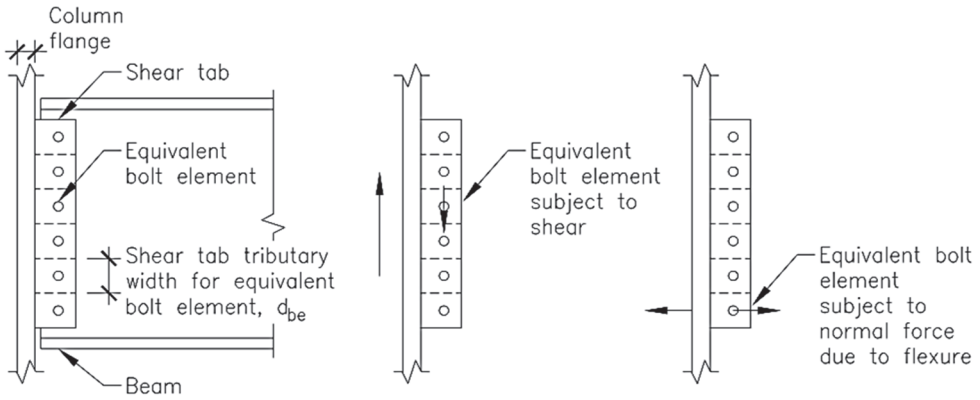

Figure 4-9 Equivalent bolt elements in shear tab connections (Liu and Astaneh-Asl, 2000b).

Table 4-1 Ductile and Brittle Failure Modes in Composite Gravity Connection

Ductile	Non-Ductile (Brittle)
Gross yielding of shear tab	Net section fracture of shear tab
Gross yielding of beam web	Net section fracture of beam web
Bolt bearing at bolt holes	Bolt fracture
Concrete floor slab crushing	Weld fracture

4.4.1 Positive Moment Capacity

As illustrated by the idealized force distribution in Figure 4-10, the positive moment capacity, M^+_{max}, can be determined by multiplying the tension resistance of bolts on the lower portion of the shear tab by an effective moment arm with compression in the slab. Based on tests of composite beam-to-column connections, bolts near the top of the shear tab are assumed to resist the applied beam shear, with the remaining bolts available to provide moment resistance. For the expected gravity shear load, $V_{u,gravity}$, the number of equivalent bolt elements required to provide shear resistance for gravity loading, N_v, is as follows:

$$N_v = V_{u,gravity} / F_{\parallel\ equiv\ bolt\ cap} \quad (4\text{-}32)$$

where N_v should be rounded up to the nearest integer, with a minimum value of one. The remaining bolts are assumed to provide tension to resist flexure. A fully plastic force distribution can be assumed for bolt equivalents ($F_{\perp\ equiv\ bolt\ cap}$) governed by ductile failure modes, and a linear force distribution can be assumed for brittle failure modes. The linear force distribution is determined by setting the force in the bottom bolt to $F_{\perp\ equiv\ bolt\ cap}$, and assuming a linear decrease among the remaining tension bolts. Figure 4-10 provides representations of the force distribution.

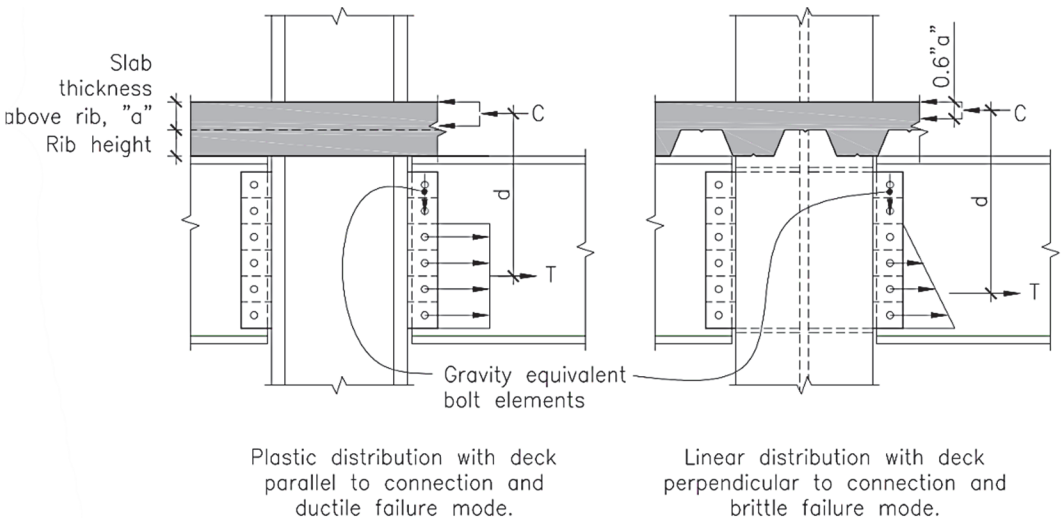

Figure 4-10 Force distribution in composite shear tab connection (Liu and Astaneh-Asl, 2000b).

The maximum normal force that can be developed is the lower of the total tension resistance of the equivalent bolt elements, T, or the compressive capacity of the slab, C, where:

$$C = 0.85 f_c' b_{eff} a \tag{4-33}$$

and b_{eff} is either (1) the column flange width for bending about column strong axis, or (2) the column depth for bending about column weak axis. If T exceeds C, the concrete slab is the weak link and governs connection capacity. If T is less than C, then the effective slab compression depth, a_{eff}, is calculated as:

$$a_{eff} = T / 0.85 f_c' b_{eff} \tag{4-34}$$

As shown in Figure 4-11, the lever arm dimension d is then determined based on the distance between the centroid of the bolt tension force T and the compression depth (lesser of slab thickness a or a_{eff}). The positive moment capacity, M_{max}^{+}, can then be calculated as:

$$M_{max}^{+} = d(\min(T, C)) \tag{4-35}$$

Referring to Figure 4-8, the positive moment capacity is assumed to be reached at a connection rotation of 0.03 radians. Beyond this, the moment resistance reduces linearly to M_{drop} at a rotation of 0.04 radians, where

$$M_{drop} = M^{-}_{max} \tag{4-36}$$

and M^{-}_{max} is equal in magnitude to the negative moment capacity, as determined in the next section.

4.4.2 Negative Moment Capacity

The tests by Liu and Astaneh-Asl (2000a, 2004) showed the presence of a slab could increase the negative moment capacity, M^{-}_{max}, up to 50% above the bare steel connection, due to continuity of the slab, metal deck, and nominal slab reinforcement. However, the slab effect contribution in negative bending was inconsistent. Therefore, it is suggested to evaluate the negative moment capacity as a bare steel connection. Similar to the calculation for M^{+}_{max}, the number of gravity shear bolts N_v is calculated using Equation 4-32; however, for negative bending, this number is not rounded up to the nearest integer. The bolts at the bolt group centroid are assumed to resist the shear load and assigned as shear bolts, starting at the center and distributed evenly above and below the centroid. The remaining bolts, or portion thereof, are assumed to resist flexure. A fully plastic force distribution is assumed for ductile failure modes and a linear force distribution is assumed for non-ductile failure modes. The assumed force distributions are shown in Figure 4-11.

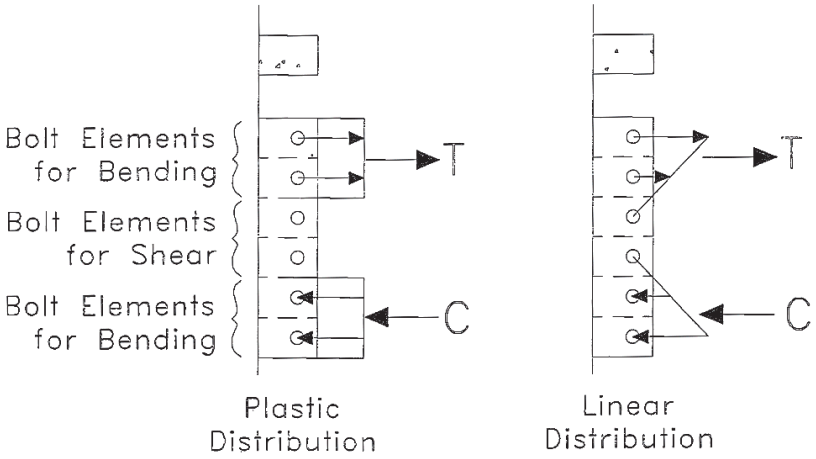

Figure 4-11 Force distribution in non-composite (bare) steel shear tab connection (Liu and Astaneh-Asl, 2000b).

Assuming that the equivalent bolt strengths, $F_{\perp\ equiv\ bolt\ cap}$, are governed by tension, the M^{-}_{max} is calculated as:

$$M^{-}_{max} = dT \tag{4-37}$$

where d is the distance between flexure bolts centroids and T is based on the bolts in tension, using either the plastic distribution (ductile failure modes) or linear distribution (non-ductile failure modes). The negative moment strength M^{-}_{max} is associated with the rotation values shown in Figure 4-8.

4.4.3 Moment at Connection Slip

The moment at connection slip, M_{slip}, is based on a plastic distribution of bolt friction forces, assuming the distribution shown in Figure 4-12. The friction force, minimum bolt pretension, and static friction coefficient for a faying surface are used to calculate M_{slip}, where the bolt slip force is calculated as follows:

$$F_{bolt\ slip} = \mu T_{bolt\ pretension} \tag{4-38}$$

where μ is 0.30 for Class A surface and 0.50 for Class B surface (Section J3.8 of ANSI/AISC 360-16), and $T_{bolt\ pretension}$ is per Table J3.1 of ANSI/AISC 360-16, Section J3.1.

For connection with slab:

$$M_{slip} = 0.67 F_{bolt\ slip}(\#\ \text{tension bolts})d \tag{4-39}$$

where d is the distance between the bolt group centroid and top of concrete.

For bare steel:

$$M_{slip} = 1.5 F_{bolt\ slip}(\#\ \text{tension bolts})d \tag{4-40}$$

where d is the distance between centroid of tension and compression bolts.

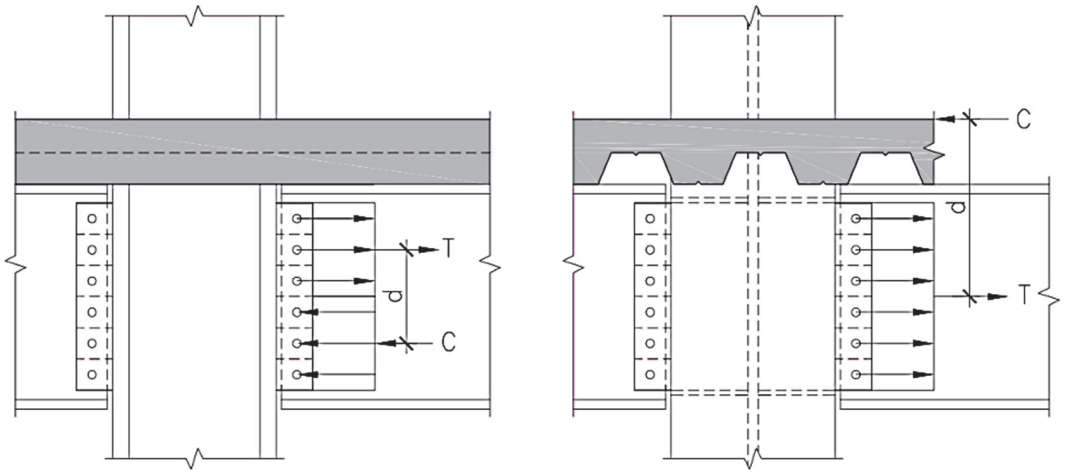

Figure 4-12 Calculation of M_{slip} in shear tab connections (Liu and Astaneh-Asl, 2000b).

4.4.4 Limitations on Procedure

The analysis procedure just described (Liu and Astaneh-Asl, 2000a, 2004) is generalized based on a limited number of tests, all of which had a single line of bolts and a one-inch gap between the column and beam. Simple connections often have multiple lines of bolts with smaller gaps. An increase in number of lines of bolts and a decrease in gap size could increase the percent M_p of the connection, as well as minimize the sharp drop off in positive flexural capacity as the beam would bear on the column at smaller drifts. Shear tabs tested were A36 steel with an average expected yield strength of 46 ksi. This is in contrast to A572 steel Grade 50, with an expected strength of 55 ksi. The higher expected yield strength for shear tabs may imply there is less ductility in the connection compared to those tested as the governing failure mode may change from ductile yielding of the tab to shear fracture of bolts.

NIST Technical Note 1749, *Robustness of Steel Gravity Frame Systems with Single-Plate Shear Connections* (NIST, 1994) describes a method developed to assess structural integrity of steel connections based on testing. It is suggested that a similar modeling methodology from this document be used to generate backbone curves for project specific connections with test results from Liu and Astaneh-Asl (2000a) serving as calibration and verification models.

4.4.5 Comparison of Liu and Astaneh-Asl versus ASCE/SEI 41 and FEMA 355D

This section compares the Liu and Astaneh-Asl procedure to those in other documents, such as ASCE/SEI 41-13 and FEMA 355D, *State of the Art Report on Connection Performance* (FEMA, 2000c). In particular, FEMA 355D includes guidance on the secant stiffness of simple shear connections and it suggests limits on connection rotation. ASCE/SEI 41-13 provides guidance on plastic and degradation rotation values, as well as a rotation at loss of gravity support. In general, the Liu and Astaneh-Asl procedure is more detailed than available information in other documents.

Figure 4-13 compares the backbone curve based on Liu and Astaneh-Asl (2000a, 2004) with the curves inferred from ASCE/SEI 41-13 and FEMA 355D. In these comparisons, the ASCE/SEI 41-13 flexural capacity is set equal to that in the Liu and Astaneh procedure. Figure 4-13a shows the backbone of a post-1980s simple shear connection for a 24-inch deep beam (55% M_p positive flexure). Figure 4-13b shows the backbone of a post-1980s simple shear connection for a 33-inch deep beam (30% M_p positive flexure). Figure 4-13c shows the backbone of a pre-1980s simple shear connection for 24-inch deep beam where behavior was controlled by bolt fracture. In all three plots there is a noticeable difference in both initial and secant stiffnesses between the two methods, as well as residual strength ratio. Hysteretic energy

dissipation (area below the curves) is considerably smaller in the positive pre-degradation section of the backbone curve for Liu and Astaneh-Asl. This difference would increase as connection stiffness degrades under cyclic loading. As the Liu and Astaneh-Asl procedure is well documented and verified with test data, it is recommended for use over the other methods.

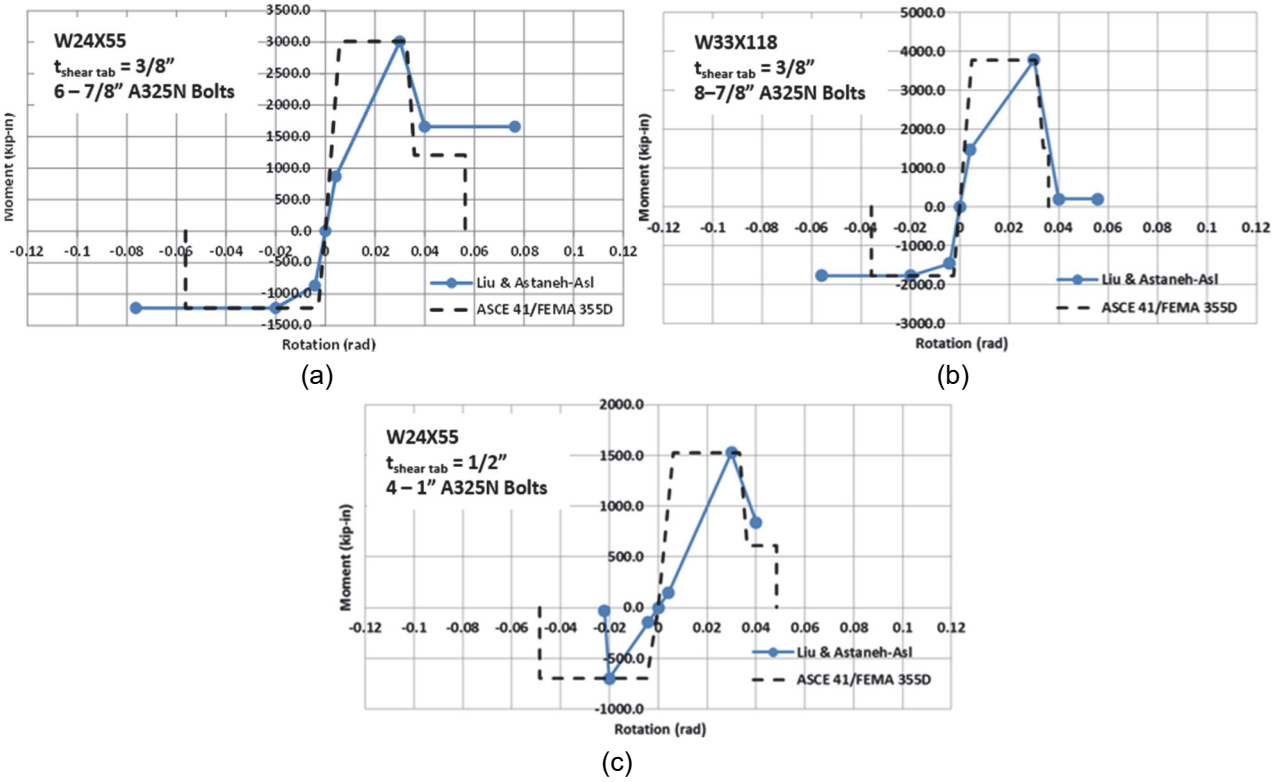

Figure 4-13 Comparison of Liu and Astaneh-Asl (2000a, 2004) and ASCE/SEI 41-13 and FEMA 355D backbone curves.

Chapter 5

Fiber-Type Beam-Column Models

5.1 Overview of Fiber-Type Models

This chapter provides guidelines for the implementation of fiber cross section models to represent axial and flexural effects (P-δ_x and M-ϕ) in either a distributed-inelastic model (Figure 3-2) or a fiber-hinge model (Figure 3-3) formulation. Compared to concentrated hinge models, fiber models generally allow a more fundamental representation of inelastic behavior, compared to the concentrated hinge models described in Chapter 4. However, fiber models generally have a higher computational cost due to the numerical integration of fiber strains within the section and of generalized cross section strains at points along the element length. This computational cost can be minimized by: (1) discretizing a section with a minimum quantity of fibers; (2) optimizing the size and distribution of fibers; (3) decreasing the number of integration points along element length; and (4) modeling fiber sections at expected locations of nonlinearity with the remainder of the element modeled as elastic or using phenomenological sections. A sensitivity analysis should confirm that the discretization through the cross section and along the member length is sufficiently accurate to simulate the necessary response quantities.

5.2 Implementation of Section and Element Models

Beam-column element formulations generally involve characterization of behavior at member cross sections and along the member length. The so-called fiber-type models described in this chapter are essentially a subset of general finite element approaches, where kinematic assumptions are used to relate strains to deflections, material constitutive models are used to relate strains to stresses, and numerical integration methods are used to integrate the stresses, strains, their derivatives and associated energy quantities over the element volume. The qualifier “fiber” generally implies representing material behavior through uniaxial stresses and strains along the member length. The “fiber” term is also often associated with implementations that employ the rectangular (or midpoint) method to integrate stresses and material stiffness quantities through simple summation of quantities through the member cross section, although, this is a detail of the numerical implementation, rather than a fundamental assumption.

In fiber-type models, a kinematic assumption is applied to relate axial strains through the cross section to the generalized cross-section deformations, and the material response is idealized in terms of uniaxial stress-strain response. A common kinematic assumption is the Euler-Bernoulli (plane sections remain plane) assumption, where the axial strains throughout the cross section can be uniquely related to the axial strain at the centroid combined with curvature about the major and minor axes. The axial fiber strains are then related to fiber stresses, which are integrated over the cross section to determine stress resultants such as axial force, major and minor axis bending moments, and torsion. Other kinematic assumptions are possible, such as the Timoshenko beam, which allows for shear deformations in the derivation, or elements that can accommodate non-uniform (warping) torsion. It is also possible to combine fiber-type discretization for some cross section response quantities, such as axial and flexural (P-δ and M-ϕ) behavior, and functional relationships for other quantities, such as shear and torsion (V-γ and T-ϕ_x) response, although, the formulations for these combinations are less standardized. Because fiber sections only account for axial and flexural response, any localized deformations, such as bolt slip and buckling, must be superimposed to the section response by using additional springs.

Where fiber sections are used in fiber-hinge formulations, the generalized cross section strains (centroidal strain and curvatures) at the midpoint or ends of the hinge are related to the hinge deformations (axial deformation and rotation) through an assumed hinge length and strain gradient. By assuming constant values of strains over the hinge length, the conversion between section strains/curvatures and hinge deformation/rotations reduces to a simple multiplication of curvature/strain times hinge length.

When fiber sections are implemented into distributed-plasticity elements, the section strains are related to member deformations through either displacement (shape functions) or force interpolation functions along the member. Integrations along the member length are accomplished through numerical integration techniques, such as Gauss quadrature or one of its many variants, where the section response is evaluated at a specified number of integration points along the member.

5.3 Fiber-Section Modeling

Fiber sections are most useful for cross sections whose behavior cannot be characterized via calibration, such as composite sections, as well as structural components subjected to varying axial loads or biaxial bending. Because integration of strains over the section depth at each force recovery step can be computationally expensive, the number, size and location of fibers should be optimized. For example, in unidirectional bending of beams and beam-columns, the fibers only need to be discretized through the depth of the member, and not the width, as shown in Figure

5-1. For the case of biaxial bending, 2D fiber discretization is needed. Since the fibers that contribute the most to the equilibrium forces are the extreme fibers which have strains of the highest amplitude, a finer mesh is general recommended at these section extremities, as shown in Figure 5-1.

It should be noted that the typical fiber discretization, such as shown in Figure 5-1, is essentially equivalent to discretizing through the cross section using the rectangle method (or midpoint rule). While this is commonly employed in structural engineering software, such as PERFORM-3D and OpenSees, it is less common in general purpose analysis software, such as ABAQUS or ANSYS. General purpose programs may employ other methods of numerical integration through the cross section such as Simpson's rule or any one of a variety of quadrature integration rules.

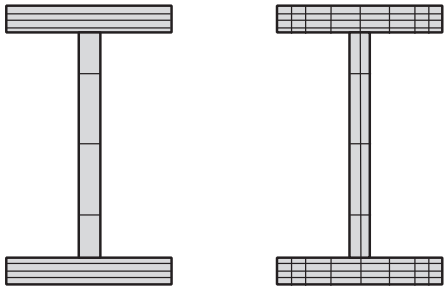

Figure 5-1 Fiber-section discretization of I-shape member: (a) uniaxial bending; (b) biaxial bending.

5.4 Uniaxial Moment and Axial Force Model

For a moment frame beam, or other members subject to uniaxial bending, the fibers can be defined through the depth of the member, as shown in Figure 5-1a. Defining the fibers along this axis captures only strong-axis moment and axial force. Weak-axis beam behavior can usually be ignored in design of building moment frames, where the frames are designed as planar and the beams are restrained in the out-of-plane (weak-axis) direction by the slab. The flanges and webs can be subdivided to produce a more realistic representation of expected capacity, but it comes at an additional computational cost. In general, it is recommended to include at least two fibers (integration points) through the flange depth, although similar to mesh refinement in finite element analysis, it is recommended to conduct some sensitivity analyses to determine an appropriate level of fiber mesh refinement.

For modeling of beams (flexural members where the axial restraint is small), the fiber sections are defined such that the axial cross-section strain is free (releases), such that no axial stress resultant will develop during the analysis (i.e., pure moment-curvature (or rotation) analysis with zero axial force and non-zero (unrestrained) axial cross section strain). This then implies that the member length may change during flexural

loading, which may or may not be captured in beam element formulations. In contrast, a beam-column type formulation would generally track both curvature and axial centroid strain along the member, such that there is interaction between axial and flexural effects.

5.5 Biaxial Moment and Axial Force Model

For a moment frame beam-columns subjected to biaxial (strong- and weak-axis) bending, the fibers can be defined along both axes of the column. The column flanges and web can be discretized as described in the previous section. A sensitivity study on the moment-curvature response of the biaxial moment and axial fiber section under the range of expected axial loads should verify that the number and location of fibers results in an accurate representation of behavior.

5.6 Material Modeling Requirements

A typical engineering cyclic stress-strain curve for steel members should include the key components of behavior necessary to capture distributed yielding of the member, as seen in Figure 5-2. Key characteristics of the behavior that should be captured in the formulation include: (1) modeling of yielding through a change in slope of the modulus; and (2) capturing strain hardening of the material; however, the material stress should typically be capped at a value of the tensile strength of the material

In addition, it is helpful to capture the following phenomena:

- An initial yield plateau of the virgin material.
- Cyclic hardening of the material.
- Inclusion of an elastic region prior to yielding of the member, including elastic unloading after a plastic excursion. After repeated cyclic loading, it is commonly observed that the elastic zone of the material decreases.
- Achieving a limiting bounding modulus after significant inelastic excursion in either tension or compression.
- Capturing the Bauschinger effect, whereby the material yields earlier than the virgin material after a significant inelastic excursion in the reverse direction.
- Local buckling and fracture of the material (recognizing that these require phenomenological calibration of behavior that depends on the member properties and loading).

Depending on the modeling capabilities of the software, the material response may be highly idealized through an approximate (often piecewise linear) curve.

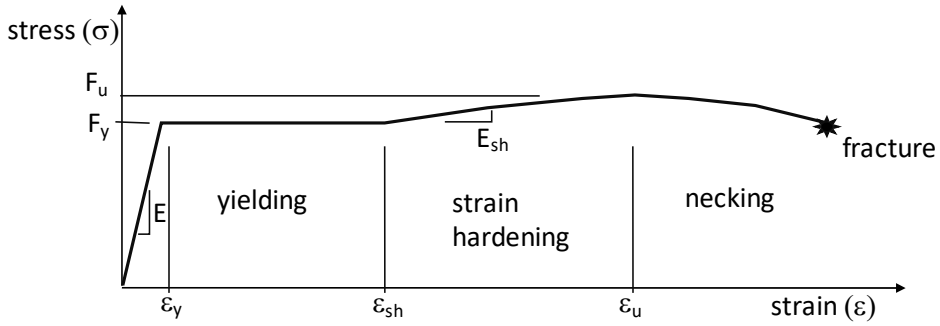

Figure 5-2 Engineering stress-strain curve for mild steel.

In the absence of having measured material properties for the structure being modeled, an expected yield and ultimate strength of the material can be obtained by multiplying the nominal yield and ultimate strengths by the R_y and R_u factors, as provided in *Part I Guidelines* or as specified in ANSI/AISC 341-16, *Seismic Provisions for Structural Steel Buildings* (AISC, 2016c). For mild structural steels, the strain at the onset of strain hardening, ε_{sh}, may be taken as 10 times the yield strain; and the ultimate strain, ε_u, may be taken as about 75 times the yield strain.

The cyclic response of the steel can be modeled by a variety of hysteretic models, which typically employ a combination of kinematic and isotropic hardening characteristics to simulate the measured cyclic stress-strain response. Figure 5-3 shows an example of a representative cyclic hysteretic response curve for steel. The specific terms of definitions of cyclic stress-strain curves will depend on the specific material formulation, which one would expect to have documented with the analysis software implementation.

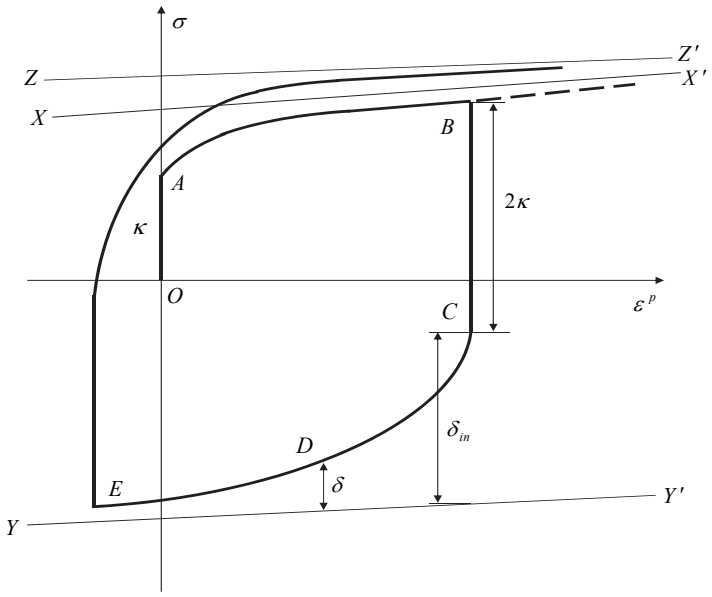

Figure 5-3 Uniaxial cyclic stress-plastic strain curve (adapted from Shen et al., 1995).

Validation studies may be conducted by comparing the results of fiber-based component model analyses to tests of steel members subjected to axial force and flexure. As the calibration is conducted at the stress-strain level, validation may be carried out adequately by comparing load-deformation results from the member experiments. More comprehensive validation is possible through comparing to frame tests. Experiments with a wide range of material and geometric parameters should be used to perform the validation of any fiber-based finite element.

Fiber-based elements can also be effective for analyzing composite steel-concrete members, in which case, equivalent uniaxial properties for concrete are necessary. *Part IIb Guidelines* (NIST, 2017c) on reinforced concrete moment frames provides information on concrete material models.

5.7 Implementation of Distributed-Inelasticity Elements

There are two fundamental formulations for distributed-inelastic elements: (1) displacement-based; (2) and force-based formulations. For standard flexural members with member end nodes and cubic polynomial displacement fields, the displacement-based formulation generally assumes a linear shape function for axial deformations and curvatures along the element. This assumption of a displacement interpolation is a standard approach applied in most structural finite element formulations. In contrast, force-based formulations assume a linear shape function for forces and moments along the element. While force-based formulations are generally more computationally efficient than displacement-based formulations, force-based formulations are more prevalent in research software (e.g., OpenSees) and are not common in commercially available analysis software (e.g., PERFORM-3D, SAP2000, or LS-DYNA).

To represent the distribution of deformations along the entire element accurately, a structural element generally needs to be discretized into several displacement-based finite elements. Each element would then have several (typically five or seven) integration points along their length. The required discretization increases as members plasticize and the distribution of curvature becomes more nonlinear. While coming with a higher computational cost than concentrated models, the displacement-based formulation is able to capture the gradual progression of the spread of plasticity along the element. Therefore, its application is best suited to cases where spread of plasticity is expected, such as in members with shallow moment gradients (in members subjected to single curvature bending and/or distributed member loads), and in members with high axial load ratios.

Force-based formulations generally assume a linear distribution of moments along the element and are best suited to members that are subjected to constant shear force and reverse curvature along their length. In such cases, force-based formulation are

often accurate enough to capture the seismic response of beams or column using a single element. To avoid problems with localization or numerical instabilities in force-based formulations, it is recommended to limit the number of integration points to between three and five. Numerical integration consists of evaluating the deformations at the integration points and multiplying them by the integration weights of the integration points, which are defined numerically and based on the integration scheme. Taucer et al. (1991) and Neuenhofer and Filippou (1997, 1998) provide more information on force-based element formulations.

One of the challenges with both displacement-based and force-based distributed plasticity formulations is that when yielding becomes large (e.g., under large moments), the curvature gradients become high, causing numerical localization of curvatures and strains. While in concept this can be controlled by adjusting the number of elements and/or number of integration points, in practice it can present a significant challenge. For this reason, and alternative type of fiber-type formulation is the so-called "fiber-hinge" model, where the yielding portion of the member is pre-defined with a specified hinge length and the portion of the member outside of the hinge is assumed to be elastic.

5.8 Hinge Length

Distributed-inelasticity models calculate strain and curvature at the element integration points. However, an acceptance criterion in design standards, such as ASCE/SEI 41, is often defined in terms of either total or plastic hinge (or chord) rotation. In order to evaluate the behavior of a fiber-type component model, a finite length of a plastic hinge must be assumed, and curvatures are integrated across this length to calculate rotation. Typically, the hinge length is assumed to be $0.5d_b$ to $1.5d_b$, where d_b is the section depth, depending on loading conditions and expected level of deformation. Based on a study of the seismic performance of steel columns, Suzuki and Lignos (2015) and Elkady and Lignos (2015, 2016) recommend using a hinge length of $1.4d_b$.

5.9 Special Considerations for Fiber Sections in Steel Structures

5.9.1 Reduced Beam Section

Reduced beam sections (RBS) pose a challenge to discrete models because the RBS cross section varies along the element length. On the other hand, by limiting yielding to a specific region of the member, the RBS can be well suited to modeling with a fiber-hinge formulation. In such cases, it is recommended to define the fiber-hinge cross section based on the cross section geometry at the center of the RBS. This will ensure that the fiber-hinge will yield at the strength of the RBS. Then, with the fiber-hinge cross section geometry set, the fiber-hinge length and material parameters can be calibrated against test data.

5.9.2 Bolt Slip and Fracture

Fiber-type approaches offer an effective approach for modeling bolt slip or weld fracture in member connections, where one can discretize the connection cross section into fibers that represent the resistance of either individual bolts or regions of a weld. In such models, the fiber-hinge should be defined with a "unit" length that is consistent with the material definitions used to represent the fibers. For example, in the case of a shear tab connections where the bolts are subjected to shear, the fiber representing each bolt should be established to have the force-deformation response of a shear bolt, which can slip for a finite distance, go into bearing, and ultimately reach a limiting strength due to bolt shear or plate tearout. These limit points should be accompanied by appropriate hysteretic functions to characterize the cyclic loading response. Similarly, connections subject to weld fracture could be modeled by discretizing the welded joints into fibers, whose tensile and compression strengths are determined considering the weld strength, based on either the ultimate strength of the weld or lower strengths that are limited by weld fracture stress. Further details on modeling weld fracture is included in Appendix A.

Chapter 6

Continuum Finite Element Component Models

6.1 Overview

General purpose, commercially-available finite element analysis software is widely used in industry to determine stress distributions and deformation characteristics of complex components. Several leading software packages (e.g., ABAQUS, LS-DYNA, and ANSYS) have the capability to perform nonlinear static, cyclic, and fully dynamic analysis of steel assemblies that will capture large deflection behavior, local and global buckling, opening and closing of gaps, and, in some cases, fracture.

While it is possible to build highly detailed 3D models of entire building frames using continuum finite elements, it is generally more effective to restrict the use of such detailed analysis to those areas where beam-column type elements would prove inadequate. This would generally apply to applications with the following attributes:

- local buckling,
- lateral-torsional buckling,
- stress path in the connection region,
- welded joints where stress concentration is of concern,
- complex connections where three-dimensional effects need to be considered, and
- any form of geometry, detail, loading pattern or loading history for which robust hysteretic beam 'hinge' rules do not exist.

The results of the study of a detailed continuum model can be used to develop a model that captures the critical characteristics of the study region using discrete elements in the model of the entire building frame. A detailed continuum model analysis often yields a simple result such that the detailing of the component is sufficient to model it as rigid or elastic in a full-building analysis. In many cases, it serves as a strategy for validating assumptions.

6.2 Quality Assurance

Modern general purpose finite element software generally includes a wide variety of different element and material types, each with many selection options. In most industries that utilize advanced continuum finite element modeling, detailed analyses

are used in conjunction with physical testing, such that the analyst's experience is developed with careful reference to the results of physical tests. As project-specific testing is not as common in the building construction industry, it is highly recommended that analysts using advanced software demonstrate that their modeling technique with a particular software package can reasonably replicate a number of published physical tests on components that exhibit the types of behavior that might be expected. For example, the results of many beam-column subassembly tests that were conducted after the 1994 Northridge earthquake are available in the literature and can be used.

6.2.1 Virtual Testing

One of the most valuable uses for continuum modeling is to develop understanding of the behavior of details and components so that simpler phenomenological models and performance criteria can be developed for 'whole building' analysis. This might be referred to as 'virtual testing,' where, for example, a detailed numerical model is built of a particular component or a beam-column subassembly which is then subjected to a sequence of loading or deformation cycles in order to simulate its hysteretic behavior. This is an exact analogy to using physical testing for the same purpose; the only difference is that the model is numerical rather than physical. Two examples are shown in Figure 6-1 and Figure 6-2.

The disadvantage of virtual testing is that numerical simulation is limited by the ability of the software to replicate all aspects of physical behavior that would affect the outcome of a corresponding physical test. However, these concerns can be largely overcome by means of proper validation and calibration against previously conducted physical tests which display similar behaviors. While one must be cautious in extrapolating analyses into territory where unexpected behaviors might occur, in general the fundamental behaviors of steel materials and fabricated components are well-known and can be modeled reliably using current software.

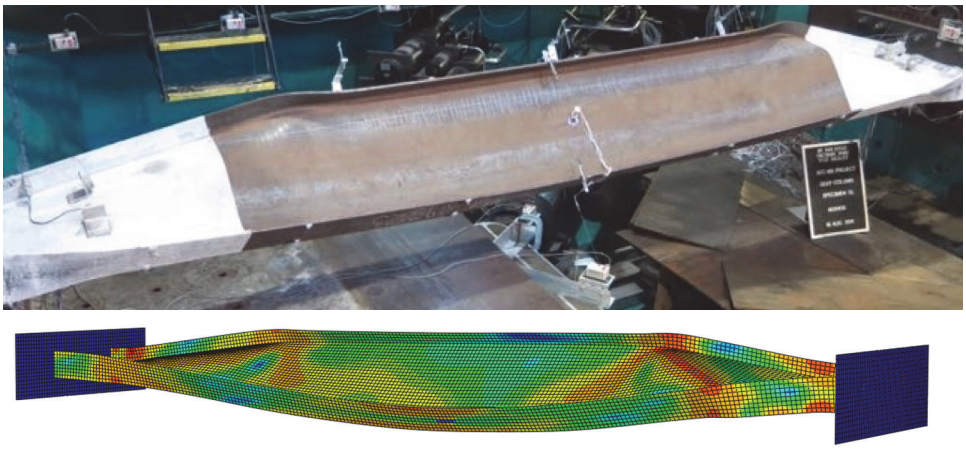

Figure 6-1 Simulation of cyclic response of a deep (W24) column with ABAQUS (Ozkula et al., 2015).

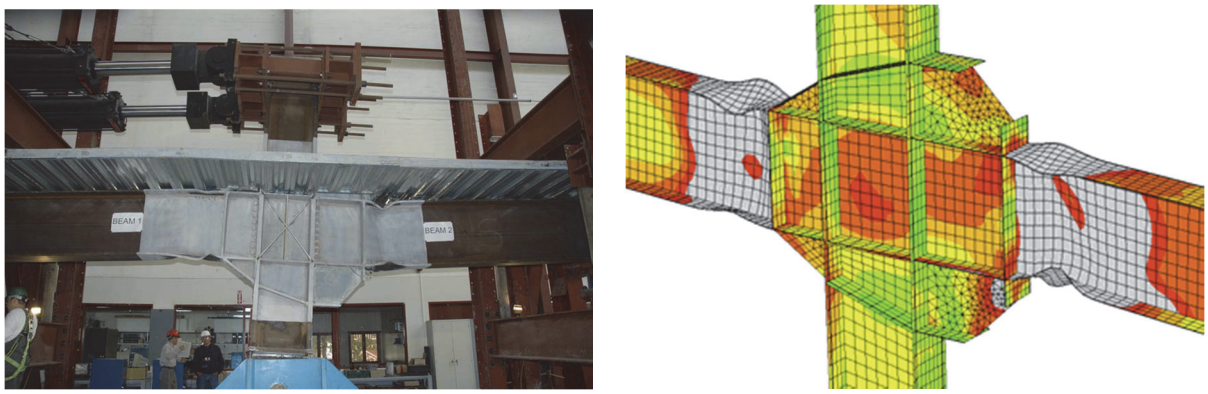

Figure 6-2 Simulation of retrofitted beam-column connection response with ABAQUS (Newell and Uang, 2006).

The advantage of virtual testing is that it is a quicker and more cost-effective method of exploring and optimizing alternative details than physical testing, thus allowing the modeler to perform sensitivity studies on a variety of design parameters. Numerical testing of a component under different loading protocols and with small modifications to geometry or detailing can be performed many times once the basic model has been built and validated. Small changes to details can dramatically improve performance and virtual testing can be used to realize such improvements.

6.3 Element Type and Convergence Test

Four-node shell elements, eight-node brick elements, or a combination of the two are commonly used to model steel members and subassemblies. Four-node shell elements are computationally efficient, especially for large models; although eight-node shell elements, with higher-order interpolation functions, can be used in combination with four-node elements to model certain regions (e.g., connection region) where an accurate prediction of the local response is important (see Figure 6-3).

Alternatively, shell elements with a coarse mesh can be used first to construct and analyze a global model. Then a sub-model with a more refined mesh or higher-order elements can be used to analyze the region of interest, and the sub-model analysis uses the results of global model analysis as boundary conditions along the perimeter edges of the model. Figure 6-4 provides an example application of the technique. In either case, convergence tests should be conducted to ensure the element (or mesh) sizes are sufficiently small for a reliable prediction of the response.

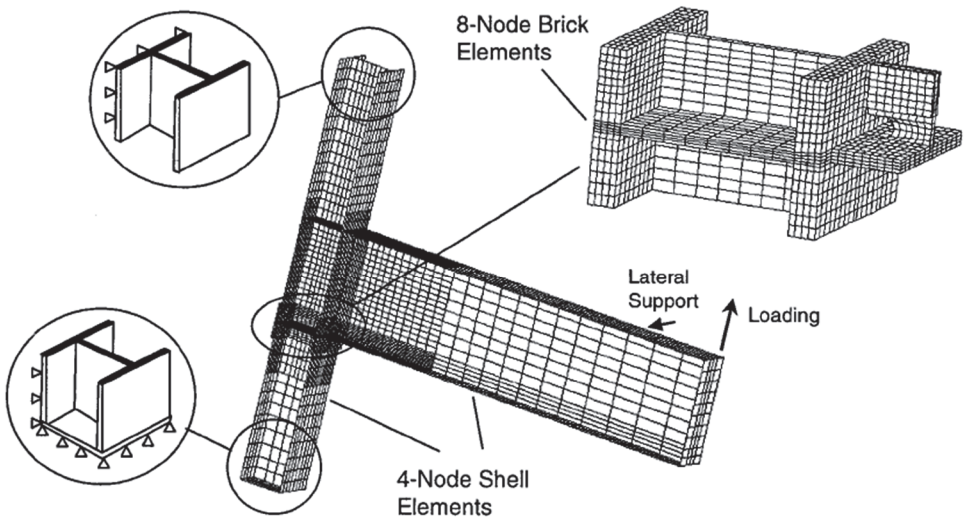

FIG. 6. Details of Finite-Element Model

Figure 6-3 Beam-column subassembly modeling with mixed shell and brick elements (El-Tawil et al., 1999).

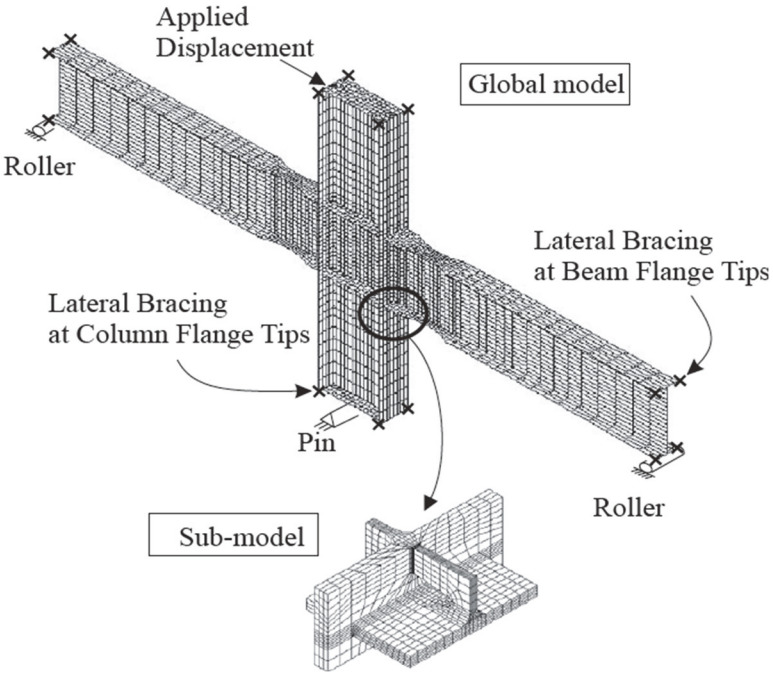

Figure 6-4 Beam-column subassembly global modeling and sub-modeling (Ricles et al., 2002).

6.4 Nonlinear Material Models

Different software packages have different material model formulations. In general, to make realistic and reliable predictions of the cyclic response, the material models should adequately account for: (1) yield and strain increment under bi-axial and tri-axial stress states; (2) cyclic strain hardening; and (3) Bauschinger unloading and re-loading behavior.

Engineering stress-strain (σ-ε) relationships can be obtained from tensile coupon testing. When such information is not available, the idealized curve shown in Figure 6-5 can be used. While such relationship can be used for nonlinear analysis with fiber elements, relationships for true stress-strain (σ_t-ε_t) are needed for continuum finite element analysis. The transformation from engineering stress-strain (σ–ε) to true stress-strain (σ_t-ε_t) is described by the following relationships:

$$\varepsilon_t = \ln(1 + \varepsilon) \quad (6\text{-}1)$$

$$\sigma_t = \sigma(1+ \varepsilon) \quad (6\text{-}2)$$

For structural steel, it is common to model the plasticity based on a von Mises yield surface and the associated flow rule. Isotropic, kinematic hardening, or combined isotropic-kinematic hardening can be assumed, with the first being more appropriate for monotonic loading analysis and the latter two for cyclic analysis. Parameters for a plastic material model can be established from results of cyclic coupon tests. If fracture is to be predicted, an appropriate low-cycle fatigue damage accumulation model is required, or alternatively a conservative strain estimate can be assumed.

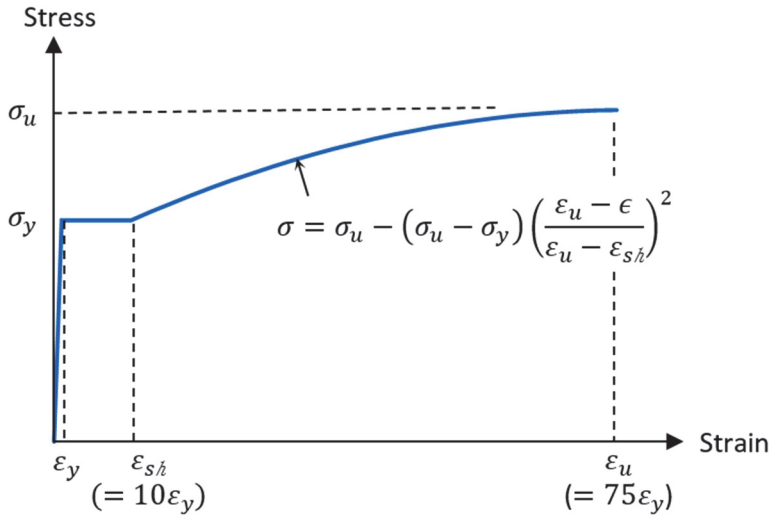

Figure 6-5 Recommended steel stress-strain relationship (A992 steel).

6.5 Geometric Imperfections, Residual Stresses, and Post-Buckling Analysis

The presence of geometric imperfections and residual stresses affects the performance of steel components to some degree. Geometric imperfections relative to the theoretically exact geometry arise due to: (1) mill straightness tolerance (camber and sweep); (2) fabrication tolerance; (3) welding distortion; and (4) erection tolerance.

Residual stresses along a member arise from rolling, cooling, and straightening. Figure 6-6 shows a commonly used residual stress pattern for rolled W-shapes. Welding can produce higher residual stresses in built-up shapes and near welded

joints. In physical tests where buckling is not a factor, the presence of geometric imperfections and residual stresses do not usually have a significant effect on the strength or cyclic response of steel elements. However, the deformations on first loading can be significantly affected by early yielding of parts of a section with residual stresses, particularly where there has been significant welding. While residual stresses due to rolling can be modeled explicitly, if desired, welding residual stresses are normally ignored mainly because little information is available on modeling these residual stresses. This practice may be acceptable as the effect of residual stresses tends to diminish in the post-buckling region.

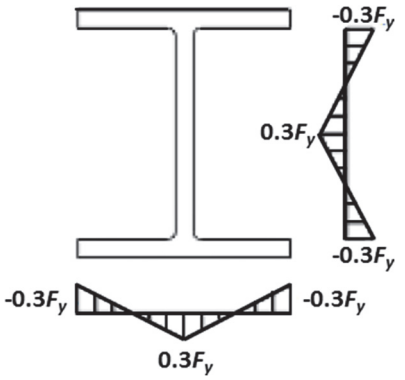

Figure 6-6 Typical residual stress pattern.

It is important that analysis models are able to simulate the development of all relevant global and local buckling mechanisms since these can significantly affect strength and cyclic response. It is common to introduce geometric imperfections of a member by means of a linear superposition of scaled buckling mode shapes, especially the lowest buckling modes, in an analysis involving post-buckling response. The magnitude of local deformations can be based on manufacturing and fabrication tolerances from the ANSI/AISC 303-16, *Code of Standard Practice for Steel Buildings* (AISC, 2016a). A member out-of-straightness equal to $L/1000$, where L is the member length between framing or brace points is commonly used to represent mill and fabrication tolerances. In tiered building structures, erection tolerances can be modeled assuming and out-of-plumbness equal to $H/500$, where H is the story height. This amount of erection tolerance can also be extended to applications other than tiered frame structures.

Opinions vary on the importance of including hypothetical imperfections in the geometry of an analysis model. Ultimately, it is the analyst that should demonstrate that the assumptions made can reproduce buckling behaviors that are observed in physical tests. A few considerations are set as follows:

- Large-deflection formulations are likely to be more reliable for nonlinear buckling regimes.

- The mesh density associated with the use of a particular element formulation must be sufficient to enable a buckle to occur.
- If imperfections are added to a model, their geometry and alignment should promote the development of potential buckled shapes under the loading protocol selected.

6.6 Strain Limits for Fracture and Low-Cycle Fatigue

While modern continuum finite element technologies can reliably model steel materials and components with large strains and cyclic plasticity, the continuum finite element analyses do not directly simulate fracture. In highly ductile members and connections fracture generally initiates by ductile fracture processes at very large strains, where the limiting strain depends on the material toughness, the triaxial stress constraint, the loading history and other parameters. In addition, when considering localized strains from detailed continuum finite element analyses, it is important to recognize that the commonly reported engineering failure (fracture) strain limits from conventional tension coupon tests can be quite different from the localized true strains at failure. For example, whereas the typical engineering fracture strain measured over a one-inch to two-inch gage length for a mild structural steel typically ranges from 0.2 to 0.3 (20% to 30%), the true localized strain in the necked section is often on the order of 1.0 (100%). In addition, the fracture strains under cyclic loads with large inelastic stress reversals will be much smaller than the strains under monotonic loading.

In the absence of a detailed investigation that rigorously considers localized fracture phenomena, current standards limit the calculated steel strains to about 0.02 to 0.05 (2% to 5%) to avoid fracture under cyclic loading. These are for cases where the steel material has reasonable fracture toughness (e.g., Charpy V-Notch toughness on the order of 40 ft-lb or greater at the expected ambient temperature of the steel). While these strain limits should be reasonably conservative for most cases, there is certainly room to apply more detailed methods to assess fracture in continuum finite element analyses (e.g., Smith et al., 2017; Kanvinde and Deierlein, 2007).

Appendix A
Modeling Pre-Northridge (Fracture Critical) Connections

A.1 Overview of Pre-Northridge Connections

The guidelines in this appendix are intended for analyses to assess the performance of so-called "pre-Northridge" steel moment frames. The term "pre-Northridge" refers to steel moment frame buildings that were constructed in the Western United States (primarily in California, Washington, and Oregon) between the mid-1960s and 1994, conforming to the seismic design provisions of the *Uniform Building Code* (International Conference of Building Officials, 1994). The beam-column connections of these systems typically consisted of complete penetration groove welds between the beam flanges and column, and bolted shear tab web connections. The column splices typically consisted of milled-bearing surfaces with partial penetration grove welds with a bolted shear connection. Groove welds of the beam and column flanges were typically field welds, often constructed with non-toughness rated weld metal. In response to observations of many weld fractures to such systems during the 1994 Northridge earthquake, extensive studies were conducted to investigate the premature weld fractures, which resulted from a combination of: (1) connection details and geometries with high stress and strain demands at critical welded locations; (2) large discontinuities and initial flaws in groove welds; and (3) low toughness weld metals and nearby heat affected zones (FEMA, 1996, 1997a, 2000a, 2000b). These conditions were not typically present in steel buildings constructed prior to the mid-1960s, where shop-welded flange plate connections and higher toughness weld materials were more common.

Pre-Northridge connections may develop the yield strength of the beam prior to weld fracture, but the extent of yielding is highly dependent on weld fracture toughness and size of existing cracks within welds. In beam-column connections, brittle fracture generally occurs first at the lower flange followed by weld fracture at the upper flange. As a result, pre-Northridge connections do not exhibit ductile and stable backbone curves of modern beam-column moment connections as those described in Chapter 4, which adhere to more stringent connection requirements that were introduced into seismic design provisions in 1997.

A.2 Pre-Northridge Beam-Column Connection

A.2.1 Moment Frame Beam Hinge Model

This section provides guidelines to define properties of either concentrated hinge or fiber hinge properties for steel beam-column connections in fracture-prone pre-Northridge steel moment frames. The concentrated hinge is defined by parameters of a backbone curve, relating beam end moment to plastic hinge rotation. The fiber hinge is based on critical fiber stress and strain parameters. Both the concentrated hinge and fiber hinge parameters are calibrated to test data and material properties that are derived from limit states based on either critical stress or critical plastic hinge rotation. The connection modeling parameters are based the connection geometry shown in Figure A-1 (Chi et al., 2000), where the key limit states are: (1) yielding and fracture in the bottom flange; (2) yielding and fracture in the top flange; and (3) yielding and fracture in the bolted web connection. Critical stress is the first limit state checked in both flanges. If the critical stress is larger than the effective yield stress, then the flange is checked based on a critical plastic hinge rotation (strain) criteria. Default values and procedures for applying critical stress and plastic rotation are defined first, followed by recommendations for their implementation in the concentrated hinge or fiber models.

Referring to Figure A-1, it is generally assumed that both the bottom and top flange welded joints have built in flaws created by the backing bar at the weld root. As described below, the critical flaw dimension is a_0, which corresponds to the initial flaw length extension from the backing bar into the weld root. Note that even if a_0 is equal to zero, there is still a finite initial flaw effect due to the presence of the weld backing bar. While the weld and flaw sizes are generally the same for the top and bottom flange, the bottom flange is typically more fracture critical due to the location of the flaw at the extreme fiber. Figure A-2 shows the response of a beam-column connection test where the bottom flange has fracture prior to yielding and the top flange and web connection are still intact. As shown, even after the bottom flange weld fractured, the connection has significant reserve moment strength, provided by the force couple between the intact portions of the connections and the compression bearing region of the fractured flange joint. In this case, the residual strength in the upper quadrant (positive moment) is due to the force couple between tension in the web connection and compression in the top flange. The strength in the lower quadrant (negative moment) is essentially unaffected by the bottom connection fracture, which continues to resist compression bearing stresses.

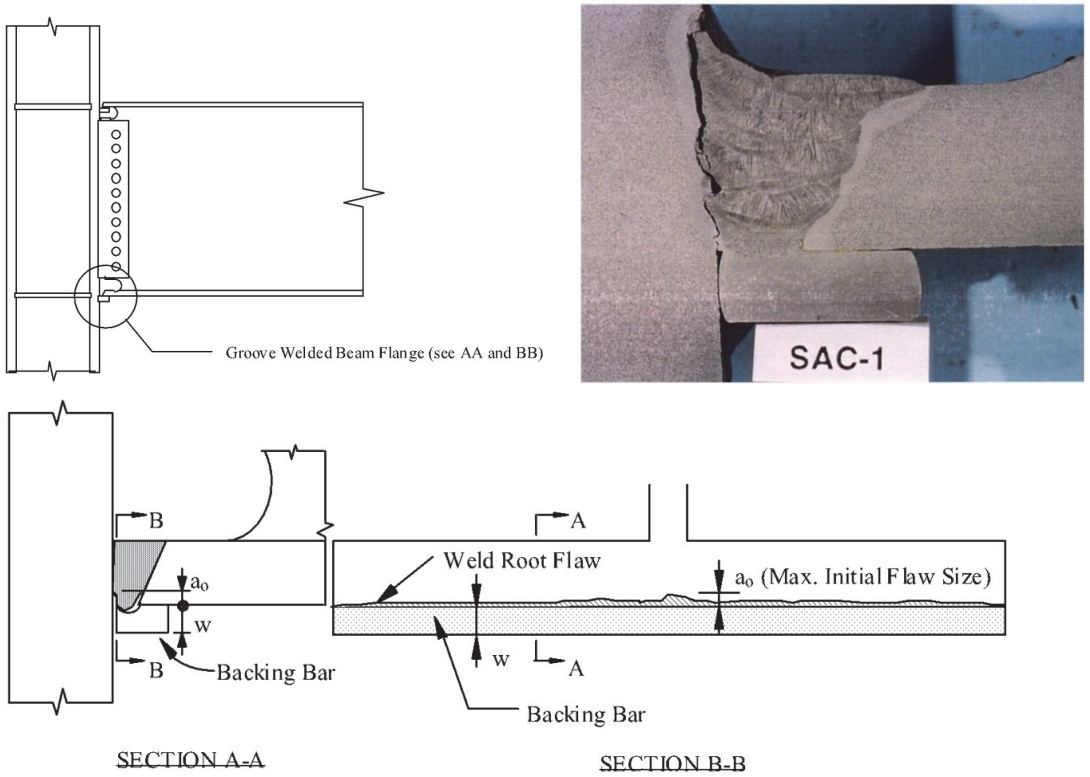

Figure A-1 Pre-Northridge beam-column connection.

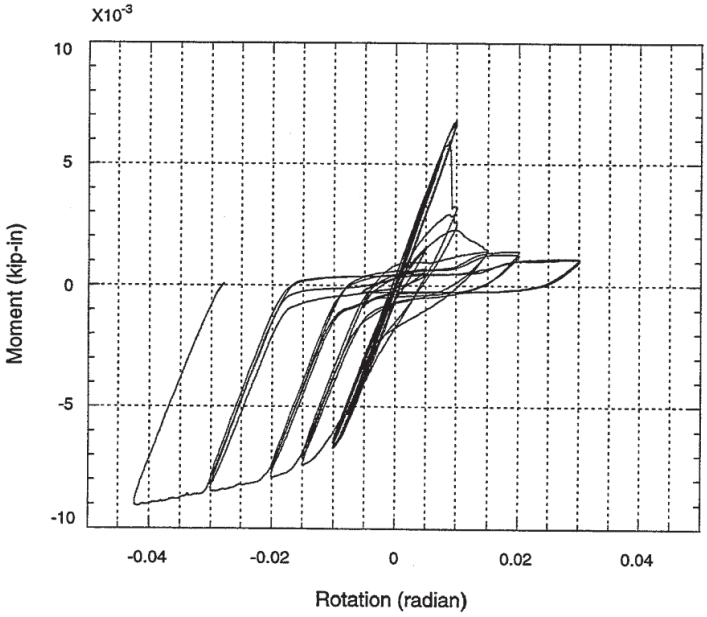

Figure A-2 Moment-rotation response of pre-Northridge connection with fractured lower flange and intact top flange (Lee et al., 1999).

A.2.2 Critical Stress

The critical nominal stress to evaluate fracture in the flanges is calculated by the following formulas, where the critical stress is compared to the axial stress in the member, calculated using standard flexure theory assumptions (i.e., plane sections remain plane):

$$\sigma_{cr} = [K_{IC}/F(a_0)] \quad \text{(A-1)}$$

where for the bottom flange:

$$F(a_0) = 1.2 + 2a_0 \quad \text{(A-2a)}$$

and for the top flange:

$$F(a_0) = 0.5 + 2a_0 \quad \text{(A-2b)}$$

where:

a_0 = the length of the flaw protruding into the flange (inches)

K_{IC} = the critical stress intensity factor of the weld material (ksi $\sqrt{\text{in}}$)

The above formulas are based on a computational fracture mechanics study by Chi et al. (2000) and supporting research by Stillmaker et al. (2015). Note that the $a_0^{1/2}$ term that generally appears in classical fracture mechanics expressions does not appear here since this effect is overwhelmed by the non-uniform stress gradient through the flange. The equations are limited to flaw sizes a_0 of less than the smaller of one-half of the flange thickness or 0.5 inches. In the absence of detailed inspection information, it is not unreasonable to assume a flaw size of $a_0 = 0.1$ inches for flange thicknesses larger than 0.5 inches.

For weld metals and the heat affected zone in the temperature transition region in the temperature-fracture toughness curve, the critical stress intensity factor K_{IC} ksi $\sqrt{\text{in}}$ can be empirically related to the Charpy V-Notch (CVN) toughness. This involves a three step process, wherein the CVN toughness is first converted to a dynamic fracture toughness through the following equation:

$$K_{IC,dynamic} \approx \sqrt{\alpha CVN^* E} \quad \text{(A-3)}$$

where CVN^* is in ft-lb units, E is the elastic modulus in psi units (29,000,000 psi for steel), and α is an empirical calibration coefficient. According to Stillmaker et al. (2015), $\alpha = 7.6$ provides an unbiased mean estimate for typical steel materials, whereas Barsom and Rolfe (1999) recommend a more conservative value of $\alpha = 5$. In the second step, the dynamic value may be converted to a static value, which is more consistent with loading rates during seismic loading. For this purpose, a temperature shift is applied, which implies that the dynamic CVN measurement is equal to the static fracture toughness K_{IC} at a temperature $T_{shift} = 215 - 1.5F_y$ (Barsom

and Rolfe, 1999) below the temperature at which the dynamic toughness is measured. Using F_y – 55 ksi, this results in a temperature shift T_{shift} = 132.5º F. For example, a room temperature (i.e., 70º F) fracture toughness of CVN = 10 ft-lb may be converted to an equivalent K_{IC}(static) = 47 ksi $\sqrt{\text{in}}$ at T = (70-133)º F = -63º F. In the final step, a "Master Curve," per ASTM E1921-16, *Standard Test Method for Determination of Reference Temperature, To, for Ferritic Steels in the Transition Range* (ASTM, 2016), is fit through this point to extrapolate a median static fracture toughness K_{IC} at 70º F. For 10 ft-lb, this value is 107 ksi $\sqrt{\text{in}}$. The Master Curve method also enables the calculation of percentile values following the work of Wallin (1991) which indicated that the toughness of structural steels follows a characteristic Weibull probabilistic distribution.

Table A-1 indicates the median as well as the 5-percentile, and 95-percentile values of K_{IC} assuming room temperature CVN toughness of 5, 10, and 20 ft-lb. According to Chi et al. (2000), 10 ft-lb is the typical CVN value in pre-Northridge weld details. The values shown in Table A-1 are calculated for the expected operating temperature of the structure, i.e., 70º F.

Table A-1 Fracture Toughness Values at 70º F

	K_{IC} (ksi $\sqrt{\text{in}}$)		
CVN (ft-lb)	*5 percentile*	*Median*	*95 percentile*
5	36	51	66
10	65	107	147
20	106	186	261

Referring to Table A-1, assuming CVN of 10 ft-lbs and the median value of α = 7.6, then the median value of K_{IC} (after adjusting for loading rate effects) is calculated as 107 ksi $\sqrt{\text{in}}$ and the 5-percentile value is 65 ksi $\sqrt{\text{in}}$.

Thus, the resulting critical stresses using Equation A.1 and Equation A.2 (and a_0 = 0.1 in for the bottom flange weld is σ_{cr} = 76 ksi and for the top flange weld is σ_{cr} = 153 ksi. This suggests that the both the bottom and the top flanges will yield prior to fracture if the median toughness values are considered. On the other hand, if 5 percentile values are considered, then the critical stress in the bottom flange is 46 ksi, indicating that brittle fracture will occur in many connections with expected yield strengths of 50 to 60 ksi. The likelihood of fracture would also increase in joints with larger weld flaws. These estimates are not inconsistent with the fractures documented after the Northridge earthquake, which likely suffered from selection bias, since connections that yielded or survived may have received less attention. Data from laboratory tests on pre-Northridge connections analyzed by Ramirez et al. (2012), and presented in the next section corroborate this; on average, the connections showed some degree of yielding prior to bottom flange fracture. On the

other hand, the top flange is not likely to be controlled by fracture unless a significantly lower toughness or higher flaw size is present.

It is recommended that frame simulations be conducted with different estimates of fracture toughness and percentile values to characterize the sensitivity of structural response to material toughness.

A.2.3 Critical Plastic Hinge Rotation

Using data from laboratory tests of pre-Northridge Welded Flange-Bolted Web Moment-Resisting Connections, Ramirez et al. (2012) developed fragility functions for the onset of yielding and fracture in terms of story drift. Assuming that the plastic (post-yield) story drift is primarily due to beam yielding, the drift data can be converted into plastic hinge rotations at fracture. The resulting data is plotted in Figure A-3, where the plastic hinge rotation at lower flange fracture is plotted (Figure A-3a) in a counted cumulative distribution function, and as a function of beam depth (Figure A-3b). In Figure A-3a, one set of data points corresponds to the full data set (51 tests of beams ranging in depth from 16 to 36 inches with flange thicknesses between 0.35 to 1.57 inches) and the other is subset of data for 15 of the tests with beams with depths of 30 to 36 inches, and flange thicknesses greater than 0.87 inches. These data show that while many tests did develop the full plastic hinge strength and sustain significant inelastic rotations, the larger beams generally performed worse. In addition, the performance data for the larger beams was highly correlated within a set of lab tests, which presumably reflects systematic differences in weld toughness and quality.

The data shown in Figure A-3a tends to fit a Weibull statistical distribution, where the calculated median (50 percentile) values of plastic hinge rotation are 0.012 radians for the full set and 0.009 radians for the deep beam set. The tenth percentile values are 0.004 and 0.002 radians, for the full set and deep beam set, respectively.

Flange Fracture. Based on the data shown in Figure A-3, for beams that meet the critical stress check, the median critical hinge rotation ($\theta_{p,fr}$) at fracture can be estimated by the following:

$$\theta_{p,fr} = \alpha_f e^{(3.6 + 0.04 d_b)} \tag{A-5}$$

where:

α_f = 1 for bottom beam flanges and 2 for top beam flanges

d_b = beam depth in inches

This expression is plotted in Figure A-3, along with the 80% prediction intervals. The lower interval curve, representing a 10% likelihood of exceedance, can be approximated by multiplying the median capacity of Equation A-5 by 0.3.

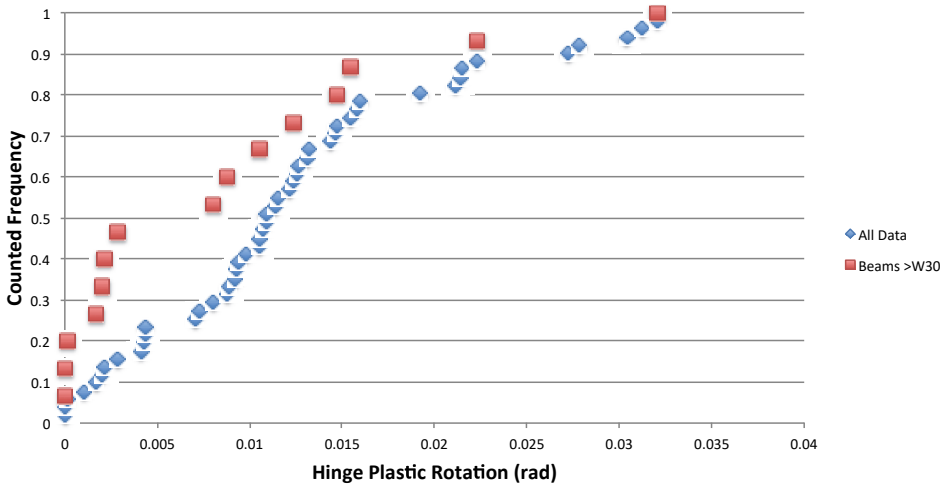

(a)

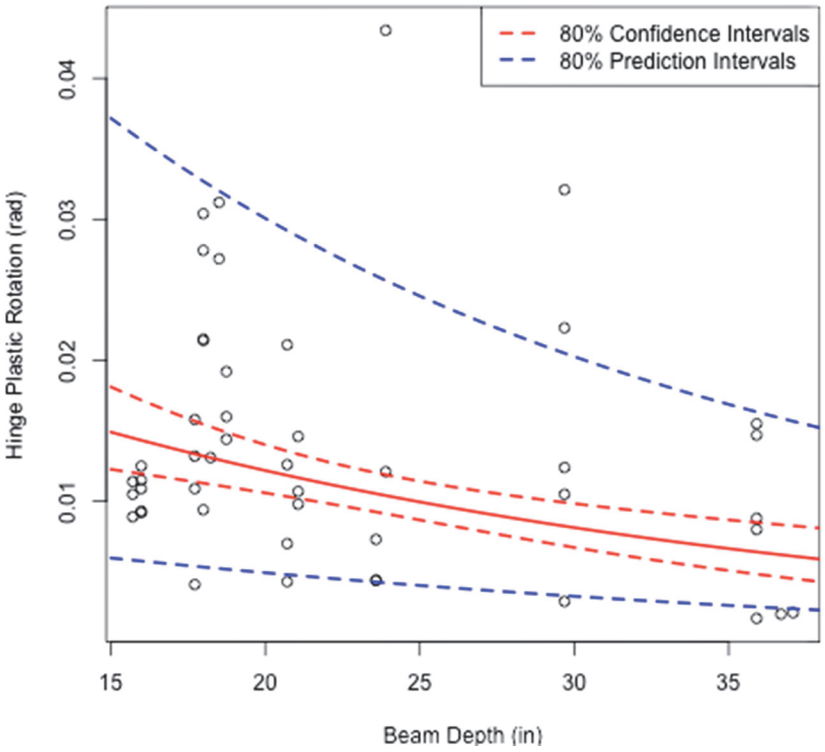

(b)

Figure A-3 Plastic hinge rotation at initial fracture in tests of pre-Northridge beam-column connections: (a) cumulative distribution (fragility) function, separated between all beams and deep beams; (b) trend of rotation capacity with beam depth (data derived from Ramirez et al., 2012).

A.2.4 Recommendations for Pre-Northridge Beam-Column Connections

In light of the data and information presented above, unless there is substantiating information (e.g., measured toughness data of weld and heat affected zones, flaw size characterization, project-specific test data), the following guidelines are

recommended for nonlinear modeling and assessment of steel frames with pre-Northridge beam-column connections:

Median Model Response. Assuming that the flange weld has a median toughness of at least 10 ft-lb (K_{IC} = 107 ksi $\sqrt{\text{in}}$) and a small (a_0 < 0.1 inch) flaw depth, then the beam flanges are expected to yield before fracture for flexural stresses up to 76 ksi, which would cover most frames. In such cases, the beam hinges can be modeled using the critical plastic rotations given by Equations A-5. Otherwise, if the material toughness is assumed to be less than 10 ft-lb or the flaw sizes larger than a_0 equal to 0.1 inch, then the beam flange fracture stress can be calculated accordingly using Eq. A-2a and Eq. A-2b.

Conservative Model Response. Given the large uncertainty in fracture response, the potential consequences of connection fracture should be checked using lower bound estimates of critical stress and critical plastic hinge rotation. In such cases, the critical stress in the beam flanges should be determined from Equations A-2a and A-2b using 10 percentile fracture toughness values from Table A-1 based on the estimated weld CVN toughness and flaw sizes. If the resulting critical fracture stress is less than the effective yield strength of the material, then the flange(s) should be modeled accordingly. To check the lower bound (worst case) effects for flanges that meet the critical stress check, it is suggested to reduce the critical plastic hinge rotation values to their 10 percentile values (equal to 0.3 times the values given by Eq. A.5).

A.2.5 Concentrated Hinge Implementation

Using the guidelines suggested above, a concentrated hinge model can be implemented using a non-symmetric moment-rotation response, similar to the behavior shown in Figure A-2. In positive bending (tension on bottom), the beam hinge loses strength at a moment corresponding to an elastic stress equal to the bottom flange critical fracture stress. Continued loading in this direction results in a steep drop in the moment-rotation curve which levels off at a residual moment strength. The residual connection strength (typically on the order of 20% of the beam strength) can be calculated based on the force couple between the tension strength of the web connection (considering bolt shear, bolt bearing, and shear tab failure) and the top beam flange. In the negative loading direction (tension on top), the beam can be assumed to yield at the effective plastic moment of the beam and sustain rotations out to the plastic hinge limit given by Equation A-5, after which the strength drops off steeply to the residual strength provided by the shear tab connection.

A.2.6 Fiber Hinge Implementation

The fracturing connection behavior can also be represented by a fiber hinge model, where the stress-strain material properties of the fibers are calibrated based on the

critical stress and plastic hinge data. For the bottom beam flange, the material could be assigned as a material with a stress-limited material in tension and a standard elastic-plastic material in compression. The top beam flange would be modeled with a strain-limited material in tension and a standard elastic-plastic material in compression. Fibers in the web region would be assigned tension and compression properties, corresponding to the strength and stiffness of the shear tab plate and bolts. As shown in Figure A-4, such models can be calibrated to generate a pinched hysteresis loop, including the effect of shear tab bolt fracture following beam flange fracture.

The stress-limit for the bottom flange can usually be set directly equal to the critical stress limits defined above. The strain-limit for the top flange generally requires some calibration. As a first-order approximation, the strain limit can be calculated from the plastic rotation limit as follows:

$$\varepsilon_{cr} = \theta_{plastic}(d_b/l_p) \quad \text{(A-6)}$$

where d_b is the beam depth and l_p is the assumed plastic hinge length (usually assumed to be about 20% of the beam shear span length). The equation above assumes that the strain profile is linear through the length of the plastic hinge; this assumption is based on fiber analysis of W sections. In practice, the critical strain-limit should be calibrated to the plastic rotation limits (or connection test data) using the specific fiber-element and software, since the relationship between plastic strain and plastic hinge rotation can depend on many aspects of the analysis model (e.g., element discretization along the member length and through its depth, interpolation functions and numerical integration methods along the member length). Calibration can be conducted using simple cantilever beam models that represent the member size, span-depth ratio, and other characteristics of the structure being analyzed. The aim is to adjust the critical strain of the materials so that the inelastic force-deformation response simulates the equivalent plastic hinge deformation limits. Consider the example of a W24 beam with a shear span of 135 inches shown in Figure A-2. In the test shown, for loading with the top flange in tension, the beam sustains an inelastic rotation of $\theta_{plastic} = 0.03$ radians. Using Equation A-6 (with $l_p = 0.2 \times 135$ inches) the critical plastic strain is $\varepsilon_{cr} = 0.027$.

It should be emphasized that explicit modeling of fracturing connections with fiber hinges suddenly unloading (steep degradation slopes) can significantly increase analysis run times and may lead to non-convergence if time-steps are too large or the number of substeps exceeds the maximum defined for the solver. Prior to running an inelastic analysis with fracturing connections, it is always recommended to run an elastic analysis and perform some hand calculations to help identify where and when fracture may occur in the structure.

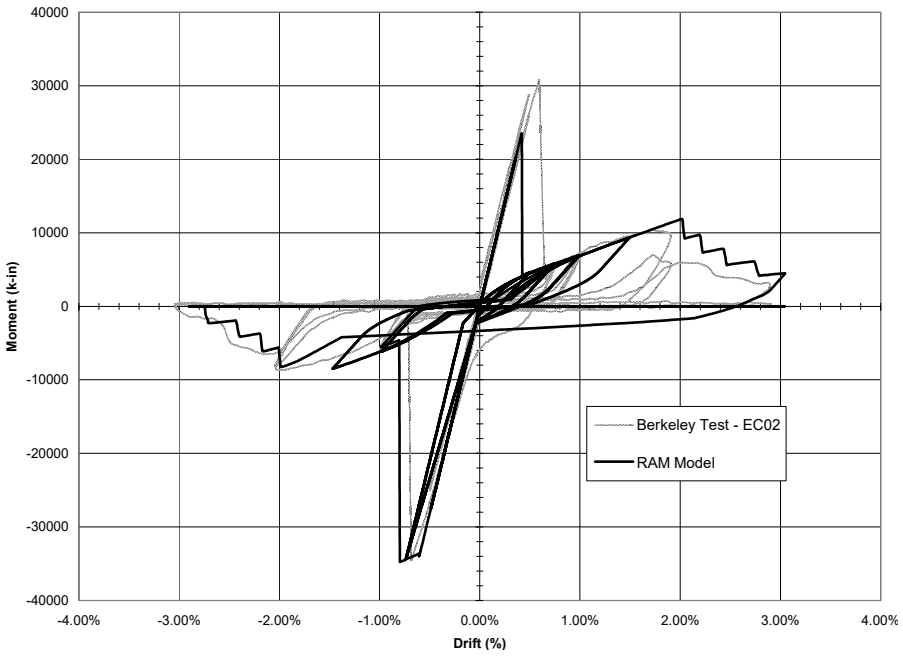

Figure A-4 Example calibration of fiber-hinge model.

A.3 Pre-Northridge Column Splice Connection

Shown in Figure A-5 is the typical configuration of column splices in pre-Northridge moment frames where the compression stresses are carried through a combination of milled bearing and the partial penetration welds, and any net tensile stresses due to the combination of column axial force (tension or compression) plus biaxial bending is carried by the partial penetration welds. Not shown in this figure is the web connection, which was usually a light web plate connection that is primarily for column erection. In some cases the webs may also be connected by a partial penetration weld to resist the calculated shear forces. Note that the flange welds in this figure do not include beveled transitions, which were introduced as a requirement in building codes after the Northridge earthquake.

Given the configuration of partial penetration welds and a light web connection, the column splices are not intended to develop the member section capacity or have significant post-yield ductility. Therefore, the connection behavior is usually controlled by a stress-limit, which at best will develop the intended strength of the partial penetration welds. However, in pre-Northridge connections with low-toughness materials and sharper discontinuities, the welded joint may fracture prior to reaching its strength. Thus, the stress-limit is based on a fracture mechanics approach similar to that described previously for the welded flange connections. Whether or not the welds reach their nominal strength, the post-peak response is likely to have a steep descending branch since any yielding is concentrated over the small throat length of the partial penetration weld.

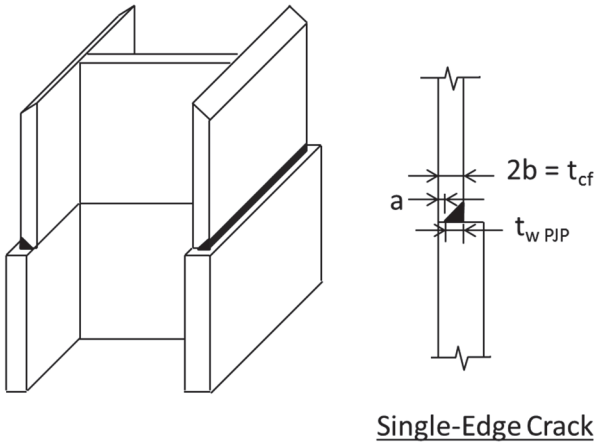

Figure A-5 Typical column splice with partial penetration flange welds.

A.3.1 Critical Stress

The critical stress for the column splice is determined in a similar manner to the beam splice, except that the relationship between nominal stress and the associated fracture indices is different due to the partial penetration weld configuration. The critical stress can be calculated by the following (adapted from Stillmaker et al., 2015):

$$\sigma_{cr} = \frac{K_{IC}}{F\left(\frac{a_0}{t_f}\right)\sqrt{\pi a_0}} \le F_{u,\exp}\left(1-\frac{a_0}{t_f}\right) \le F_{y,\exp} \tag{A-7}$$

where:

$$F\left(\frac{a_0}{t_f}\right) = \left(2.3-1.6\frac{a_0}{t_f}\right)\times\left(4.6\frac{a_0}{t_f}\right) \tag{A-8}$$

and t_f is the thickness of the column flange, a_0 is the internal flaw created by the unfused portion of the flange thickness, $F_{u,exp}$ is the lesser of the weld or base metal ultimate strength, and $F_{y,exp}$ is the expected yield strength of the upper column flange. Note that Equations A-7 and A-8 assume that the column flanges have the same thickness; Stillmaker et al., 2015 provides more comprehensive equations for splices with flanges of different thicknesses. Where $a_0/t_{f,u}$ is equal to 0.5 and K_{IC} = 107 ksi$\sqrt{\text{in}}$ (corresponding to the median value for CVN equal to 10 ft-lb), the critical fracture stress (assuming a 2 inch thick flange with a_0 equal to 1 inch) is 17 ksi, which would govern for a splice with Grade 50 steel ($F_{y,exp}$ = 55 ksi) and E70XX electrodes ($F_{u,exp}$ = 70 ksi).

The critical fracture stress should be compared to the maximum tensile stress in the column above the splice due to the combination of axial load, P, and biaxial bending moments, M_x and M_y. Ideally the maximum tensile stress should be computed based

on the instantaneous member forces at each time step, but it would be conservative to approximate the stress demand based on the combination of stresses from the peak values of P, M_x, and M_y.

A.3.2 Concentrated Hinge Implementation

In concept, the splice fracture behavior that occurs under tension stresses induced by axial load and biaxial bending could be implemented in a concentrated hinge model using a stress-resultant yield surface. However, owing to the non-symmetric nature of failure (fracture in tension, bearing in compression), the stress-resultant hinge formulation is not straightforward. Depending on the how much the axial force changes during the analysis, it may be possible to simplify the concentrated hinge implementation by assuming a fixed value of axial load. However, where column splice fracture has a significant effect on design, it is more straightforward to use a fiber hinge implementation at the splice region.

A.3.3 Fiber Hinge Implementation

Splice fracture may be implemented in a fiber hinge framework with the following considerations:

1. The lower (or larger) connected column may be modeled as a conventional fiber beam-column element. The flange may be modeled with one fiber through the thickness, and also the width (unless biaxial bending is being modeled). The web may be modeled with a suitable number of fibers (~10) to simulate the stress gradient. The flange as well as the web material may be modeled as elastic-plastic in both tension and compression.
2. The upper (or smaller) connected column may be modeled in a manner similar to the lower column, with the exception that the tension behavior in the flanges (at the splice location) is defined with a fracture stress σ_{cr} from Eq. A-7. If the stress is calculated in this manner, the width and thickness of the flange in the fiber model should reflect the dimensions of the flange without consideration of the weld flaw or effective throat. Tension behavior in the web may be represented similarly (i.e., using Eq. A-7, and the web thickness, instead of the flange thickness) if the web splice is a partial joint penetration (PJP) weld. If the web splice is bolted, then the web fibers may be simulated to reflect load deformation response of the bolts. For both the flange and the web, the compression behavior is defined by the base material.

Appendix B

Steel Moment Frame Example Building

B.1 Introduction

The following example documents the development of a computer model and a series of nonlinear analyses to assess building response by implementing these *Guidelines* and *Part I Guidelines* (NIST, 2017a). The simple and discrete nonlinearity modeled is intentional and reflects the modeling a practicing engineer may select as part of their ASCE/SEI 7-16, *Minimum Design Loads and Associated Criteria for Buildings and Other Structures* (ASCE, 2017a) design to satisfy requirements of Chapter 16. As a practical measure, foundations are modeled with elastic beam elements representing the mat foundation. For guidance on modeling soil-structure interaction, the reader is referred to NIST 12-917-21 report, *Soil-Structure Interaction for Building Structures* (NIST, 2012).

This example is organized in the same order typically employed when designing a building per ASCE/SEI 7-16 Chapter 16. Following a building description, the linear analysis and design of the building is presented. The nonlinear modeling of building components, damping and ground motions information is provided, followed by the results of the nonlinear analysis. Conclusions are found at the end of this example. A formal summary design criteria is not explicitly included as part of this example, however, the sections in this example provide a useful guide of relevant information to include in a design criteria. Additional building examples for different lateral systems can be found in other Part II series documents. Other Part II documents provide alternative examples of how to present and report results, as well as important findings which maybe applicable to other building systems and analyses.

B.2 Building Description

The example building is a five-story office building located in San Francisco, California as shown in Figure B-1. The first three stories have overall plan dimensions of 120 ft by 80 ft with a typical story height of 13’-0”. Above the fourth floor, the floor plate setbacks a single bay for an overall plan dimensions of 85 ft by 80 ft. A structural plan of the fourth floor is shown in Figure B-2. A roof top garden is located at the fourth floor setback. Mechanical equipment is located on the roof. A large conference space in the first story at the south-east corner of the building necessitated interruption of the moment frame column at grid lines B4.

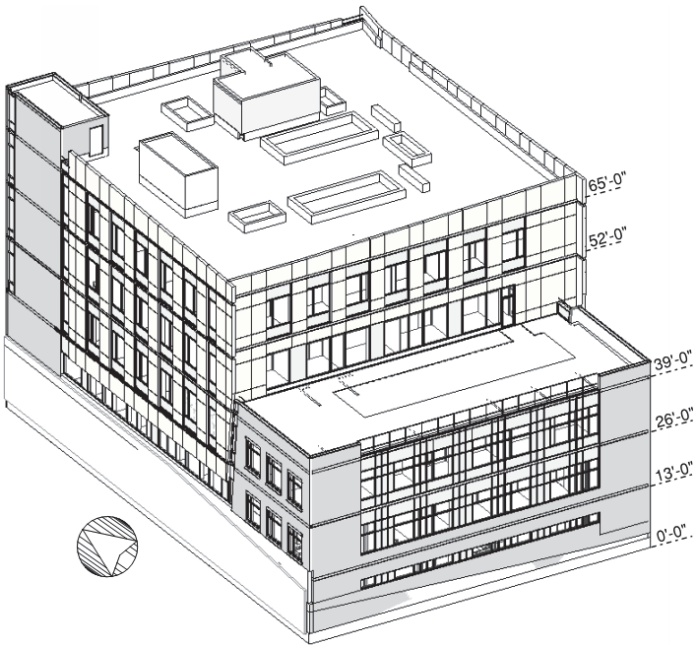

Figure B-1 Five story steel-framed building.

Floor construction consists of a 3-inch normal weight concrete slab over 3-inch ribbed deck spanning between composite beams. Gravity beams are connected to columns with bolted simple shear tabs (knife plates). The foundation consists of a 2.5-foot thick mat foundation at grade.

The building is Risk Category II and located on Soil Type D. The building is analyzed with the modal response spectrum method (MRSA) and designed for Seismic Design Category D. The seismic force resisting system consists of steel moment resisting frames in both the N-S and E-W directions (Figure B-2). A special moment-resisting frame with a response modification factor of *R* of 8 was selected for the building's lateral system. The moment frames are detailed as prequalified reduced beam section (RBS) connections per ANSI/AISC 360-16, *Specification for Structural Steel Buildings* (AISC, 2016d) and ANSI/AISC 358-16, *Prequalified Connections for Special and Intermediate Steel Moment Frames for Seismic Applications* (AISC, 2016b). There are two corner columns, subjected to biaxial bending, at gridlines A4 and D4. The building has the following structural irregularities:

- **Out-of-plane offset irregularity.** The south E-W moment frame shifts a bay at level 4 to accommodate a building setback.
- **Weight irregularity.** Increase in plan dimension at level 4 and a roof top garden located on the same floor add significant mass.
- **Vertical geometric irregularity.** At N-S transition from 2 bays to 3 bays and at E-W transition from 4 bays to 2 bays.

- **In-plane discontinuity in vertical lateral force-resisting element irregularity.** Discontinuous moment frame column in first-story at B4.

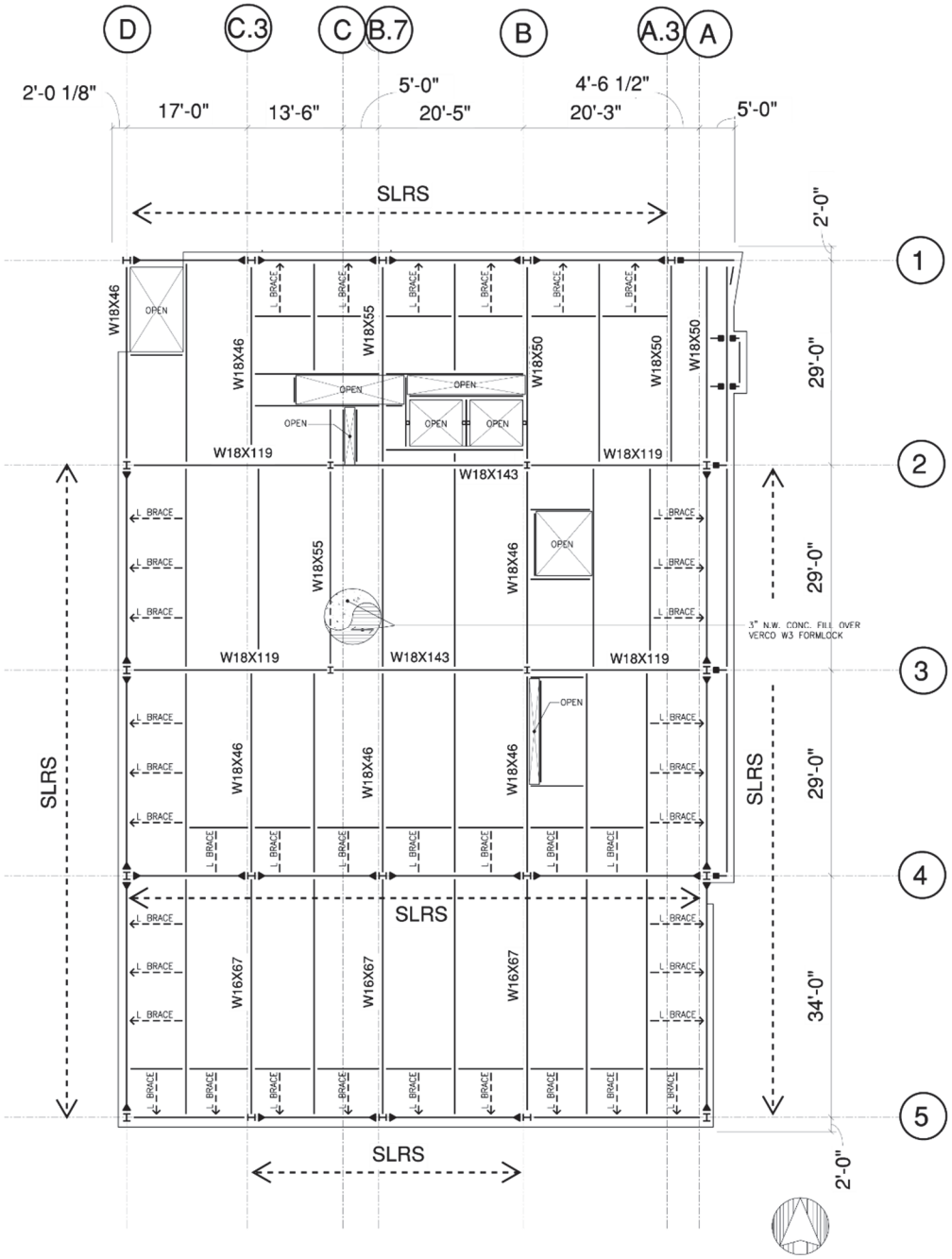

Figure B-2 Fourth floor framing plan of building.

B.3 Linear Structural Analysis and Design

The steel special moment frame is proportioned and designed under elastic analysis per prescriptive requirements of Chapter 12 of ASCE/SEI 7-16 and ANSI/AISC 341-16, ANSI/AISC 358-16, and ANSI/AISC 360. One exception is that the connection design does not satisfy the minimum PZ shear strength per Section

E3.6e.(1) ANSI/AISC 341-16. Weak PZs represent a non-conforming code condition, which is done in this example to help illustrate modeling of PZ response. A Chapter 16 ASCE/SEI 7-16 evaluation of the building is necessary to demonstrate that the PZ shear strains satisfy the design criteria defined in Section B.5. The elastic analysis and design process is not documented in its entirety as the interest of this guideline is focused on the nonlinear modeling and evaluation. However, some important elastic modeling assumptions and analysis results and structural designs are provided below. Table B-1 summarizes linear elastic design information and Table B-2 summaries equivalent lateral force analysis information.

Table B-1 Building Seismic Design Information

Code:	ASCE/SEI 7-16
Occupancy Category:	II
Design Live Loads:	
Roof:	30 psf
Floors:	100 psf
Mechanical and Electrical Rooms:	50 psf
Storage and File Rooms:	150 psf
Earthquake Design Data	
Seismic Importance Factor:	1.0
Mapped Spectral Response:	
S_s:	1.50 g
S_1:	0.67 g
Site Class:	D
Spectral Response Coefficients:	
S_{MS}:	1.50 g
S_{M1}:	1.01 g
S_{ds}:	1.00 g
S_{d1}:	0.67 g
Seismic Design Category:	D
SFRS:	Steel Spectral Moment Frame
Response Modification Coefficient, R:	8.0
Overstrength Factor, Ω_0:	3.0
Detection Amplification Factor, C_d:	5.5
Seismic Response Coefficient, C_s:	0.07
Analysis Procedure:	Modal Response Spectrum
Design Base Shear, V:	431 kips

Table B-2 Summary of Equivalent Lateral Seismic Design Forces

Floor	h_x (ft)	w_x (kips)	$w_x h_x^k$	C_{vx}	F_x (kips)	V (kips)
Roof	65	1241	285870	0.388	167	167
Level 5	52	912	157021	0.312	92	259
Level 4	39	1434	169729	0.230	99	358
Level 3	26	1245	86889	0.118	51	409
Level 2	13	1317	37257	0.051	22	431
Base	0					
		6150	736766	1.00	431	

T = 1.106 s — ρ = 1.0

k = 1.3 — $V = \rho C_s W$ = 431 kips

B.3.1 Modeling Criteria

A three-dimensional mathematical model using RAM Structural System was created for the linear elastic design (see Figure B-3). Elastic displacements are calculated with effective RBS properties.

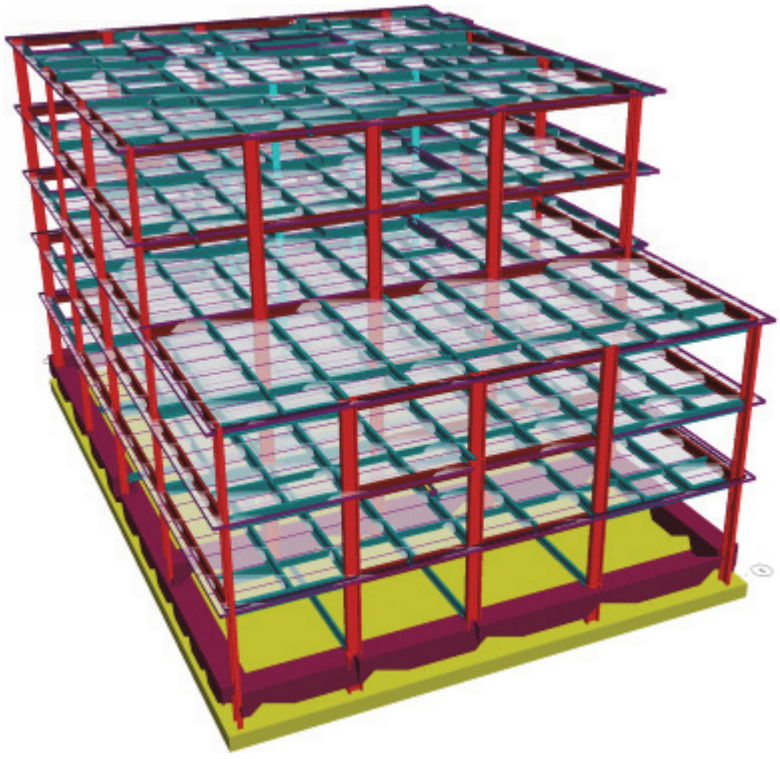

Figure B-3 Structural model used for elastic analysis and design.

B.3.2 Fundamental Periods

The fundamental mode for the N-S direction is 2.01 seconds with 76% mass participation and in the E-W is 1.38 seconds with 81% mass participation. Table B-3 summarizes the modal response characteristics of the building.

Table B-3 Dynamic Properties of Elastic Analysis Model

Mode No.	Period (s)	Mode Mass Ratio		Cumulative Mass Ratio	
		E-W	*N-S*	*E-W*	*N-S*
1	2.01	0.00	0.76	0.00	0.76
2	1.38	0.81	0.00	0.81	0.76
3	0.98*	0.02	0.00	0.83	0.76
4	0.68	0.00	0.15	0.83	0.91
5	0.46	0.10	0.00	0.93	0.91
6	0.36*	0.01	0.00	0.94	0.91
7	0.31	0.00	0.07	0.94	0.98
8	0.24	0.05	0.00	0.98	0.98
9	0.18	0.00	0.00	0.98	0.98
10	0.18	0.00	0.00	0.98	0.98

B.3.3 Modal Analysis

In accordance with ASCE/SEI 7-16 Section 12.9.4, the results of the modal response spectra analysis (MRSA) are scaled such that the MRSA base shear is no less than that of equivalent lateral force procedure. The computed seismic story shears and overturning moments and building story drifts are shown in Table B-4 and Table B-5, respectively.

Table B-4 Design Story Shears and Overturning Moment from MRSA

Story	V_{EW} (kips)	$M_{OT\,EW}$ (kip-ft)	V_{NS} (kips)	$M_{OT\,EW}$ (kip-ft)
5	162	2,103	-201	-2618
4	233	5,128	248	601
3	328	9,386	305	4,564
2	389	14,444	370	9,368
1	431	20,041	431	14,965

Table B-5 Elastic Design Story Drifts and Drift Ratios from MRSA

	E-W				N-S			
	+ecc		-ecc		+ecc		-ecc	
Story	δ_{xe} (in)	Δ_x (radians)	δ_{xe} (in)	Δ_x (radians)	δ_{xe} (in)	Δ_x (radians)	δ_{xe} (in)	Δ_x (radians)
5	1.16	0.7%	1.13	0.7%	2.41	1.5%	2.40	1.5%
4	1.86	1.2%	1.23	0.8%	2.53	1.6%	2.48	1.6%
3	1.37	0.9%	1.69	1.1%	2.46	1.6%	2.51	1.6%
2	1.62	1.0%	1.80	1.2%	2.44	1.6%	2.42	1.6%
1	1.46	0.9%	1.64	1.1%	1.71	1.1%	1.73	1.1%

B.3.4 Structural Design of Primary Moment-Resisting Members

Figure B-4 shows an elevation of the moment frames along grid lines A and D, Figure B-5 grid line 1, Figure B-6 on grid line 4 and Figure B-7 on grid line 5 with beam and column member sizes. Member sizes were selected to satisfy drift requirements of ASCE/SEI 7-16 and ANSI/AISC 341-16. Table B-6 lists the RBS flange cut dimensions.

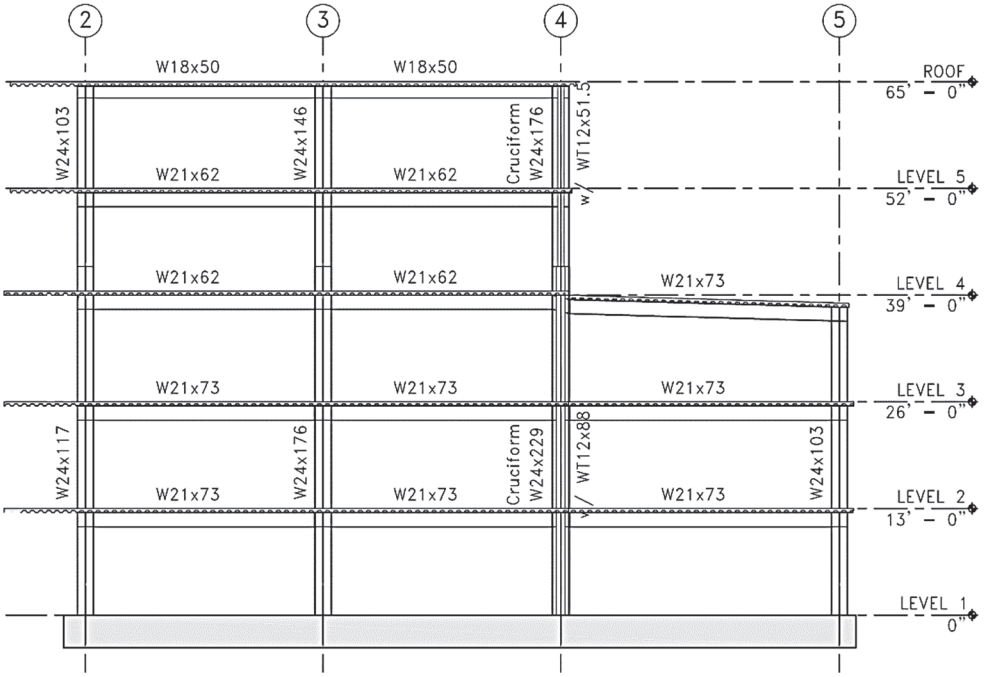

Figure B-4 Framing elevation on column lines A and D.

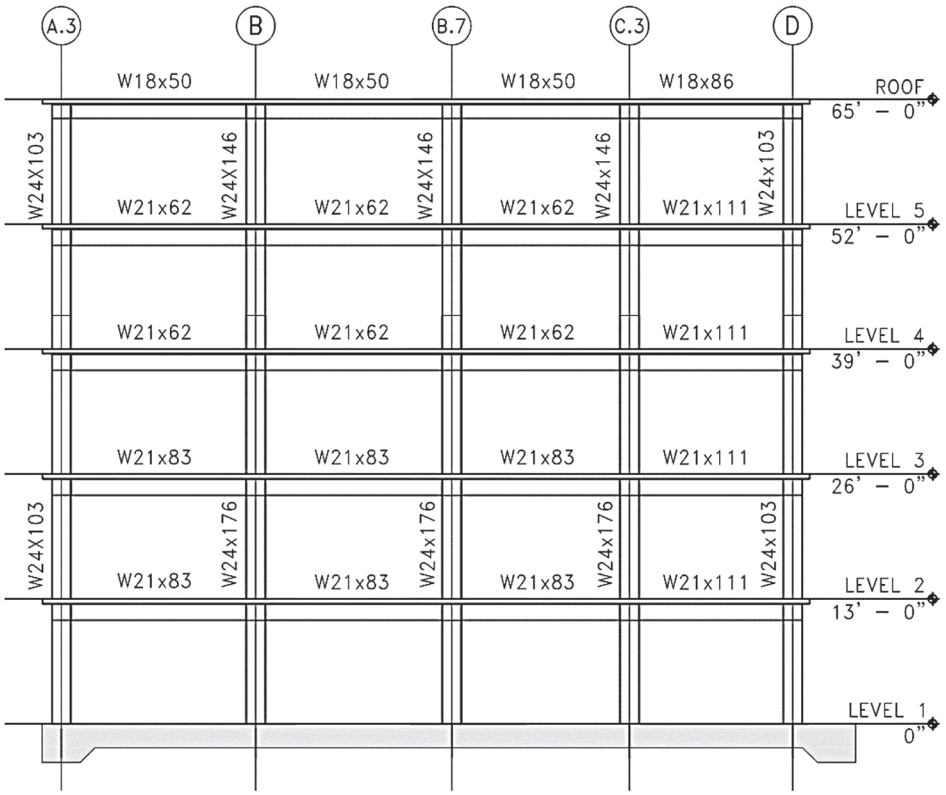

Figure B-5 Framing elevation on column line 4.

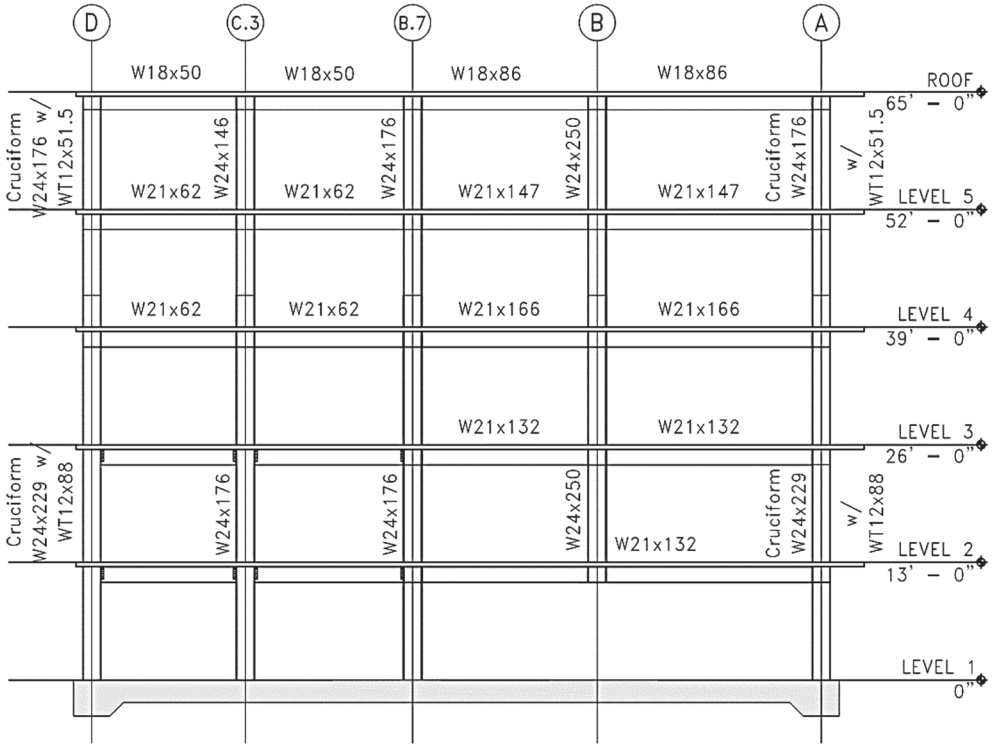

Figure B-6 Framing elevation on column line 5.

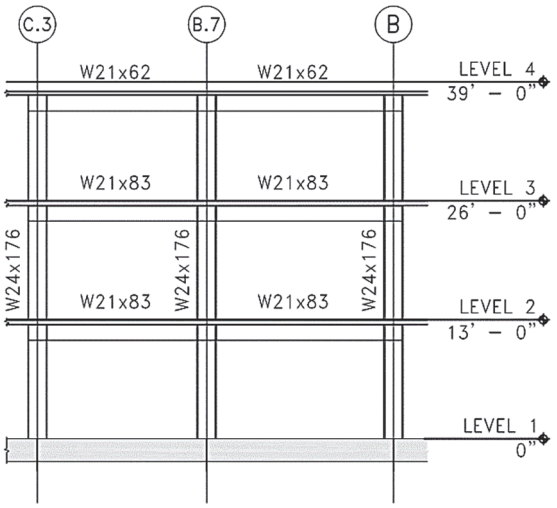

Figure B-7 Framing elevation on column line 1.

Table B-6 Beam Flange Cut Dimensions for RBS Connections

Beam Size	"a" (in)	"b" (in)	"c" (in)	"radius" (in)
W18×50	4-3/4	13-1/2	1-1/2	15-15/16
W18×86	7	13-3/4	2-1/2	10-11/16
W21×62	5-1/4	15-3/4	1-3/4	18-5/8
W21×73	6	15	1-1/2	19-1/2
W21×83	5	15	1-3/4	16-15/16
W21×111	7-3/4	16-1/2	2-3/4	13-3/4
W21×132	7-1/2	15-1/2	2-1/2	13-1/4
W21×147	7-1/2	15-1/2	2-1/2	13-1/4
W21×166	7-1/2	15-1/2	2-1/2	13-1/4

B.3.5 Structural Design of Secondary Members

Table B-7 provides typical connection information for the secondary members shown in the framing plan Figure B-2.

Table B-7 Gravity Framing Connection Information

	Bolts				
Beam Size	*No.*	*Dia.*	*Type*	Web PL. Thickness	Weld Size
W8, W10, C8, C10	2	3/4"	A325-N	3/8"	5/16"
W12, W14, C12	3	3/4"	A325-N	3/8"	5/16"
W16	4	3/4"	A325-N	3/8"	5/16"
W18, W21	5	3/4"	A325-N	3/8"	5/16"
	10	3/4"	A325-N	1/2"	7/16"
W24	7	3/4"	A325-N	3/8"	5/16"

B.4 Nonlinear Modeling of Building

The nonlinear analysis is modeled using V5.0.1 of PERFORM-3D, *Nonlinear Analysis and Performance Assessment for 3D Structures* (Computers and Structures, Incorporated), a program that is commonly used for nonlinear analyses in earthquake engineering practice. The modeling flowchart from the *Part I Guidelines* is revised and adapted to describe the approach for assessing elastic (force-controlled) and inelastic (deformation-controlled) elements in this study, as shown in Figures B-8 and B-9, respectively.

The isometric view of the lateral system in Figure B-10 illustrates the primary components of the perimeter moment frames and the gravity beams supporting the discontinuous column at B4. The more detailed view of the fourth floor framing in Figure B-11 shows both the lateral and gravity elements and the concentrated hinge model types.

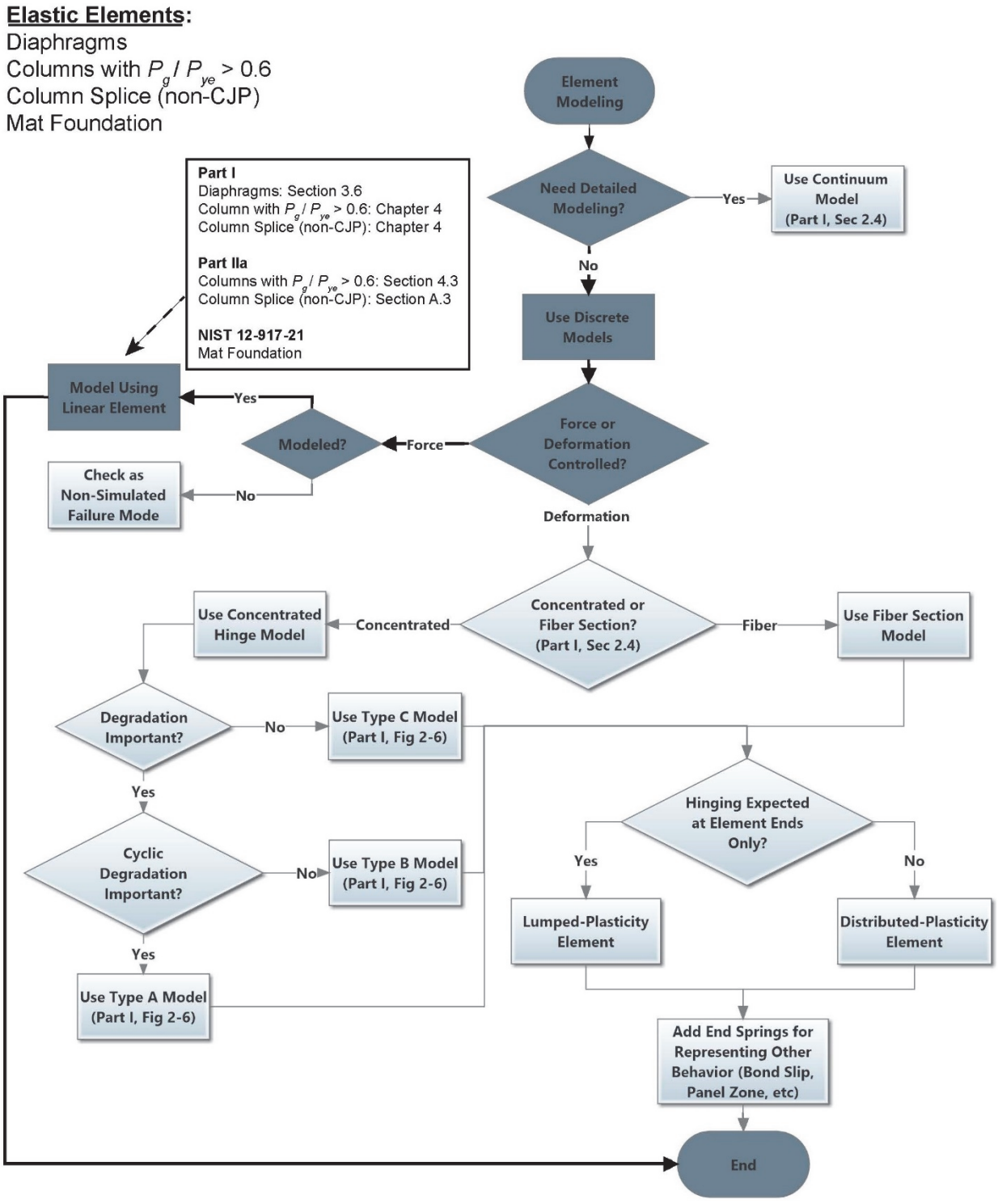

Figure B-8 Flow chart of analysis and assessment approach for force-controlled components.

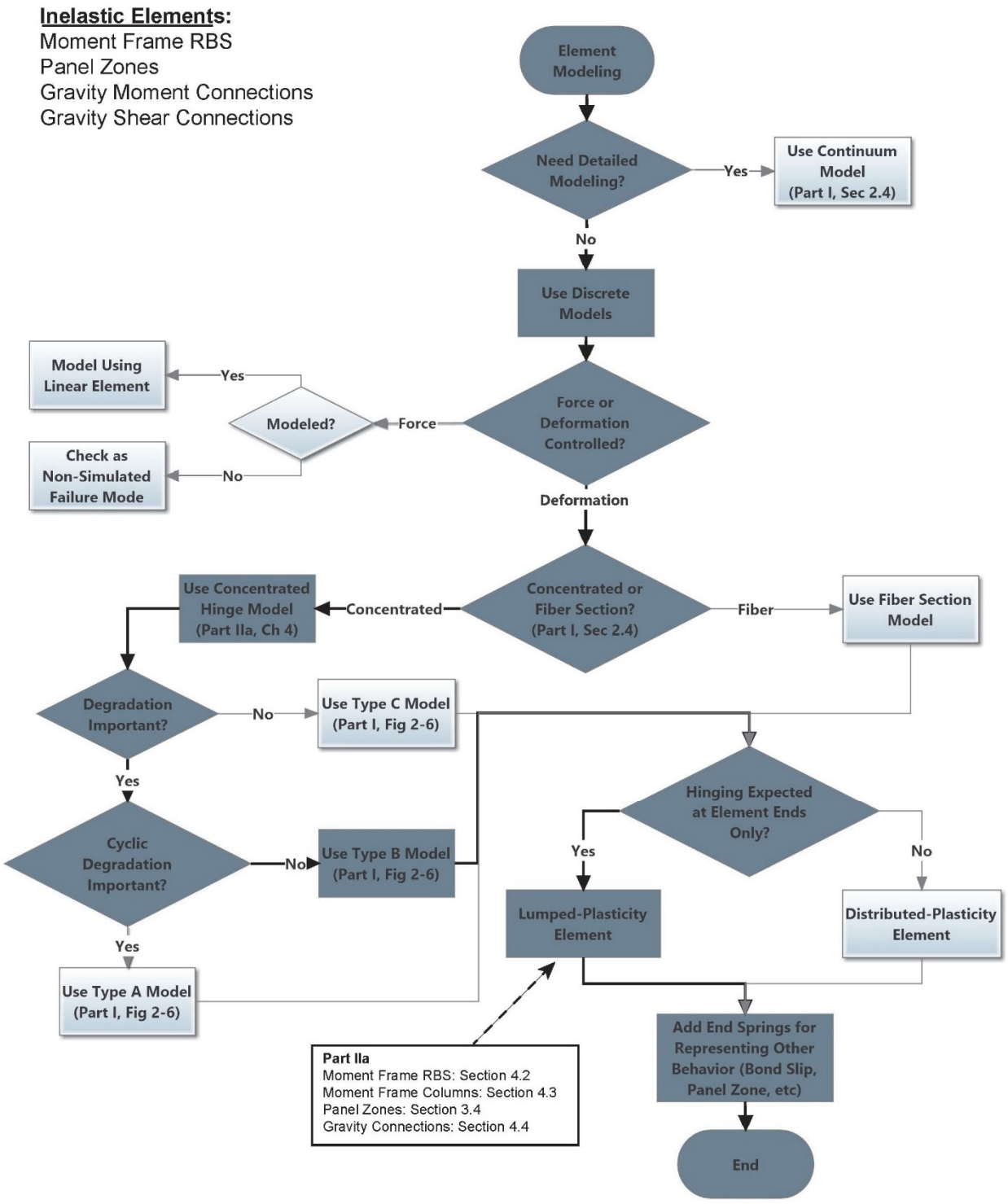

Figure B-9 Flow chart of analysis and assessment approach for deformation-controlled components.

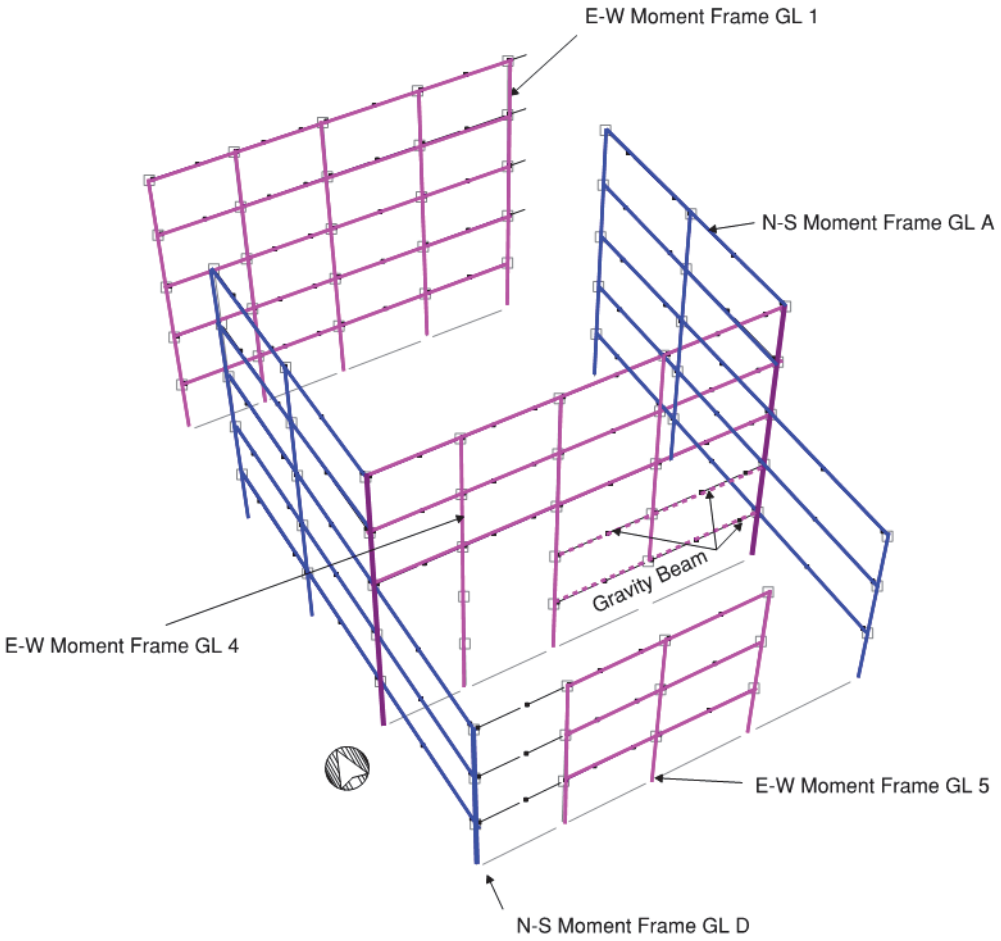

Figure B-10 Isometric view of nonlinear PERFORM-3D analysis model.

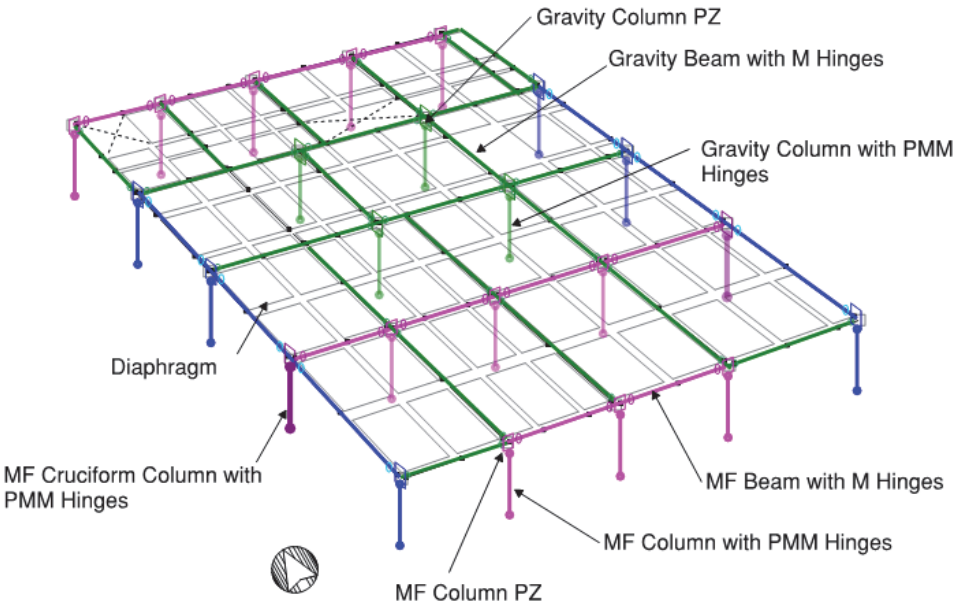

Figure B-11 Isometric view of nonlinear PERFORM-3D analysis model.

B.4.1 Material Strengths

The nominal and expected strengths of the structural materials are summarized in Tables B-8 through B-11. The expected material strengths are used to define all of the component model parameters and expected strengths of force-controlled components.

Table B-8 Structural Steel Nominal and Expected Strengths

Structural Steel Properties		Strength	
Shape	*Grade*	*Nominal*	*Expected*
Wide Flange Shapes	ASTM A992	F_y = 50 ksi	F_{ye} = 55 ksi
HSS Rectangular	ASTM A500 Gr C	F_y = 50 ksi	F_{ye} = 65 ksi
HSS Round	ASTM A500 Gr C	F_y = 46 ksi	F_{ye} = 59 ksi
Pipe	ASTM A53 Gr B	F_y = 35 ksi	F_{ye} = 56 ksi
Angle and Channel	ASTM A36	F_y = 36 ksi	F_{ye} = 54 ksi
Misc. PL	ASTM A572 Gr 50	F_y = 50 ksi	F_{ye} = 55 ksi

Table B-9 Steel Bolts Nominal and Expected Strengths

Shape	Grade	Strength Expected
High Strength Bolts	ASTM A325-N	F_u = 120 ksi

Table B-10 Concrete Nominal and Expected Strengths

Concrete Properties		Strength	
Purpose	*Weight*	*Nominal*	*Expected*
Foundations	NW	f_c' = 4000 psi	f'_{ce} = 5200 psi
Walls	NW	f_c' = 4000 psi	f'_{ce} = 5200 psi
Shotcrete	NW	f_c' = 4000 psi	f'_{ce} = 5200 psi
Fill over metal deck	NW	f_c' = 3000 psi	f'_{ce} = 3900 psi

Table B-11 Concrete Reinforcement Nominal and Expected Strengths

Concrete Reinforcement Properties		Strength	
Purpose	*Grade*	*Nominal*	*Expected*
Reinforcing steel	ASTM A615 Gr 60	F_y = 60 ksi	F_{ye} = 72 ksi
Welded wire fabric	ASTM A1064 GR 65	F_y = 65 ksi	F_{ye} = 72 ksi

B.4.2 Moment Frame Beam

Moment frame beams are modeled as deformation controlled elements using the Cyclic Envelope for RBS beams or non-RBS (as appropriate) presented in Section 4.2.2 and modified to account for composite behavior per Section 4.2.5. The

different positive and negative force deformation behavior is modeled through the use of an asymmetric moment hinge in PERFORM-3D. Inelastic behavior is assigned to a compound element with moment hinges at the ends of moment frame beams connected to PZs. The hinge is located at a distance from the face of the column equal to $a + b/2$ (the RBS cut dimensions) for RBS beams and $d/2$ (the beam depth) for non-RBS beams.

B.4.3 Moment Frame Column

All columns in the model have axial loads below the limiting value of $P_g/P_{ye} < 0.6$ (for force-controlled components in ASCE/SEI 41-17), such that they are modeled as deformation controlled elements using the Cyclic Envelope for wide-flange column members, as presented in Section 4.3.2 in these *Guidelines*. Inelastic behavior is assigned to a compound element with PMM hinges at the top and bottom of each column. The columns at grid lines A4 and D4 are modeled as cruciform columns per Section 4.3.2. Both columns have L/r_y values less than the lower bound L/r_y limit used to define the backbone. ANSI/AISC 341-10, *Seismic Provisions for Structural Steel Buildings* (AISC, 2010b) permits the use of a corner column condition with a preapproved connection for either a cruciform or box column.

B.4.4 Panel Zone

The Auto Connection Panel Zone model in CSI-Perform is defined by the Krawinkler (1978) PZ model. CSI-Perform's Auto Connection Panel Zone includes the formulas for the capacity and stiffness of the Krawinkler PZ, which are described in Section 3.4. In PERFORM-3D, PZs are assigned directly to nodes. The alternative PZ model described in Section 3.4 can be defined with a Connection Panel Zone element where backbone parameters are manually entered.

B.4.5 Diaphragm

All diaphragms are modeled as semi-rigid, using shell finite elements. Parameters to define the effective stiffness for out-of-plane plate action and in-plane membrane action are assigned by varying slab thickness in the slab cross section definition. The plate and membrane stiffness are generated with an elastic slab material defined with the expected modulus of elasticity of the concrete over metal deck and Poisson ratio for a shear modulus of $0.4E_c$. To model the $0.3E_c$ effective membrane stiffness, the 3-inch thickness of concrete over metal deck is modified by the ratio, $0.3E_c/0.4E_c$ = 2-$^1/_4$ inches. For the $0.05E_c$ effective membrane stiffness, the ratio $0.05E_c/0.4E_c$ = $^3/_8$ inches. Figure B-12 identifies where $0.05E_c$ elements were assigned on the fourth floor for the lower bound diaphragm stiffness model.

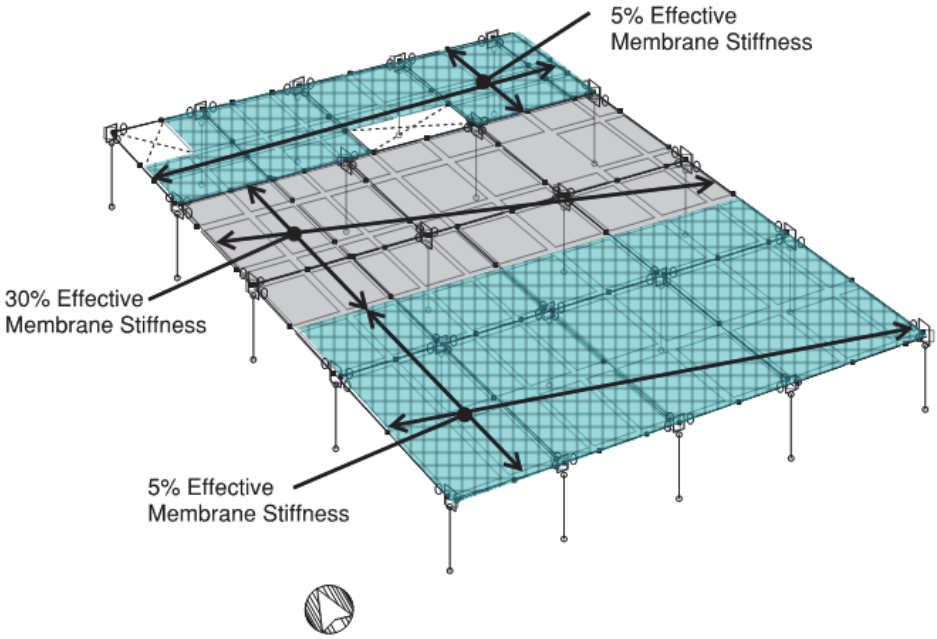

Figure B-12 Diaphragm model using shell finite elements.

B.4.6 Gravity Beam

All gravity framing connections are modeled as deformation controlled elements per Section 4.4. The different positive and negative force deformation behavior is modeled through the use of an asymmetric semi-rigid moment hinge in PERFORM-3D. Inelastic behavior is assigned to a compound element with semi-rigid moment hinges at the ends of gravity frame beams connected to PZs. The hinge is located beyond an auto end zone component (with length equal to half the column depth) at the face of the column.

B.4.7 Damping

Modal damping is primarily used to account for inherent damping in the structure. Specifically, 2% modal damping for all modes in combination with 0.1% Rayleigh damping at periods equal to $2T_1$ and $0.1T_1$, where T_1 is the first fundamental mode period is modeled. The small amount of Rayleigh damping adds a negligible amount of damping within the period range of interest to the total amount of damping, i.e., the 2% modal damping plus the intrinsic hysteretic camping. Rayleigh damping is a useful tool to damp localized, short period modes, which improves the numerical convergence of the analysis. In assigning Rayleigh damping, one should be careful to avoid cases where Rayleigh damping may over dampen higher mode effects in the building. This situation can arise when the period range of interest in a building is broad, e.g., such as for capturing high frequency floor accelerations that may affect nonstructural components.

B.4.8 Ground Motions

Ground motions are developed based on the risk-targeted Maximum Considered Earthquake (MCE_R). The target response spectrum was developed per ASCE/SEI 7-16 Section 16.2.1.1 Method 1 (based on the Uniform Hazard Spectrum). Eleven horizontal ground motion pairs were selected. It could be argued that vertical ground motion components are required per ASCE/SEI 7-16 Section 16.1.3, due to the discontinuous column at B4. However, since this is considered to be beyond the scope of this simplified example, vertical ground motion components were not considered in the analysis.

Ground motions were selected from events within the same general tectonic regime and have magnitudes and fault distances that are generally consistent with the events controlling MCE_R ground motion. This site's location in San Francisco is located outside the near-fault zone and within the deterministic cap. Ground motions were scaled between the period range of $2.0T_1 = 3.2$ s and $0.2T_2 = 0.23$ s per ASCE/SEI 7-16 Sections 16.2.3.1 and 16.2.3.2. Figure B-13 shows the target response spectrum developed for this building and site.

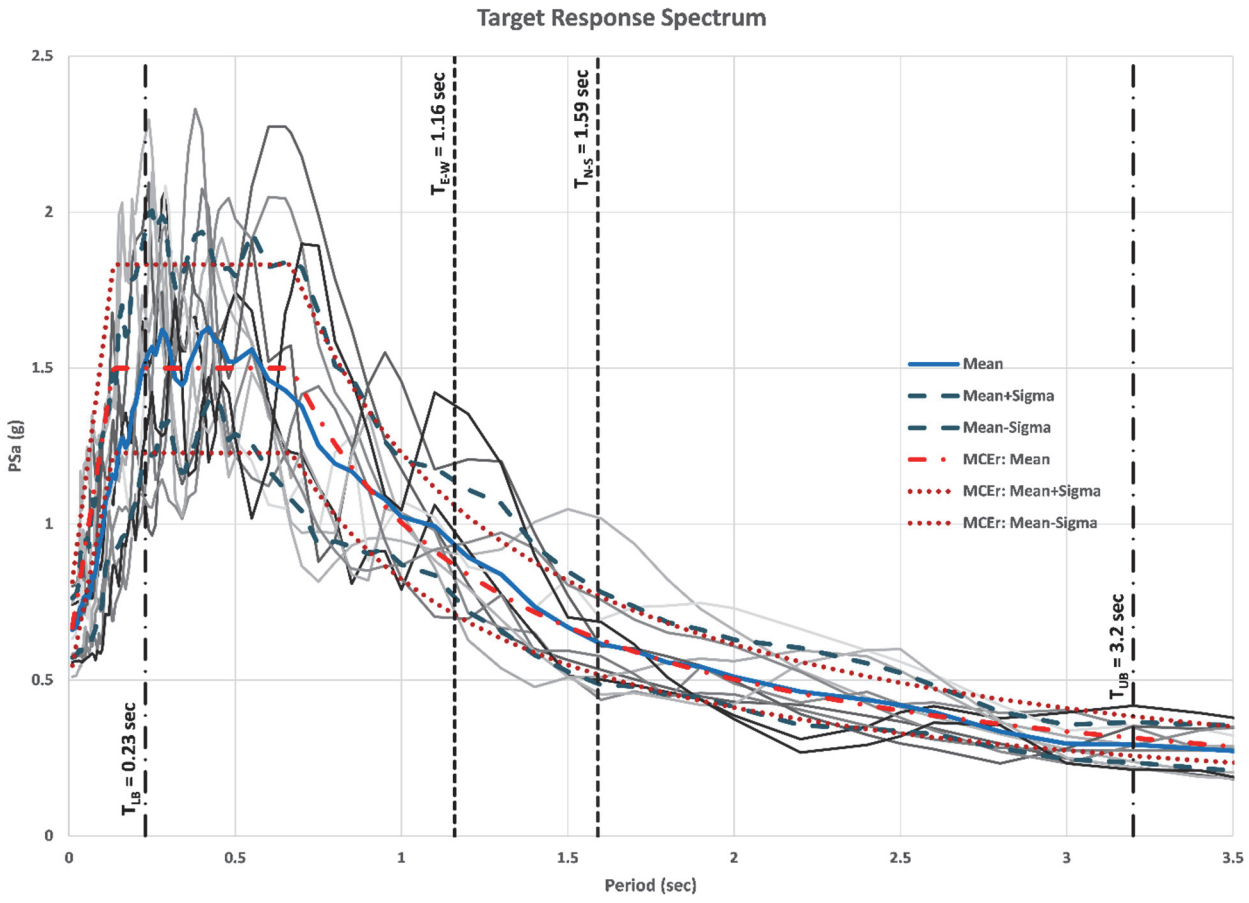

Figure B-13 Response spectra of the eleven pairs of ground motions that are selected and scaled to the MCE Uniform Hazard Spectrum.

B.5 Nonlinear Response History Analysis

In accordance with Chapter 16 of ASCE/SEI 7-16, the gravity load combination used in the nonlinear dynamic analysis is $1.0D + 0.5(0.4L_0)$ where L_0 is the unreduced live load. Tables B-12 and B-13 summarizes the acceptance criteria checks for deformation controlled actions (modeled inelastically) and force controlled actions (modeled elastically) in accordance with ASCE/SEI 7-16 Section 16.1.4. Please note that at the time Tables B-12 and B-13 were developed the ASCE/SEI 41-17 Standard was still in development.

Table B-12 Demand Parameters and Acceptance Criteria for ASCE/SEI 7-16 MCE Analysis – Inelastic Behavior

Item	Action	Type	Acceptance Criteria	Capacity
RBS Hinges	Deformation-Controlled	Ordinary	$\theta_u \le \theta_{CP}$	ASCE/SEI 41-17 Table 9-6.2 and NIST GCR 17-917-45 Sec 4.5
Non RBS Hinges at Transfer	Deformation-Controlled	Critical	$\theta_u \le \theta_{CP}$	ASCE/SEI 41-17 Table 9-6.2 and NIST GCR 17-917-45 Sec 4.5
Column with $P_G/P_{ye} > 0.6$	Deformation-Controlled	Critical	$\theta_u \le \theta_{CP}$	ASCE/SEI 41-17 Table 9-6.1 and NIST GCR 17-917-45 Sec 4.5
Column Hinges at Base	Deformation-Controlled	Ordinary	$\theta_u \le \theta_{CP}$	NIST GCR 17-917-45 Sec 4.5
Panel Zone	Deformation-Controlled	Ordinary	$\gamma_u \le \gamma_{CP}$ and $\gamma_{PZ,limit}$	ASCE/SEI 41-17 Table 9-6.2 and ASCE/SEI 41-17 Eq. 9-18 and NIST GCR 17-917-45 Sec 4.5
Gravity Connection	Deformation-Controlled	Ordinary	$\theta_u \le \theta_{CP}$	ASCE/SEI 41-17 Table 9-6.2 and NIST GCR 17-917-45 Sec 4.5

Table B-13 Demand Parameters and Acceptance Criteria for ASCE/SEI 7-16 MCE Analysis – Elastic Behavior

Item	Action	Type	Acceptance Criteria	Capacity
Non-Transfer Diaphragms	Force-Controlled	Ordinary	$V_{ne} \ge 1.5(V_s - V_{ns}) + V_{ns}$	ACI 318
Transfer Diaphagms	Force-Controlled	Critical	$V_{ne} \ge 2.0(V_s - V_{ns}) + V_{ns}$	ACI 318
Column with $P_G/P_{ye} > 0.6$	Force-Controlled	Critical	$P_{ne} \ge 2.0(P_s - P_{ns}) + P_{ns}$ and $M_{ne} \ge 2.0(M_s - M_{ns}) + M_{ns}$	AISC 341 and 360
Column Splice (non-CJP)	Force-Controlled	Critical	$P_{ne} \ge 2.0(P_s - P_{ns}) + P_{ns}$ and $M_{ne} \ge 2.0(M_s - M_{ns}) + M_{ns}$ and $V_{ne} \ge 2.0(V_s - V_{ns}) + V_{ns}$	NIST GCR 17-917-45 Sec 4.5
Mat Foundation	Force-Controlled	Ordinary	$q_{ne} \ge 1.5(q_s - q_{ns}) + q_{ns}$	Geotechnical Report and ASCE/SEI 41-17 Chapter 8

B.5.1 Nonlinear Model Fundamental Periods

The modal periods of the PERFORM-3D model are summarized in Table B-14. Comparing these periods to those of the elastic ETABS model (Table B-3), inclusion of secondary (gravity) member stiffness significantly decreased the primary vibration periods of the building. For example, the periods for the first two modes are 2.0 s and 1.4 s in the elastic model, in contrast to periods of 1.6 s and 1.2 s in the nonlinear model. By including modes 1 to 5, 90% mass participation in the two horizontal principal directions of the building is achieved with periods down to about 0.37 s.

Table B-14 Vibration Periods from Nonlinear PERFORM-3D Model

		Mode Mass Ratio		Cumulative Mass Ratio	
Mode No.	Period (s)	*E-W*	*N-S*	*E-W*	*N-S*
1	1.59	0.00	0.77	0.00	0.77
2	1.16	0.73	0.00	0.73	0.77
3	0.77*	0.09	0.00	0.82	0.77
4	0.53	0.00	0.14	0.82	0.91
5	0.37	0.10	0.00	0.92	0.91
6	0.29*	0.01	0.00	0.92	0.91
7	0.27	0.00	0.06	0.92	0.97
8	0.18	0.05	0.00	0.97	0.97
9	0.14*	0.01	0.00	0.98	0.97
10	0.14	0.00	0.02	0.98	0.99

* Torsional Mode

B.5.2 Story Drift

Story drift ratios under the MCE level ground motions for the moment frames at grid lines 1 and D are shown in Figure B-14. The peak transient drift ratios at each story for each ground motion are presented in order from the bottom of the plot, along with the mean of the peak story drifts represented by the top red shaded bar. In the N-S direction, story drift demands are similar for grid lines A and D, where the largest drifts occur in the fifth story, with a mean story drift ratio of 3.3% and a range of 2.2% to 6.2%. In the E-W direction the largest story drift demands occur at grid line 1, where the largest drifts occur in the second story with a mean story drift of 2.2% and a range of 1.2% to 3.3%. The N-S and E-W drifts are roughly 1.3 to 2.2 times and 1.6 to 2.5 times larger than the drifts approximated by the DBE linear analysis.

Chapter 16 ASCE/SEI 7-16 limits drift to twice the standard design limits of ASCE/SEI 7-16 Table 12.12-1. For this building (Risk Category II non-masonry building taller than four stories), this implies a mean story drift limit of 4%, which is satisfied in all stories and column lines.

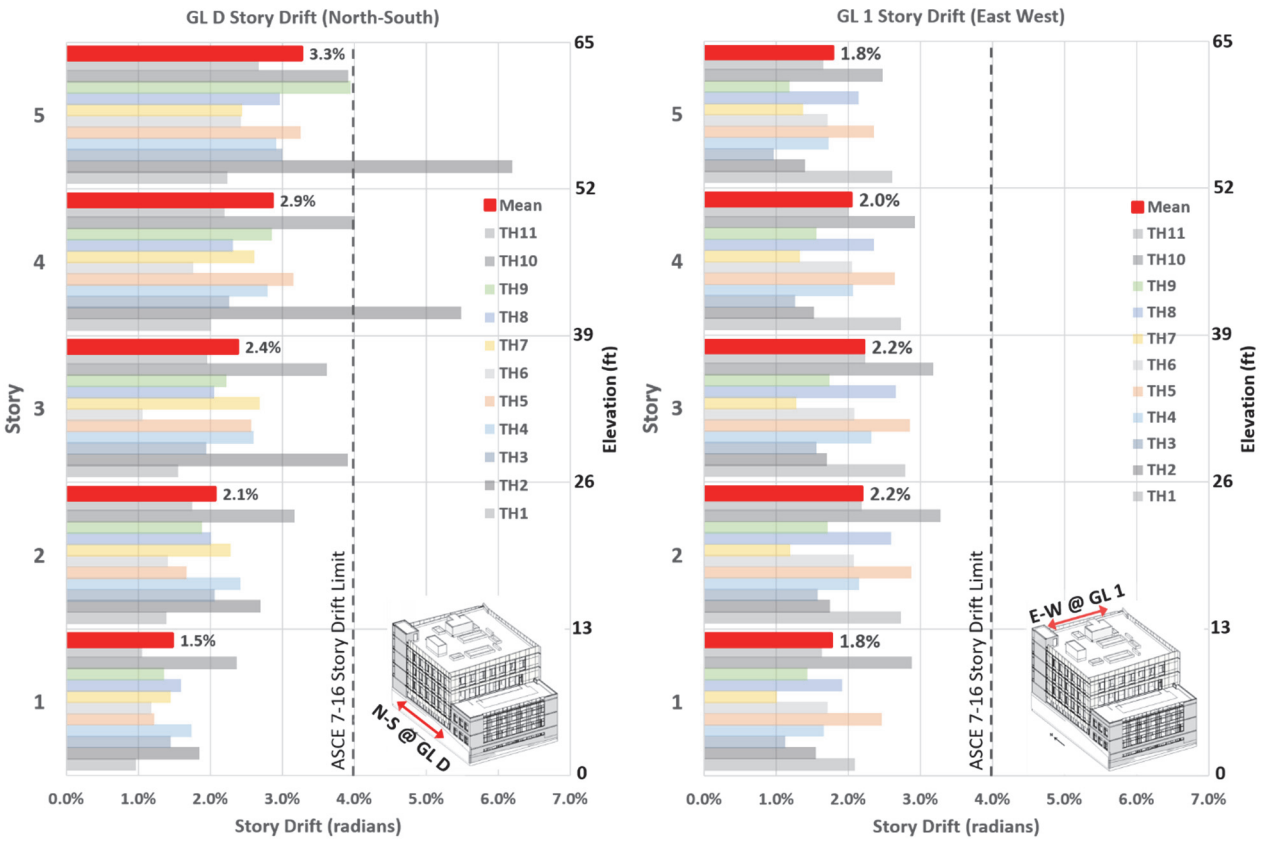

Figure B-14 Peak story drift ratios under MCE ground motions.

Figure B-15 shows the peak story drifts for an alternate analysis model in which gravity beams are modeled as pin-pin. Modeling gravity beams as pin-pin is a common modeling assumption in new design. Comparing the values in Figures B-14 and B-15, the mean story drifts increase by less than 10% and peak story drifts by less than 20% when gravity beams are modeled as pin-pin compared to the model where gravity beam strength and stiffness are included in the model.

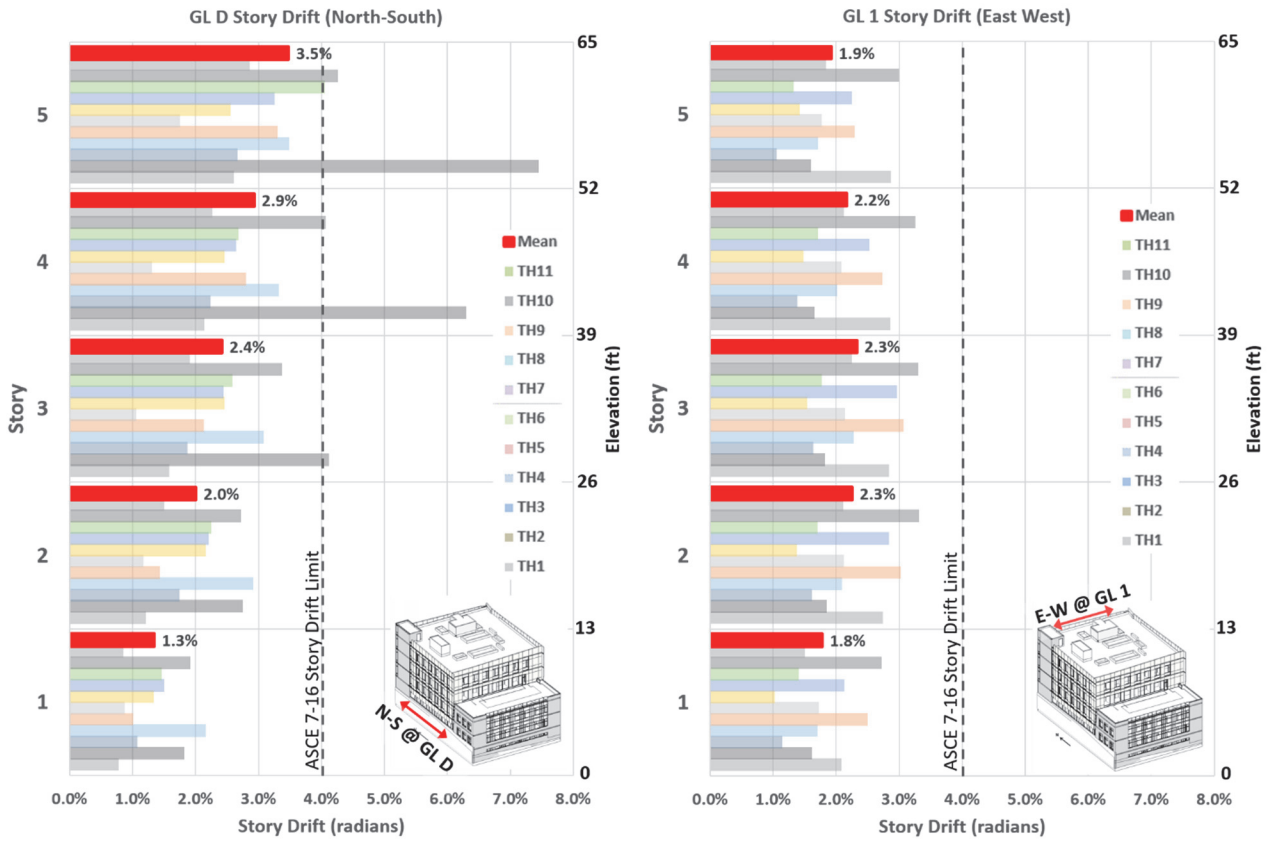

Figure B-15 Peak story drift ratios under MCE ground motion determined using an alternative model with pin-connected gravity beams.

B.5.3 Story Shear and Overturning Moment

Story shear and overturning moment in the N-S and E-W directions are shown in Figures B-16 and B-17, respectively. Section cuts were defined at each story level to output story shear and moment from the PERFORM-3D model. Results for each ground motion are presented at each story, along with the mean MCE_R story shear or moment at each story, represented by the top red shaded bar. The dashed lines represent various DBE level story shears or moments determined using $R = 8$ and $R/\Omega = 8/3 = 2.67$. The N-S and E-W shears are roughly 3.5 to 4.5 and 4.7 to 6.1 times larger respectively than the DBE story shears (with $R = 8$) previously reported in Table B-4. The MCE_R base shears are roughly 1.7 and 1.3 times larger than the DBE base shear including overstrength (with $R/\Omega = 2.67$) for the N-S and E-W directions, respectively. The MCE_R base moments are roughly 2.2 and 1.4 times larger than the DBE base moments, including overstrength, for the N-S and E-W directions, respectively.

Figure B-16 Peak story shear forces under MCE ground motions.

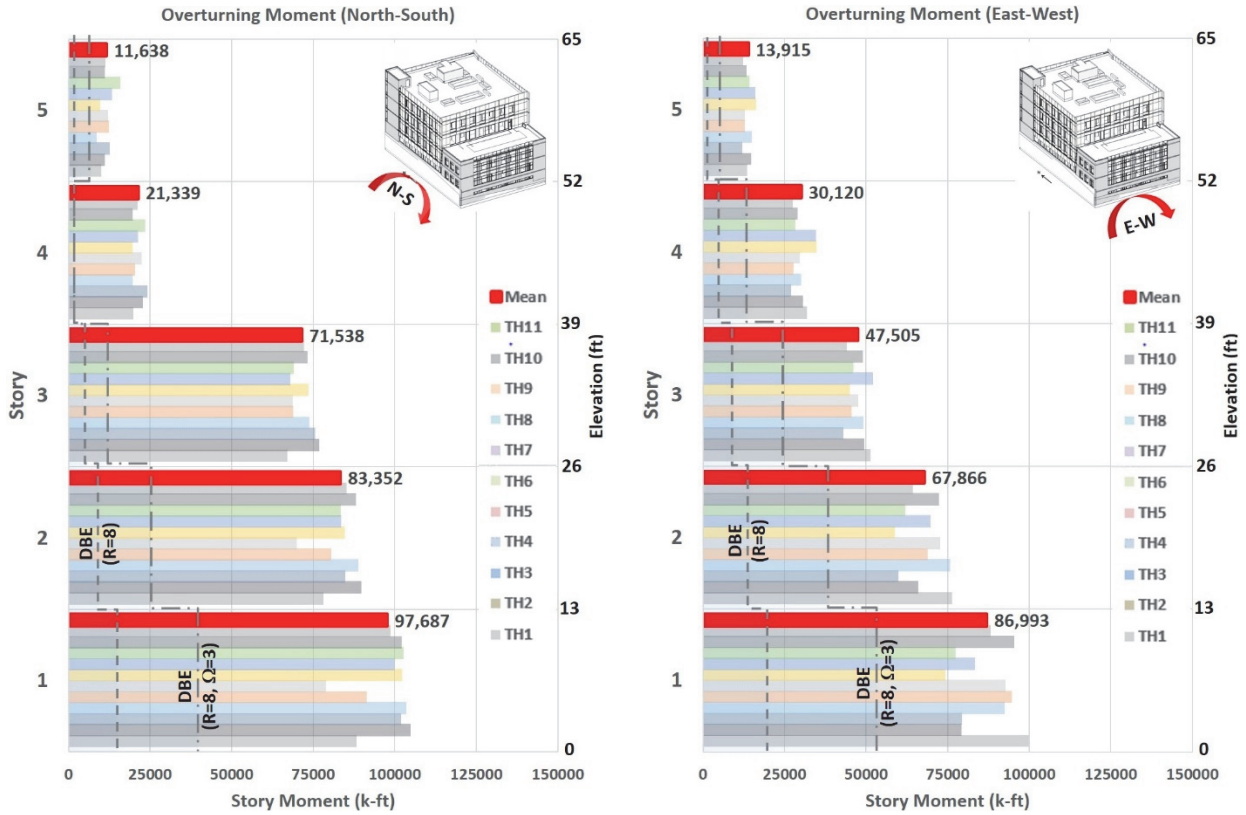

Figure B-17 Overturning moment under MCE ground motions.

B.5.4 RBS Hinges

RBS hinge rotation results along grid line A are shown in Figure B-18. The results are reported for each ground motion, along with the mean hinge rotation represented by the top red shaded bar. The largest mean rotation demand for a RBS hinge occurs on the roof at grid line A4, where the mean rotation is 0.027 radian with a range of 0.011 to 0.052 radian.

The moment frame beams in the building are evaluated using two alternative criteria. One criterion is per ASCE/SEI 7-16 with ASCE/SEI 41-17 Collapse Prevention (CP) acceptance rotation limits, and the second criterion is based on the limits on modeling parameters in Sections 4.2.2 and 4.2.5. The purpose of showing both is to compare the two documents.

The ASCE/SEI 41-17 CP rotation limit for RBS beams is $\theta_{CP} = 0.07\text{-}0.00030d$, where d is the beam depth as defined in ASCE/SEI 41-17 Table 9-6. This limit, θ_{CP} needs further adjustment using modification factors from ASCE/SEI 41-17 Section 9.4.2.4.3 to account for the variation in the detailing of continuity plates, the strength of the panel zone, the beam span-to-depth ratio, and the slenderness of the beam web and flanges. Based on these requirements, the θ_{CP} rotation limit is 0.052 radians and the maximum ratio of the mean rotation demand to capacity, θ_u/θ_{CP} is 0.52.

According to Chapter 16 of ASCE/SEI 7-16, the deformation controlled beam rotations should also satisfy, $Q_u \leq \phi_s Q_{ne}$, where $\phi_s = 0.5/Ie$ for an ordinary component per ASCE/SEI 7-16 Table 16.4-2 and Q_{ne} is the rotation at which point gravity load resistance is lost. Assuming the loss of gravity resistance as being equal to the ultimate ductile fracture rotation of 0.08 radians per Section 4.2.2, the limit state check would be $\theta_u < 0.4$ radians. Using this criterion, the maximum ratio of mean rotation demand to capacity ratio, θ_u/θ_{ne} is 0.50. Moreover, only a couple ground motions have hinge rotation demands that exceed 0.04 radians, and all are less than the ultimate limit on the analysis model of 0.08 radians.

Comparing the two alternative acceptance criteria, the second approach (ASCE/SEI 7-16 resistance factor with the Section 4.2.2 rotation limit) is more stringent than the former (ASCE/SEI 41-17 θ_{CP} limit).

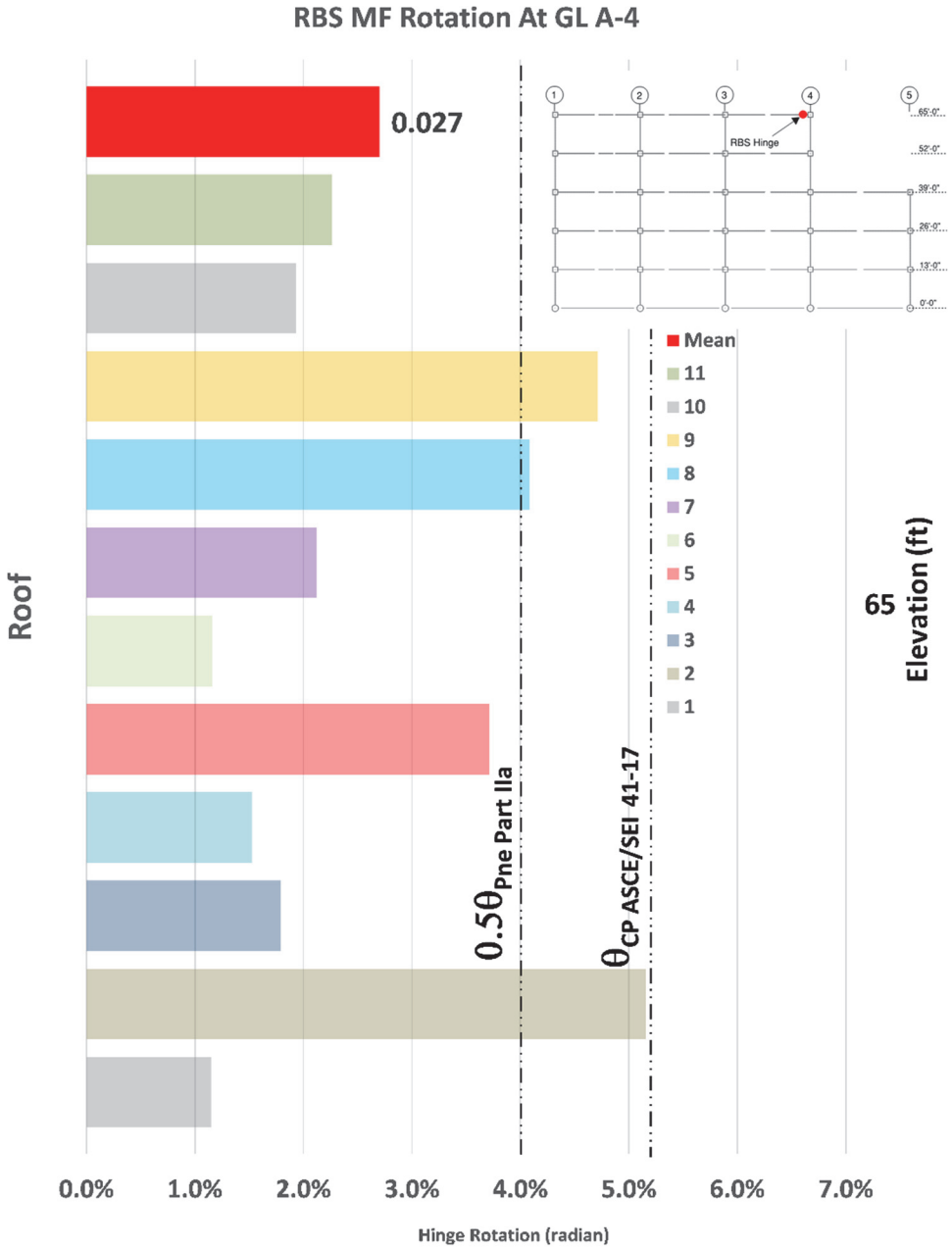

Figure B-18 Peak RBS hinge rotations and acceptance criteria under MCE ground motions.

To investigate the effect of composite slab behavior, an alternative model was analyzed in which composite behavior is ignored. In this case, the maximum mean beam rotation increases to 0.029 radians, which is about 9% larger than the analysis including composite behavior. One can imagine that the effect of modeling composite slab behavior will depend on the relative thickness of the concrete slab to the steel beam depth.

B.5.5 Columns

Ground floor column hinge rotations at grid lines 1-A.3 and 1-D are shown in Figure B-19. Similar to the beam hinges, values are reported for each ground motion and then a mean value for the set. Values are reported for both strong and weak axis rotations. For strong axis bending, the mean peak hinge rotation is 0.012 radian with a range of 0.005 to 0.026 radians. For weak axis hinge rotation, the mean is 0.012 radians with a range of 0.003 to 0.026 radians. Column hinge rotations are concentrated at the base of the structure, where the rotations in columns above the ground floor are all less than 0.005 radians.

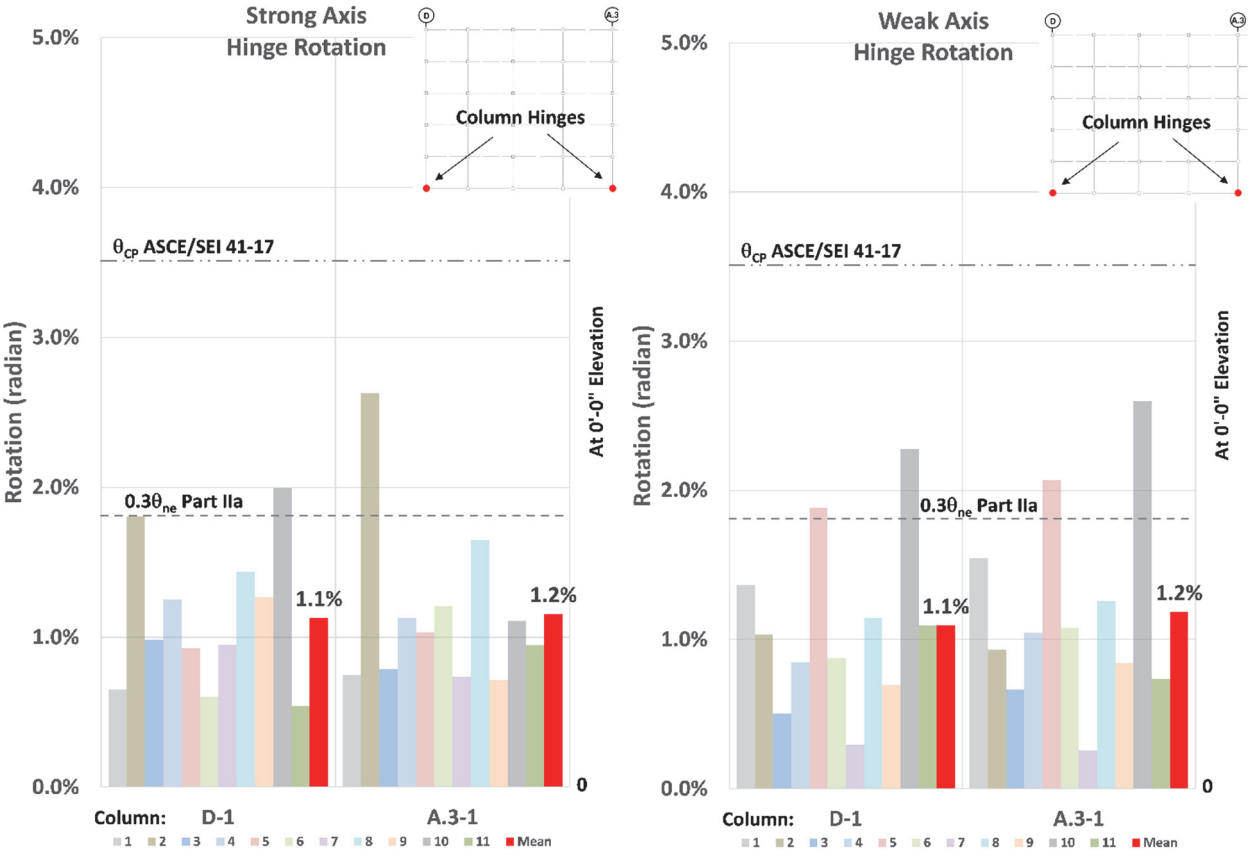

Figure B-19 First-story column hinge rotations under MCE ground motions.

The columns are evaluated per ASCE/SEI 7-16, using alternative acceptance criteria based on ASCE/SEI 41-17 and Section 4.3.2 modeling parameters.

Both ASCE/SEI 41-17 and Section 4.3.1 utilize a ratio, P_g/P_{ye}, to differentiate between deformation and force controlled flexural behavior in beam-column elements, where P_g is the axial load due to gravity in a column and P_{ye} is the expected yield strength of the column. Both qualify flexural behavior in columns as deformation controlled when $P_g/P_{ye} \leq 0.6$. ASCE/SEI 41-17 also differentiates the modeling parameters and acceptance criteria between columns with small gravity load, $P_g/P_{ye} < 0.2$, and moderate gravity load, $0.2 \leq P_g/P_{ye} \leq 0.6$; and it utilizes

another ratio, $|P|/P_{ye}$ to modify expected column flexural capacity and rotational capacity (where $|P|$ is the absolute maximum axial load due to gravity and seismic in a column).

ASCE/SEI 41-17 specifies the rotation limit for CP in ASCE/SEI 41-17 Table 9-6.1 as $\theta_{CP} = 0.035$ radians. Alternatively, Section 4.3.2 of this document specifies the ultimate rotation $\theta_u = 0.06$ radians, which is a median value. Similar to the limits on beams, it is not unreasonable to reduce this ultimate limit by the ASCE/SEI 7-16 resistance factor of $\phi_s = 0.3/Ie$ for a critical component (ASCE/SEI 7-16 Table 16.4-2). This would result in a limiting mean value rotation of $\phi_s \theta_u = (0.3)(0.06) = 0.018$ radians, which is about half that of the ASCE/SEI 41-17 limit. As shown in Figure B-19, the mean rotation demands at the column base are all well within these limits, and all of the individual demands are less than either the ASCE/SEI 41-17 θ_{CP} limit and the median modeling limit θ_u.

If any column with $P_g/P_{ye} > 0.6$ had hinged, the column would need to either: (1) be upsized such that with P_g/P_{ye} still > 0.6 no yielding occurs; or (2) upsized such that $P_g/P_{ye} < 0.6$ and flexural deformations are within acceptable rotation limits. This process may take several iterations until the column design criteria is satisfied.

In this building, column acceptance parameters from both ASCE/SEI 41-17 and these *Guidelines* resulted in columns satisfying the design criteria. In a building where overturning effects are more significant, there might be disparity between the two documents since ASCE/SEI 41-17 incorporates the ratio $|P|/P_{ye}$ in backbone parameters and acceptance criteria.

The ANSI/AISC 341-10 seismic provisions for steel special moment frames impose a strong-column-weak beam design check to avoid the premature formation of story mechanisms. This is accomplished by the $\Sigma M^*_{pc}/\Sigma M^*_{pb}$ ratio as defined in E3.4a ANSI/AISC 341-10. The provisions only require consideration of the steel beam properties to establish the beam strengths, and accordingly, the frame members were initially proportioned based on the steel beams along. However, for the nonlinear analysis, the positive flexural capacity of the moment frame beam did include composite action. Except at the base of the column, the analysis confirmed that the column hinge rotations were small (negligible), which indicates that the standard (bare steel) beam design check was reasonable. However, to promote strong column-weak beam behavior in the nonlinear analysis, one might consider using the composite flexural capacity in the ΣM^*_{pb} term of the column design equation E3.4a.

In this example, column nonlinearity was included in all columns. As a simplification, columns could have been modeled elastic with strength sections to confirm column hinging did not occur in the analysis. If the strength sections indicate column hinging would have occurred, hinges should either be modeled as

inelastic. Or, alternatively, the yielding columns would need to be strengthened and the analysis rerun. Note, however, that it is generally very difficult if not practically impossible to eliminate column yielding at a fixed column base.

B.5.6 Panel Zones

Figure B-20 shows Panel Zone deformations at the fifth floor on grid line 3A, which is the location of the largest PZ deformation demands. The mean PZ shear strain demand is 0.022 radians with a range of 0.010 to 0.048 radians.

The collapse prevention PZ deformation criterion, per ASCE/SEI 41-17, $\gamma_{CP} = 12\gamma_y$ for columns with $|P|/P_{ye} < 0.4$, where γ_y is defined by ASCE/SEI 41-17 Equation 9-3. In addition, γ_{CP} should not exceed $\gamma_{PZ,\,limit}$, where $\gamma_{PZ,\,limit}$ is defined by ASCE/SEI 41-17 Equation 9-18 and represents PZ strain which may instigate CJP weld fracture at the beam-flange to column-flange connection. For $0.58F_{ye} = 31.8$ ksi, $G = 11154$ ksi, $P_G/P_{ye} = 0.08$, $|P|/P_{ye} = 0.09$, and $\gamma_y = 0.003$ radian, $\gamma_{CP} = 0.035$ radian and $\gamma_{PZ,\,limit} = 0.015$ radians. As shown in Figure B-20, the mean PZ shear strain is less than γ_{CP}, however it exceeds $\gamma_{PZ,\,limit}$, indicating that the non-conforming fifth floor PZ at 3A does not satisfies the design criteria. Of the sixty-three non-conforming PZs in the building, only nine have shear strains that exceed $\gamma_{PZ,\,limit}$, representing roughly 10% of the total moment frame PZs. All of the conforming PZs have deformation demands that are less than both limits, thus confirming the effectiveness of the PZ design criteria to avoid fracture critical situations. Note, however, that this assessment is based on comparing the mean PZ shear deformation demand directly to $\gamma_{PZ,\,limit}$, without considering any reduction due to the resistance factor for deformation controlled components in ASCE/SEI 7-16. Thus, if the PZ were judged to be critical components, the acceptance criteria would need to be modified by the resistance factor.

To further investigate the PZ behavior, the panel zone model parameters were recalculated using the alternative PZ model by Kim et al. (2015), which would tend to give larger PZ strength and stiffness than the default Auto Connection Panel Zone in PERFORM-3D. This revision increased the PZ yield strength from 486 kips to 510 kips and the ultimate strength from 558 kips to 630 kips. The building was reanalyzed and the mean PZ shear strain demand reduced from 0.022 radians to 0.015 radians. With these reduced mean PZ shear strains, the PZ deformations all meet the limit of $\gamma_{PZ,\,limit} = 0.015$ radians.

The non-conforming PZs could also be modified to satisfy the design criteria by either adding a PZ doubler plate or increasing the column size (web thickness), which would tend to decrease the shear deformation demands and increase the PZ deformation limits. In particular, thickening the PZ would increase the ratio $\alpha = d_b/t_{cf}$, which would increase $\gamma_{PZ,\,limit}$ and $\gamma_{CP\,Alt}$. When the model was reanalyzed with

$^1/_2$ inch. A572 Grade 50 doubler plates, the mean PZ shear strain demands in the nine critical PZs to 0.003 radians, thereby eliminating any PZ concerns.

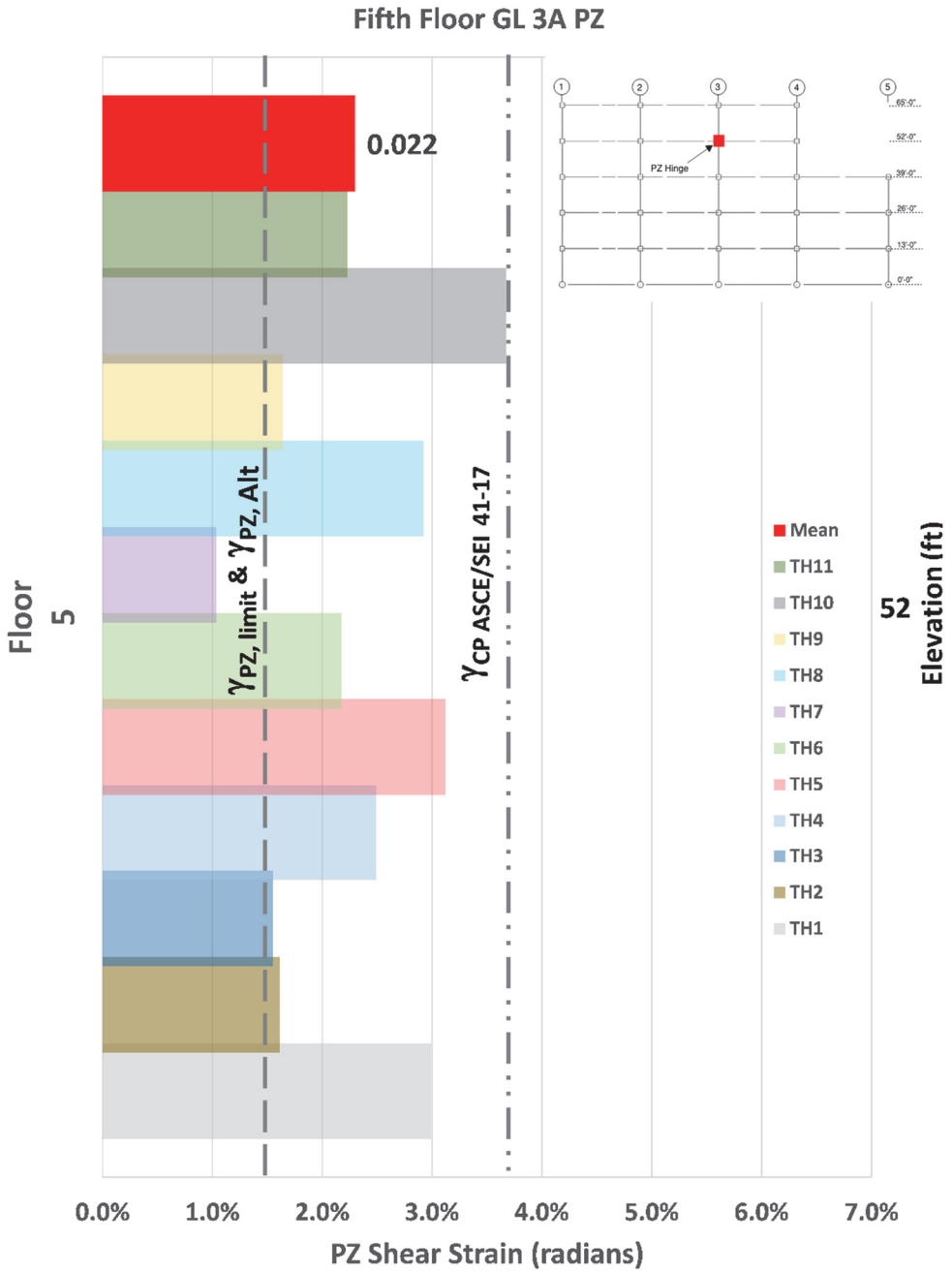

Figure B-20 Panel Zone shear strains under MCE ground motions.

B.5.7 Diaphragm Transfer at Fourth Floor

Two models with different diaphragm membrane stiffnesses were analyzed to assess the influence of diaphragm stiffness on overall building behavior. The first model uses 30% effective membrane stiffness for the diaphragms. The second model uses 5% effective membrane stiffness for diaphragm elements with shear stress exceeding

$0.5V_n$ and 30% elsewhere, as shown in Section B.4.4. The lower effective stiffness represents a case where large shear demands in the diaphragm cause cracking in the slab and a reduction in shear transfer through the diaphragm. Section 3.6 in the *Part I Guidelines* provides for more information concerning effective diaphragm properties. Grid Lines 1, 4, and 5 moment frame mean story shear and moment demands are shown in Figure B-21. Section cuts were defined at each floor level and each grid line to output diaphragm shear from the PERFORM-3D model. The results are grouped by moment frame line and listed in the following descending order at each story: Line 1 30%, Line 1 5%, Line 4 30%, Line 4 5%, Line 5 30%, and Line 5 5% where 30% represents the stiffer membrane model and 5% the softer membrane model.

An isometric view indicating the E-W moment frames along with an elevation of the moment frame at grid line 4 is included in the plots. Grid Line 1 moment frames are colored blue, grid line 4 moment frames are colored green and grid line 5 moment frames are colored orange. Below the fourth floor in the grid line 4 moment frame, the number of bays decreases from four to two bays. In Figure B-21, the grid line 4 moment frame sheds lateral load into the diaphragm shown by a decrease in story shear between the fourth and third story and the vertical dashed line. The grid line 4 moment frame maintains the remaining shear load and picks up some additional load from the second floor as shown by the change in story shear and moment demands relative to the grid line 1 moment frame.

The load shed out of the moment frame at the fourth floor is considered a transfer load. The diaphragm transfer shear demand at this floor is 7.6 klf and 7.4 klf for 30% and 5% effective diaphragm stiffness respectively. This demand represents $\gamma Qe = 2.0V_u$ where $\gamma = 2$ per Table 16.4-1 of ASCE/SEI 7-16. At other levels, the diaphragm shear demands range from 7.5 klf to 2.6 klf. These demands represent the range of values from 30% and 5% effective diaphragm stiffness with $\gamma = 1.5$.

In this building, varying diaphragm effective stiffnesses does not result in a significant change in results. To confirm this finding, another model with rigid diaphragms was analyzed. The difference between the rigid diaphragm and semi-rigid diaphragm assumption is negligible with grid line 4 moment frame story shears differing by less than ±5%. For an alternate lateral system where the beams supporting the discontinuous B4 column below the fourth floor are not moment connected, the grid line 4 moment frame sheds 20% more lateral load into the diaphragm. This alternate would eliminate seven moment connections, however, it requires a deep transfer girder at the second floor which encroaches into the conference room head space and would be unacceptable.

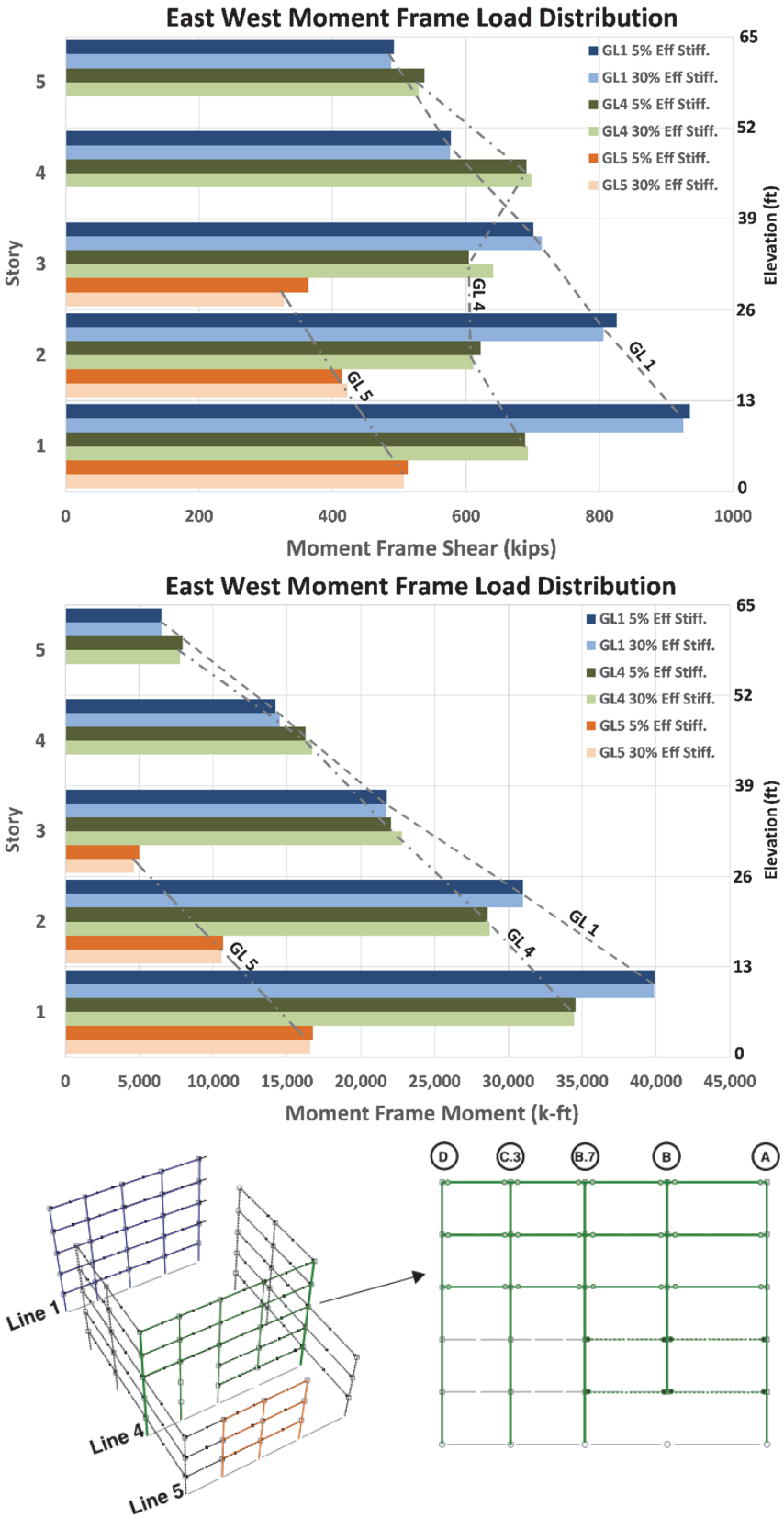

Figure B-21 Comparison of resultant shear and overturning moments in moment frames from analyses with variable floor diaphragm stiffness.

B.5.8 Gravity System

Secondary gravity systems have been traditionally ignored in the seismic design of buildings. However, where the goal is to simulate the system response as realistically as possible, gravity beam effects should be included in the analysis models.

The maximum gravity hinge rotation occurs at grid line C.3-1, with a mean rotation of 0.037 radians and a range of 0.025 to 0.072 radians. The gravity beams in the building are evaluated using alternative acceptance criteria, based on either ASCE/SEI 41-17 or the modeling parameters of Section 4.4.

According to ASCE/SEI 41-17, the rotation limit for collapse prevention (Table 9-6.2), is $\theta_{CP} = 0.15\text{-}0.0036 d_{bg}$ and d_{bg} is the depth of the bolt group. Using this criteria, the θ_{CP} limit is 0.10 radians, and all of the gravity connections meet the criteria, with the maximum rotation demand to capacity ratio, θ_u/θ_{CP} is 0.35.

According to the modeling parameters of Section 4.4, $\theta_u = g/d_f$ where g = gap between beam and column and d_f = distance from CG of shear tab or bolt group to furthest beam flange. Using this criteria, the θ_u limit is about 0.09 radians, and all of the gravity connections meet the criteria, with the maximum the max demand to capacity ratio, $\theta_u/\theta_{Gravity\ Loss}$ is 0.40.

To investigate the effect of the gravity system on global behavior, an alternative model was analyzed in which gravity beams are modeled pin-pin. In this case, rotation demands increased by roughly 12%. However, at the roof, the maximum mean RBS rotation for N-S beams increases 25-30% to 0.034 radians from the results described in Section B.5.4. The resulting ratios of the maximum RBS mean rotation demands to the capacities (acceptance criteria) increase to 0.83 and 0.85, based on the ASCE/SEI 41-17 and Section 4.2.2 criteria, respectively. At the fifth story in the N-S direction, the gravity system stiffness is a larger percentage of the total story stiffness compared to the lower levels. When this gravity stiffness is removed from the analysis, the N-S moment frame RBS rotations increase as inelastic deformation demand is dissipated in fewer elements. Although the global drift and shear results are similar when the gravity system is modeled and when it is not, this is not the case for the N-S moment frames at the roof.

B.6 Conclusions

This appendix illustrated the application of the analysis *Guidelines* to the nonlinear response history analysis of a steel moment frame building that generally conforms to current building code requirements for a high-seismic region. In general, the analysis results confirmed that the building performs within expectations and meets the ASCE/SEI 7-16 (Chapter 16) requirements for response under MCE level ground motions. The following are some specific observations regarding the analyses:

- The mean peak story drifts of 3.3% under MCE ground motions are within expectations and less than the 4% limit specified by ASCE/SEI 7-16. Further, the peak story drift ratio of 6.2% for the worst ground motion is considered within the range of modeling parameters, as further supported by checks on the local component deformations.
- The local demands on deformation controlled components (RBS hinge rotations, column base rotations, gravity beam-column connection rotations, and panel zone shear deformations) are generally less than required for collapse safety, as judged by either the CP limits of ASCE/SEI or the ultimate modeling limits of Chapters 3 or 4. One notable exception is that the panel zone deformations exceeded the limits at a few locations, which is attributed to the fact that some of the connection details do not meet the seismic design requirements of ANSI/AISC 341. When reanalyzed with code-confirming PZ doubler plates, the PZ deformation demands were all within the limits.
- Comparisons between the CP deformation limits of ASCE/SEI and the ultimate modeling deformation limits of Chapters 3 and 4 generally showed the latter to be more liberal (less severe). However, if the ASCE/SEI 7-16, *Minimum Design Loads and Associated Criteria for Buildings and Other Structures* (ASCE, 2017a) resistance factors are applied to the median values of modeling limits from Chapters 3 and 4 (e.g., $\phi_s = 0.3$ for critical components), then these limits were more restrictive.
- Force controlled checks were not presented in this appendix with the exception that axial forces in columns are checked to confirm that the columns are below the limit of $P_g/P_{ye} < 0.6$ for force controlled members. However, comparisons of resultant frame shears and moments do indicate that the forces developed under MCE ground motions are generally larger than what one would calculate using the design basis forces with an Ω (overstrength) factor. Therefore, local checks should be made to confirm that the force controlled members meet the requirement strengths (e.g., connection design forces, and shear strengths of beams and columns).
- Sensitivity analyses of selected modeling parameters confirmed that the MCE response is not overly sensitive to variations in analysis including: (1) diaphragm membrane stiffness; (2) inclusion of gravity framing; and (3) consideration of composite beam action. With regard to the latter two, they both do improve response by reducing the story drifts and local deformations on the order of 10% to 20%, compared to analyses that consider only the bare steel frames of the seismic force resisting system.

Finally, it should be emphasized that these observations are based on the one example building and that the observations and conclusions are not meant to

generally apply to other buildings. Indeed, the intent of these *Guidelines* is to facilitate the use of nonlinear analysis to investigate the specific characteristics of any building, and the purpose of this appendix is to illustrate application of the *Guidelines*.

References

AISC, 1999, *Seismic Provisions for Structural Steel Buildings (1997)*, American Institute of Steel Construction, Chicago, Illinois.

AISC, 2010a, *Prequalified Connections for Special and Intermediate Steel Moment Frames for Seismic Applications*, ANSI/AISC 358-10, American National Standards Institute/American Institute of Steel Construction, Chicago, Illinois.

AISC, 2010b, *Seismic Provisions for Structural Steel Buildings*, ANSI/AISC 341-10, American National Standards Institute/American Institute of Steel Construction, Chicago, Illinois.

AISC, 2016a, *Code of Standard Practice for Steel Buildings and Bridges*, ANSI/AISC 303-16, American National Standards Institute/American Institute of Steel Construction, Chicago, Illinois.

AISC, 2016b, *Prequalified Connections for Special and Intermediate Steel Moment Frames for Seismic Applications*, American Institute of Steel Construction, AISC 358-16, Chicago, Illinois.

AISC, 2016c, *Seismic Provisions for Structural Steel Buildings*, ANSI/AISC 341-16, American National Standards Institute/American Institute of Steel Construction, Chicago, Illinois.

AISC, 2016d, *Specification for Structural Steel Buildings*, ANSI/AISC 360-16, American National Standards Institute/American Institute of Steel Construction, Chicago, Illinois.

Almufti, I., Hutt, C.M., Willford, M., and Deierlein, G.G., 2012, "Seismic assessment of typical 1970s tall steel moment frame buildings in downtown San Francisco," *15WCEE Proceedings*, Lisbon, Portugal.

Altoontash, A., 2004, *Simulation and Damage Models for Performance Assessment of Reinforced Concrete Beam-Column Joints*, Ph.D. dissertation, Stanford University, Stanford, California.

ASCE, 2014, *Seismic Evaluation and Retrofit of Existing Buildings*, ASCE/SEI 41-13, American Society of Civil Engineers, Reston, Virginia.

ASCE, 2017a, *Minimum Design Loads and Associated Criteria for Buildings and Other Structures*, ASCE/SEI 7-16, American Society of Civil Engineers, Reston, Virginia.

ASCE, 2017b, *Seismic Evaluation and Retrofit of Existing Buildings*, ASCE/SEI 41-17, American Society of Civil Engineers, Reston, Virginia.

ASTM, 2016, *Standard Test Method for Determination of Reference Temperature, To, for Ferritic Steels in the Transition Range,* ASTM E1921-16*,* ASTM International, West Conshohocken, Pennsylvania.

Barsom, J.M., and Rolfe, S.T., 1999, *Fracture and Fatigue Control in Structures: Applications of Fracture Mechanics,* Third Edition, ASTM MNL41, American Society for Testing and Materials, ASTM Press, West Conshohocken, Pennsylvania.

Bech, D., Houston, J., and Tremayne, B., 2016, "Implementation of ASCE 41-17 steel column modeling & acceptance criteria," *Proceedings*, 2016 SEAOC Convention, Structural Engineers Association of California.

Charney, F.A., and Downs, W.M., 2004, "Modeling procedures for panel zone deformations in moment resisting frames," *Connections in Steel Structures V: Innovative Steel Connections*, Amsterdam, the Netherlands.

Charney, F.A., and Marshall, J., 2006, "A comparison of the Krawinkler and scissors models for including beam-column joint deformations in the analysis of moment resisting steel frames," *Engineering Journal*, First Quarter, pp. 31-48.

Chi, W-M., Deierlein, G.G., and Ingraffea, A.R., 2000, "Fracture toughness demands in welded beam-column moment connections," *Journal of Structural Engineering*, Vol. 126, No. 1, pp. 88-97.

Elkady, A., and Lignos, D.G., 2014, "Modeling of the composite action in fully restrained beam-to-column connections: implications in the seismic design and collapse capacity of steel special moment frames," *Earthquake Engineering and Structural Dynamics*, Vol. 43, No. 13, pp. 1935-1954.

Elkady, A., and Lignos, D.G., 2015, "Analytical investigation of the cyclic behavior and plastic hinge formation in deep wide-flange steel beam-columns," *Bulletin of Earthquake Engineering*, Vol. 13, No. 4, pp. 1097-1118.

Elkady, A., 2016, *Collapse Risk Assessment of Steel Moment Resisting Frames Designed with Deep Wide-Flange Columns in Seismic Regions*, Ph.D. Thesis, Dept. of Civil Engineering and Applied Mechanics, McGill University, Montreal.

Elkady, A., and Lignos, D.G., 2016, "Dynamic stability of deep and slender wide-flange steel columns – Full scale experiments," *Proceedings* of the Annual Stability Conference, Structural Stability Research Council (SSRC), Orlando, Florida, April 12-15, 2016.

El-Tawil, S., Mikesell, T. D., Vidarsson, E., and Kunnath, S. K., 1999, "Inelastic behavior and design of steel panel zones," *Journal of Structural Engineering*, Vol. 125, No. 2, pp. 183-193.

FEMA, 1996, *Background Reports on Metallurgy, Fracture Mechanics, Welding, Moment Connections and Frame Systems Behavior*, FEMA 288, prepared by the SAC Joint Venture, a partnership of the Structural Engineers Association of California (SEAOC), Applied Technology Council (ATC), and California Universities for Research in Earthquake Engineering (CUREE), for the Federal Emergency Management Agency, Washington, D.C.

FEMA, 1997a, *Connection Test Summaries*, FEMA-289, SAC Report 96-02, prepared by the SAC Joint Venture, a partnership of the Structural Engineers Association of California (SEAOC), Applied Technology Council (ATC), and California Universities for Research in Earthquake Engineering (CUREE), for the Federal Emergency Management Agency, Washington, D.C.

FEMA, 1997b, *Interim Guidelines for Steel Moment Resisting Frame Construction*, FEMA 267, prepared by the SAC Joint Venture, a partnership of the Structural Engineers Association of California (SEAOC), Applied Technology Council (ATC), and California Universities for Research in Earthquake Engineering (CUREE), for the Federal Emergency Management Agency, Washington, D.C.

FEMA, 2000a, *Recommended Seismic Design Criteria for New Steel Moment-Frame Buildings*, FEMA 350, prepared by the SAC Joint Venture, a partnership of the Structural Engineers Association of California (SEAOC), Applied Technology Council (ATC), and California Universities for Research in Earthquake Engineering (CUREE), for the Federal Emergency Management Agency, Washington, D.C.

FEMA, 2000b, *Recommended Seismic Evaluation and Upgrade Criteria for Existing Welded Steel Moment-Frame Buildings*, FEMA 351, prepared by the SAC Joint Venture, a partnership of the Structural Engineers Association of California (SEAOC), Applied Technology Council (ATC), and California Universities for Research in Earthquake Engineering (CUREE), for the Federal Emergency Management Agency, Washington, D.C.

FEMA, 2000c, *State of the Art Report on Connection Performance*, FEMA 355D, prepared by the SAC Joint Venture, a partnership of the Structural Engineers

Association of California (SEAOC), Applied Technology Council (ATC), and California Universities for Research in Earthquake Engineering (CUREE), for the Federal Emergency Management Agency, Washington, D.C.

Hall, J.F., 1995, *Parameter Study of the Response of Moment-Resisting Steel Frame Building to Near-Source Ground Motions*, Report EERL 95-08, California Institute of Technology.

Hartloper, A., and Lignos, D.G., 2016, *Updates to the ASCE-41-13 Nonlinear Modeling Provisions for Performance-Based Seismic Assessment of New And Existing Steel Moment Resisting Frames*, M.Eng., Thesis, McGill University, Montreal, Canada.

Ibarra, L.F., Medina, R.A., and Krawinkler, H., 2005, "Hysteretic models that incorporate strength and stiffness deterioration," *Earthquake Engineering and Structural Dynamics*, Vol. 34, No. 12, pp. 1489-511.

International Conference of Building Officials, 1994, *Uniform Building Code*, Whittier, California.

Kanvinde, A.M., and Deierlein, G.G., 2007, "A cyclic void growth model to assess ductile fracture in structural steels due to ultra-low cycle fatigue," *Journal of Engineering Mechanics*, Vol. 133, No. 6, pp. 701-712.

Kim, D.W., Blaney, C., and Uang, C-M., 2015, "Panel zone deformation capacity as affected by weld fracture at column kinking location," *Engineering Journal*, Vol. 53, No. 1, pp. 27-46.

Krawinkler, H., 1978, "Shear design of steel frame joints," *Engineering Journal*, Vol. 15, No. 3.

Lee, K-H., Stojadinovic, B., Goel, S.C., Margarian, A.G., Choi, J., Wongkaew, A., Reyber, B.P., and Lee, D-Y., 1999, *Parametric Tests on Unreinforced Connections, Volume I – Final Report,* Report No. SAC/BD-00/01, prepared by the SAC Joint Venture, a partnership of the Structural Engineers Association of California (SEAOC), Applied Technology Council (ATC), and California Universities for Research in Earthquake Engineering (CUREE), for the Federal Emergency Management Agency, Washington, D.C.

Lignos, D.G., and Krawinkler, H., 2010, "A steel database for component deterioration of tubular hollow square steel columns under varying axial load for collapse assessment of steel structures under earthquakes," *Proceedings*, 7th International Conference on Urban Earthquake Engineering (7CUEE) & 5th International Conference on Earthquake Engineering (5ICEE), Tokyo Institute of Technology, Tokyo, Japan.

Lignos, D.G., and Krawinkler, H., 2011, "Deterioration modeling of steel components in support of collapse prediction of steel moment frames under earthquake loading," *Journal of Structural Engineering*, Vol. 137, No. 11, pp. 1291-1302.

Lignos, D.G., and Krawinkler, H., 2012, *Sidesway Collapse of Deteriorating Structural Systems Under Seismic Excitations*, Report 177, the John A. Blume Earthquake Engineering Center, Stanford University, Stanford, California.

Liu, J., and Astaneh-Asl, A., 2000a, "Cyclic testing of simple connections, including effects of the slab," *Journal of Structural Engineering*, Vol. 126, No. 1, pp. 32-39.

Liu, J., and Astaneh-Asl, A., 2000b, *Cyclic Testing on Simple Connections, including Effects of the Slab*, Report No. SAC/BD-00/03, prepared by the SAC Joint Venture, a partnership of the Structural Engineers Association of California (SEAOC), Applied Technology Council (ATC), and California Universities for Research in Earthquake Engineering (CUREE), for the Federal Emergency Management Agency, Washington, D.C.

Liu, J., and Astaneh-Asl, A., 2004, "Moment-rotation parameters for composite shear tab connections," *Journal of Structural Engineering*, Vol. 130, No. 9, pp. 1371-1380.

Neuenhofer, A., and Filippou, F.C., 1997, "Evaluation of nonlinear frame finite-element models," *Journal of Structural Engineering*, Vol. 123, No. 7, pp. 958-966.

Neuenhofer, A., and Filippou, F.C., 1998, "Geometrically nonlinear flexibility-based frame finite element," *Journal of Structural Engineering*, Vol. 124, No. 6, pp. 704-711.

Newell, J., and Uang, C.M., 2006, *Cyclic Testing of Steel Moment Connections for the Caltrans District 4 Office Building Seismic Rehabilitation*, Structural Systems Research Project Report No. SSRP-05/03, Department of Structural Engineering, University of California, San Diego, La Jolla.

Newell, J.D., and Uang, C.M., 2008, "Cyclic behavior of steel wide-flange columns subjected to large drift," *Journal of Structural Engineering*, Vol. 134, No. 8, pp. 1334-1342.

NIST, 1994, *Robustness of Steel Gravity Frame Systems with Single-Plate Shear Connections*, Technical Note 1749, National Institute of Technology and Standards, Gaithersburg, Maryland.

NIST, 2009, *Research Required to Support Full Implementation of Performance-Based Seismic Design*, NIST GCR 09-917-2, prepared by the Building Seismic Safety Council of the National Institute of Building Sciences for the National Institute of Standards and Technology, Gaithersburg, Maryland.

NIST, 2010, *NEHRP Seismic Design Technical Brief No. 4: Nonlinear Structural Analysis for Seismic Design: A Guide for Practicing Engineers*, NIST GCR 10-917-5, prepared by the NEHRP Consultants Joint Venture, a partnership of the Applied Technology Council and the Consortium for Universities for Research in Earthquake Engineering, for the National Institute of Standards and Technology, Gaithersburg, Maryland.

NIST, 2011, *NEHRP Seismic Design Technical Brief No. 5: Seismic Design of Composite Steel Deck and Concrete-filled Diaphragms: A Guide for Practicing Engineers*, NIST GCR 10-917-4, prepared by the NEHRP Consultants Joint Venture, a partnership of the Applied Technology Council and the Consortium for Universities for Research in Earthquake Engineering, for the National Institute of Standards and Technology, Gaithersburg, Maryland.

NIST, 2012, *Soil-Structure Interaction for Building Structures*, NIST GCR 12-917-21, prepared by the NEHRP Consultants Joint Venture, a partnership of the Applied Technology Council and the Consortium for Universities for Research in Earthquake Engineering, for the National Institute of Standards and Technology, Gaithersburg, Maryland.

NIST, 2013, *Nonlinear Analysis Research and Development Program for Performance-Based Engineering*, NIST GCR 14-917-27, prepared by the NEHRP Consultants Joint Venture, a partnership of the Applied Technology Council and the Consortium for Universities for Research in Earthquake Engineering, for the National Institute of Standards and Technology, Gaithersburg, Maryland.

NIST, 2016, *NEHRP Seismic Design Technical Brief No. 2: Seismic Design of Steel Special Moment Frames: A Guide for Practicing Engineers*, NIST GCR 16-917-41 Second Edition, prepared by the NEHRP Consultants Joint Venture, a partnership of the Applied Technology Council and the Consortium for Universities for Research in Earthquake Engineering, for the National Institute of Standards and Technology, Gaithersburg, Maryland.

NIST, 2017a, *Guidelines for Nonlinear Structural Analysis for Design of Buildings, Part I – General*, NIST GCR 17-917-46v1, prepared by the Applied Technology Council for the National Institute of Technology and Standards, Gaithersburg, Maryland.

NIST, 2017b, *Recommended Modeling Parameters and Acceptance Criteria for Nonlinear Analysis in Support of Seismic Evaluation, Retrofit, and Design*, NIST GCR 17-917-45, prepared by the Applied Technology Council for the National Institute of Technology and Standards, Gaithersburg, Maryland.

NIST, 2017c, *Guidelines for Nonlinear Structural Analysis for Design of Buildings, Part IIb – Reinforced Concrete Moment Frames*, NIST GCR 17-917-46v3, prepared by the Applied Technology Council for the National Institute of Technology and Standards, Gaithersburg, Maryland.

Ozkula, G., Harris, J., and Uang, C-M., 2015, "Observations from cyclic tests on deep wide-flange beam-column members," *Proceedings*, 2015 SSRC Annual Stability Conference, Structural Stability Research Council.

Ozkula, G, Harris, J., and Uang, C.M., 2017, "Observations from cyclic tests on deep wide-flange beam-columns," *Engineering Journal*, First Quarter, pp. 45-59.

PEER/ATC, 2010, *Modeling and Acceptance Criteria for Seismic Design and Analysis of Tall Buildings*, PEER/ATC 72-1, prepared by the Pacific Earthquake Engineering Research Center (PEER) and Applied Technology Council (ATC), Redwood City, California.

Ramirez, C.M., Lignos, D.G., Miranda, E., and Kolios, D., 2012, "Fragility functions for pre-Northridge welded steel moment-resisting beam-column connections," *Engineering Structures*, Vol. 45, pp. 574-584.

Ricles, J. M., Mao, C., Lu, L-W., and Fisher, J. W., 2002, "Development of improved welded moment connections for earthquake-resistant design," *Journal of Constructional Steel Research*, Vol. 58, No. 5, pp. 565-604.

Ricles, J.M., Zhang, X., Lu, L-W., and Fisher, J., 2004, *Development of Seismic Guidelines for Deep-Column Steel Moment Connections*, ATLSS Report No. 04-13, Advanced Technology for Large Structural Systems, Bethlehem, Pennsylvania.

Shen, C., Mamaghani, I. H. P., Mizuno, E., and Usami, T., 1995, "Cyclic behavior of structural steels. II: Theory," *Journal of Engineering Mechanics*, Vol. 121, No. 11, pp. 1165–1172.

Shen, J., Sabol, T., Akabas, B., and Sutchiewcharn, C., 2010, "Seismic demand on column splices in steel moment frames," *Engineering Journal*, American Institute of Steel Construction, Vol. 47, pp. 223-240.

Smith, C.M., Kanvinde, A.M., and Deierlein, G.G., 2017, "A local criterion for ductile fracture under low-triaxiality axisymmetric stress states," *Engineering Fracture Mechanics*, Elsevier, Vol. 169, pp. 321-335.

Stillmaker, K., Kanvinde, A., and Galasso, C., 2015, "Fracture mechanics-based design of column splices with partial joint penetration welds," *Journal of Structural Engineering*, Vol. 142, Issue 2.

Suzuki, Y., and Lignos, D.G., 2015, "Large-scale collapse experiments of wide flange steel beam-columns," *Proceedings*, 8th International Conference on the Behavior of Steel Structures in Seismic Areas, Shanghai, China, July 1-3, 2015.

Taucer, F., Spacone, E., and Filippou, F., 1991, *A Fiber Beam-Column Element for Seismic Response Analysis of Reinforced Concrete Structures*, UCB/EERC-91/17, Earthquake Engineering, Research Center, Berkeley, California.

Tremblay, R., Tchebotarev, N., and Filiatrault, A., 1997, "Seismic performance of RBS connections for steel moment-resisting frames: influence of loading rate and floor slab," *Behavior of Steel Structures in Seismic Areas, Proceedings of the Second International Conference*, STESSA, Kyoto, Japan, pp. 664-671.

Wallin, K., 1991, "Statistical modelling of fracture in the ductile-to-brittle transition region," *Defect Assessment in Components-Fundamentals and Applications*, ESIS/EGF9, edited by J.G. Blauel and K.-H. Schwalbe, Mechanical Engineering Publications, London, pp. 415-445.

Yu, Q-S., and Uang, C-M., 2001, "Effects of near-fault loading and lateral bracing on the behavior of RBS moment connections," *Steel and Composite Structures*, Vol. 1, No. 1, pp. 145-158.

Project Participants

National Institute of Standards and Technology

Steven L. McCabe
Engineering Laboratory (MS8604)
National Institute of Standards and Technology
100 Bureau Drive
Gaithersburg, Maryland 20899

Matthew S. Speicher
Engineering Laboratory (MS8604)
National Institute of Standards and Technology
100 Bureau Drive
Gaithersburg, Maryland 20899

Jay Harris
Engineering Laboratory (MS8604)
National Institute of Standards and Technology
100 Bureau Drive
Gaithersburg, Maryland 20899

Kevin K. F. Wong
Engineering Laboratory (MS8604)
National Institute of Standards and Technology
100 Bureau Drive
Gaithersburg, Maryland 20899

Siamak Sattar
Engineering Laboratory (MS8604)
National Institute of Standards and Technology
100 Bureau Drive
Gaithersburg, Maryland 20899

Applied Technology Council

Jon A. Heintz (Program Manager)
Applied Technology Council
201 Redwood Shores Parkway, Suite 240
Redwood City, California 94065

Veronica Cedillos (Associate Project Manager)
Applied Technology Council
201 Redwood Shores Parkway, Suite 240
Redwood City, California 94065

Ayse Hortacsu (Associate Program Manager)
Applied Technology Council
201 Redwood Shores Parkway, Suite 240
Redwood City, California 94065

Program Committee on Seismic Engineering

Jon A. Heintz (Chair)
Applied Technology Council
201 Redwood Shores Parkway, Suite 240
Redwood City, California 94065

James R. Harris
J.R. Harris & Company
1775 Sherman Street, Suite 1525
Denver, Colorado 80203

Michael Cochran
Thornton Tomasetti
4551 Glencoe Avenue, Suite 350
Marina del Rey, California 90292

James Jirsa
Department of Civil, Architectural and Environmental Engineering
University of Texas at Austin
301 E. Dean Keeton Street, Stop C1700
Austin, Texas 78712

Roberto Leon
Department of Civil and Environmental Engineering
Virginia Tech
102-D Patton Hall
Blacksburg, Virginia 24061

Stephen Mahin
Department of Civil and Environmental Engineering
University of California, Berkeley
721 Davis Hall
Berkeley, California 94720

James O. Malley
Degenkolb Engineers
375 Beale Street, Suite 500
San Francisco, California 94105

Donald Scott
PCS Structural Solutions
811 First Avenue, Suite 620
Seattle, Washington 98104

Andrew Whittaker
Department of Civil, Structural and Environmental Engineering
University at Buffalo
230 Ketter Hall
Buffalo, New York 14260

Project Technical Committee

Gregory G. Deierlein (Project Director)
Dept. of Civil and Environmental Engineering
Blume Earthquake Engineering Center
MC 3037
Stanford, California 94305

Stephen T. Bono
Simpson Gumpertz & Heger, Inc.
100 Pine Street, Suite 1600
San Francisco, California 94111

James O. Malley
Degenkolb Engineers
375 Beale Street, Suite 500
San Francisco, California 94105

Silvia Mazzoni
325 Davis Hall
University of California
Berkeley, California 94720

Chia-Ming Uang
Dept. of Structural Engineering
University of California, San Diego
409 University Center
La Jolla, California 90293

Project Review Panel

Jerome F. Hajjar
Dept. of Civil and Environmental Engineering
400 Snell Engineering Center
360 Huntington Avenue
Northeastern University
Boston, Massachusetts 02115

Charles Roeder
University of Washington
Dept. of Civil Engineering
Seattle, Washington 98195

Thomas Sabol
Englekirk Institutional
888 South Figueroa Street, 18th Floor
Los Angeles, California 90017

Mark Saunders
Rutherford + CHekene
375 Beale Street, Suite 310
San Francisco, California 94105

Kent Yu (ATC Board Contact)
SEFT Consulting Group
4800 SW Griffith Drive, Suite 100
Beaverton, Oregon 97005

Working Group Members

Gulen Ozkula
Dept. of Structural Engineering
University of California, San Diego
409 University Center
La Jolla, California 90293

Zhi Zhou
Simpson Gumpertz & Heger, Inc.
100 Pine Street, Suite 1600
San Francisco, California 94111